e-ISSN: 3061-9939

JOURNAL OF NAVAL ARCHITECTURE AND MARINE TECHNOLOGY

ISSUE 226 December 2024

www.jnamt.org

JOURNAL OF NAVAL ARCHITECTURE AND MARINE TECHNOLOGY

Publisher
Galenos Yayınevi
Address: Molla Gürani Mah. Kaçamak Sk. No: 21/1
34093 İstanbul, Turkey
Phone: +90 (530) 177 30 97 / +90 (539) 307 32 03
E-mail: info@galenos.com.tr/yayin@galenos.com.tr
Web: www.galenos.com.tr
Publisher Certificate Number: 14521

Online Publication Date: January 2025

E-ISSN: 3061-9939

JOURNAL OF NAVAL ARCHITECTURE AND MARINE TECHNOLOGY

GMO

www.jnamt.org

Please refer to the journal's webpage (**https://www.jnamt.org/**) for "Aims and Scope", "Instructions to Authors", and "Ethical Policy".

The editorial and publication processes of the Journal of Naval Architecture and Marine Technology are shaped in accordance with the ethical guidelines provided by COPE (Committee on Publication Ethics), EASE (European Association of Science Editors), SNAME (Society of Naval Architects and Marine Engineers), and IMarEST (Institute of Marine Engineering, Science and Technology). The journal adheres to the Principles of Transparency and Best Practice in Scholarly Publishing.

Journal of Naval Architecture and Marine Technology is indexed in **ULAKBİM TR Index, EBSCO Host, CNKI, I2OR, DRJI, Sobiad, Google Scholar**, and **RootIndex**.

The journal is published online.

Owner: Mr. Bülent Hüseyinoğlu, Naval Architect and Marine Engineer, on behalf of UCTEA Turkish Chamber of Naval Architects and Marine Engineers (TMMOB GMO).

JOURNAL OF NAVAL ARCHITECTURE AND MARINE TECHNOLOGY

EDITORIAL

31.01.2024

Dear Readers,

We are pleased to present seven research articles in Issue 226. These articles cover a diverse range of topics, including parametric roll analysis, ship airwake analysis, optimal structures for submarine pressure hulls, bridge resource management for navigational safety, curriculum evaluation in naval architecture and marine engineering, maritime accidents in Turkish territorial waters, and the design of long sandwich plates. We sincerely acknowledge the scientific contributions and valuable efforts of the authors, reviewers, and editors.

Following recommendations from publishing experts, we will transition to a continuous publication (CP) model starting in 2025. This model will allow articles to be made available online as soon as they are finalized, in a fully citable format with a DOI code.

As we step into a new year, we extend our heartfelt gratitude for your continued support and engagement. May the year ahead bring you joy, success, and inspiration. We invite you to submit your articles and look forward to sharing more exciting content with you in the coming months and years.

Editorial Board
Journal of Naval Architecture and Marine Technology

JOURNAL OF NAVAL ARCHITECTURE AND MARINE TECHNOLOGY

CONTENTS

ISSUE 226 DEC 2024

RESEARCH ARTICLE

DOI: 10.54926/jnamt.2024.1516922

J Nav Architect Mar Technol 2024;226(2):1-11

Non-Linear Numeric Parametric Roll Analysis for the DTMB 5512 in Regular Waves

Fikret Dündar, Ferdi Çakıcı

Department of Naval Architecture and Marine Engineering, Faculty of Marine Sciences, Yıldız Technical University, İstanbul, Türkiye

To cite this article: F. Dündar, and F. Çakıcı. Non-linear numeric parametric roll analysis for the DTMB 5512 in regular waves. *J Nav Architect Mar Technol*. 2024;226(2):1-11.

Received: 16.07.2024 - **Revised:** 29.10.2024 - **Accepted:** 30.10.2024 - **Publication Date:** 31.01.2025

Abstract

Parametric roll motion is a phenomenon that occurs within seconds, and it can reach high roll degrees. If the periodic stability of a ship changes, it may cause roll angles over 25 degrees, threatening the safety of the crew and the ship. This also threatens the operational skills of the ship. To investigate this phenomenon, a navy combatant model DTMB 5512 is selected. The model also has a bilge keel. Himeno's method was employed to calculate damping coefficients based on roll decay experiments (from literature) conducted at various model speeds and initial angles. This approach facilitated the extraction of both linear and non-linear damping coefficients from experimental data. Additionally, extinction coefficients were also obtained. Maxsurf stability software was utilized to compute *GM* values and generate the *GZ* curve. A Runge-Kutta method implementation in Python programming enabled numerical analysis, comprising a total of 240 simulations across 10 wave heights and 24-speed scenarios. For each scenario, the maximum roll angle was determined. It was observed that roll angles increased notably when the encounter frequency approached twice the natural roll frequency. Based on the analysis findings, maximum roll angles did not exceed 25 degrees, indicating that the DTMB 5512 model is not vulnerable to parametric roll resonance.

Keywords: DTMB 5512, parametric roll resonance, damping, roll decay

1. Introduction

Parametric roll motion is a rapid phenomenon characterized by high roll angles (exceeding 25 degrees) occurring within seconds. Research on parametric roll began in the 1930s, marked by seminal theoretical analyses by Watanabe [1] and Kempf [2]. Subsequent studies integrated nonlinear damping and Mathieu-type equations, notably by Kerwin [3] and Paulling and Rosenberg [4]. Experimental investigations by Paulling [5] in 1972 further contributed to understanding this phenomenon. The practical significance of parametric roll gained prominence in the 1990s following accidents, such as the damage to a post-panamax C11 type cargo ship in 1998, which prompted detailed publications emphasizing its importance [6]. Bulian [7] explored the nonlinear damped 1-degree-of-freedom motion associated with the parametric roll. The International Maritime Organization (IMO) included parametric roll in the second-generation stability criteria for ship safety [8], while recent studies continue to investigate various aspects of parametric roll [9,10,11]. Parametric roll analysis plays a critical role in maritime safety guidelines established by classification societies such as ClassNK [12] and ABS [13], as well as the updated guidelines from the IMO in 2020 [14]. The metacentric height (*GM*) is a pivotal factor in parametric roll analysis,

Address for Correspondence: Ferdi Çakıcı, Department of Naval Architecture and Marine Engineering, Faculty of Marine Sciences, Yıldız Technical University, İstanbul, Türkiye

E-mail: fcakici@yildiz.edu.tr

ORCID ID: orcid.org/0000-0001-9752-1125

varying with different loading conditions. Recent research has also explored computational fluid dynamics solutions tailored to specific vessel types, including fishing boats [15].

In this study, we conducted numerical parametric roll analysis for the DTMB 5512 model. Damping coefficients were derived using roll decay data specific to the DTMB 5512, as detailed by Irvine et al. [16]. Both linear and nonlinear damping coefficients were considered, adhering closely to IMO guidelines [17]. The restoring term *GZ* was modelled using a seventh-degree equation, while *GM* was approximated using a cosine function. The numerical analysis was executed utilizing the Runge-Kutta method.

2. Physical Background

Parametric roll can occur when the ship length and the wavelength of encountered waves are closely aligned, and the wave encounter frequency is twice the ship natural roll frequency. Changes in transverse inertia in the head or following seas lead to fluctuations in *GM* (metacentric height).

Ships typically have a wider beam at upper decks, especially in cargo ships, where the underwater portion is streamlined compared to the above-water structure. Consequently, when the wave trough is amidships, the ship experiences greater inertia, enhancing its stability. Conversely, when the wave crest is amidships, the ship encounters less inertia, resulting in decreased stability. The variation in *GM* mentioned above is influenced by factors such as wavelength, wave height, and the wave position. Figures 1 and 2 illustrate the submerged portions of the ship at different wave positions.

Figures 3 and 4 depict the submerged waterplane area of the ship at various positions relative to the wave. These perspectives should be considered together for a comprehensive evaluation. As the wave moves past the ship, the relationship with width becomes crucial, significantly as the height varies at different points along the ship.

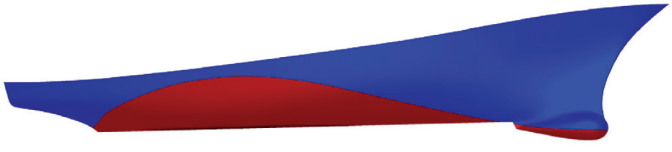

Figure 1. View of the DTMB 5512 when the ship is on the wave crest.

Figure 2. View of the DTMB 5512 when the ship is on the wave trough.

The variation of these two variables relative to the wave's position defines the changes in *GM*.

Parametric roll is characterized by periodic changes influenced by the relationship between the ship's natural roll frequency and the encounter frequency of waves. Figure 5 illustrates a scenario where the encounter frequency is twice the ship's natural roll frequency. Initially, at the zero-roll degree point with the wave crest position, the ship experiences zero roll angle. As the wave progresses, the ship reaches its maximum roll angle with the wave in a trough position. The ship's stability is enhanced during this phase due to a greater restoring moment. Subsequently, as the ship continues to roll, the wave position returns to a crest. At this stage, the ship's stability decreases, leading to increased rolling compared to earlier stages, the ship reaches its maximum roll angle again when the wave returns to a trough position. Consequently, stability improves once more. This cyclic pattern of roll and stability changes is characteristic

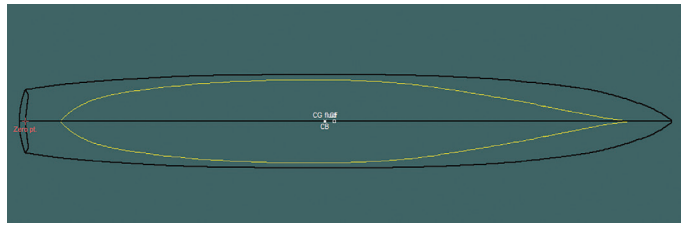

Figure 3. Waterplane area view of the DTMB 5512 when the ship is on the wave crest.

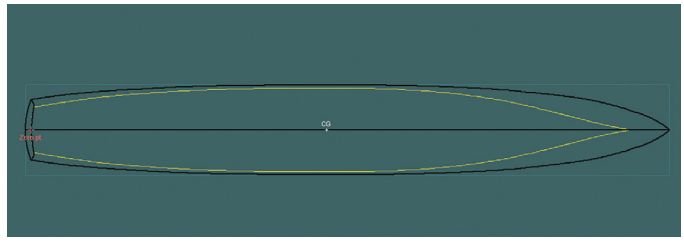

Figure 4. Waterplane area view of the DTMB 5512 when the ship is on the wave trough.

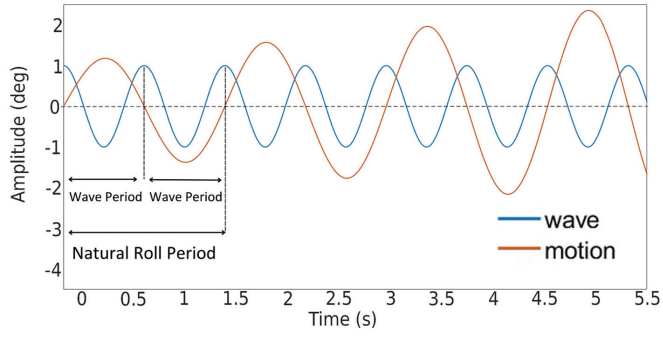

Figure 5. Sample wave profile (x-axis is time in seconds, y-axis is motion in degrees).

of parametric roll phenomena, influenced by the dynamic interplay between wave conditions and the ship's response.

According to Luthy [11], the following conditions are required for parametric roll to occur:

- Wavelength should be close to the length of the ship,
- *GM* value should be affected as much as possible by the interaction of the hull of the ship with the wave profile,
- Encounter frequency should be twice the natural roll frequency of the ship,
- Head or following seas,
- Insufficient damping.

3. The Method of Analysis

3.1. General Information About Analysis

The main parameters of DTMB 5512 (Iowa scale) is given in Table 1 [16].

In many studies, observing different *GM* values for DTMB 5512 is possible. The reason of the difference is caused by the baseline selection. In this study, Figure 6 is used as the baseline, representing the lowest point of the sonar dome.

The equation of roll motion can be found in various forms in the literature. As a basis, the Mathieu-type (the changing *GM* in time) in Equation 1 can be used if the ship is sailing in longitudinal seas and there is no wave roll moment:

$$\left(I_{44}+A_{44}\right)\ddot{\phi}+B_{44}\dot{\phi}+\Delta GM(t)\phi \;=\; 0 \tag{1}$$

Here B_{44} is the linear or linearized damping coefficient and $\Delta GM(t)\phi$ is the linear restoring moment. These linear terms can be used at the lower roll degrees, but parametric roll resonance reaches high roll degrees, and this formula can not be used in this situation. Also, the Mathieu equation can only indicate whether parametric rolling starts or not. At higher roll degrees, the solution goes to infinite. Therefore, the Mathieu equation is insufficient to find the final degree of parametric roll resonance. Therefore, a non-linear equation can be used to better express the dynamics at higher roll degrees. After introducing the non-linear terms, the Equation 2 becomes the following:

$$\left(I_{44}+A_{44}\right)\ddot{\phi}+B_{44L}\dot{\phi}+B_{44NL}\dot{\phi}^{3}+\Delta GZ(\phi,t) \;=\; 0 \tag{2}$$

Table 1. Ship data of DTMB 5512.

Symbol	Unit	Value
L_{PP}	m	3.048
L_{WL}	m	3.052
B_{WL}	m	0.409
C_B	-	0.506
T	m	0.132
Displacement force	N	843.66
KG	m	0.163
GM	m	0.043
$\lambda_w = L_{WL}$	m	3.052

3.2. Restoring Term

$$GZ(\phi,t) \;=\left[GM_m + GM_a cos(\omega_e \;\; t)\right] \left[a\phi^7 + b\phi^5 + c\phi^3 + d\phi\right] \tag{3}$$

The restoring term is expressed as Equation 3 [9]. As seen, *GZ* is a function that has different parameters. GM_{max} and GM_{min} are maximal and minimal instantaneous values of *GM* for several wave crest positions along the ship hull as stated in Belenky et al., [18].

$$GM_m \;=\; 0.5\left(GM_{max}+GM_{min}\right) \tag{4}$$

$$GM_a \;=\; 0.5\left(GM_{max}-GM_{min}\right) \tag{5}$$

Also, wave height is defined as follows :

$h_j \;=\; 0.01\,jL\,,\;$ where $j \;=\; 0,1,2,3\ldots9,10$

Table 2 shows GM_m and GM_a values for different wave heights calculated with the help of the Maxsurf Stability [19]. The wave heights listed in the Table 2 are 0.065 meters less than the actual values. This is because the baseline has been chosen as the reference point. The distance of 0.065 meters is the gap between the baseline and the orange line seen in Figure 6.

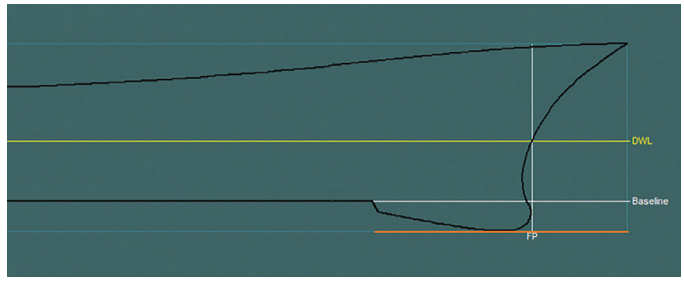

Figure 6. Baseline selection

Table 2. GM_m, GM_a and wave height values.

H (m)	0.024	0.048	0.072	0.096	0.120	0.144	0.168	0.192	0.216	0.240
GM_a (m)	0.0025	0.0050	0.0065	0.0085	0.0100	0.0120	0.0140	0.0155	0.0180	0.0185
GM_m(m)	0.0425	0.0420	0.0415	0.0425	0.0430	0.0440	0.0450	0.0465	0.0480	0.0485

To make it easier to express the *GM* changing with the position of the wave, the encounter frequency and time are used. An example result is shown in Figure 7. The curves in Figure 7, are calculated for DTMB 5512 and show an example cosine approximation for DTMB 5512.

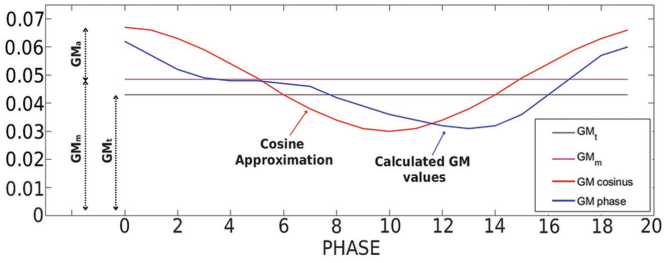

Figure 7. Cosine function of *GM* values.

To find a, b, c, and d coefficients, the *GZ* (Restoring moment arm) graph was obtained with the help of the Maxsurf Stability software. Then *GZ* values were divided by GM_T value. Using Matlab, a curve was fitted for GZ/GM_T values by the form in Equation 3. The fitted curve can be seen in Figure 8. The a, b, c, and d coefficients obtained as a result of curve fitting are as in Table 3.

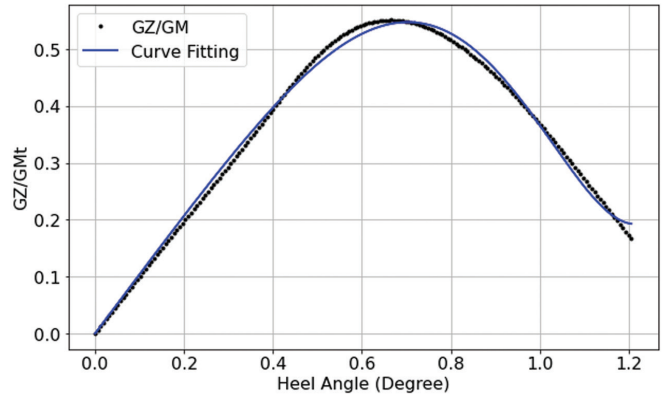

Figure 8. *GZ* curve fitting.

3.3. Mass Moment of Inertia and Hydrodynamic Added Inertia

As stated in Equation 6, a restoring term and model natural roll period are needed to find inertia and added inertia. The restoring term was calculated with the help of Equation 7. When the roll decay results of the model are examined, different natural roll periods are observed at various speeds and initial angles. The natural roll period was calculated at all speeds and initial angles. Table 4 shows a natural roll period with the average of these values was obtained.

Table 3. *GZ* coefficients.

Symbol	Value
a	0.4518
b	-0.9550
c	-0.1745
d	1.0440

$$T_\phi = 2\pi\sqrt{\frac{I_{44}+A_{44}}{C_{44}}} \tag{6}$$

$$C_{44} = \Delta\ GM \tag{7}$$

Table 4. Froude numbers, initial angles, and natural roll periods (s).

Fn	10 Degree	15 Degree	20 Degree	Mean
0.069	1.610	1.616	1.629	1.618
0.096	1.615	1.621	1.622	1.619
0.138	1.613	1.615	1.617	1.615
0.190	1.599	1.603	1.609	1.604
0.280	1.579	1.585	1.583	1.582
0.340	1.550	1.559	1.562	1.557
0.410	1.531	1.520	1.543	1.531
			Total mean:	1.590

The average inertia of the ship was found using the average natural period and restoring term.

$$I_{44} + A_{44} = 2.322\ \ kg\ m^2$$

3.4. Coefficients of Non-linear Representation of Roll Damping

Equation 8 is the general formula for the nonlinear damping coefficients. In this study, the B_2 term will be ignored since the quadratic damping coefficient will not be used. In the rest of the study, B_L stands for B_1 as it represents the linear coefficient of roll damping and B_{NL} stands for the B_3 as cubic coefficient of roll damping.

$$\Delta\phi = \frac{\pi}{2}\frac{\omega_\phi}{C_{44}}\phi_m\left[B_1 + \frac{8}{3\pi}\omega_\phi\phi_m B_2 + \frac{3}{4}\omega_\phi^2\phi_m^2 B_3\right] \tag{8}$$

To determine the damping coefficients, roll decay test data were analyzed across all speeds and initial angles of 10°, 15°, and 20°. Given the intention to incorporate coefficients of non-linear representation of roll damping in the study, Himeno's method [20] was employed. This method is suited explicitly for extracting non-linear damping characteristics from experimental data, ensuring accurate characterization of the ship's damping behavior during roll decay tests. In experimental data, as in Figure 9, the red points where the roll degree of the model peaks are determined. Using Equations 9 and 10, the difference between the peak points

and, after that, the averages of the peak points are calculated (Table 5).

$$\Delta\phi = \phi_{n-1} - \phi_n \tag{9}$$

$$\phi_m = \frac{\phi_{n-1} + \phi_n}{2} \tag{10}$$

After calculating ϕ_m and $\Delta\phi$ values, a curve fitting was performed using Matlab software. In Figure 10, the curve fitting using peak values can be seen. With the equation obtained with the curve, Equation 8 can be equated. This can be seen in Equation 11. The transformation in Equation 7 is used for the restoring term (C_{44}). With the modifications made to the Equation 11, and B_L, B_{NL} are obtained in Equation 12 and Equation 13.

The process in Figure 10 was performed for each speed and initial angle. Table 6 shows the values of k_1 and k_3.

$$k_1\phi_m + k_3\phi_m^3 = \frac{\pi}{2}\frac{\omega_\phi}{C_{44}}\phi_m B_L + \frac{\pi}{2}\frac{\omega_\phi}{C_{44}}\phi_m\frac{3}{4}\omega_\phi^2\phi_m^2 B_{NL} \tag{11}$$

$$B_L = \frac{\left(2\,k_1\,\Delta GM\right)}{\pi\omega_\phi} \tag{12}$$

$$B_{NL} = \frac{\left(8k_3\,\Delta GM\right)}{3\pi\omega_\phi^3} \tag{13}$$

The relation of the extinction coefficients can be seen in Equation 14 and 15. "a and c" are called the decay coefficients (obtained from free-roll test). In our equation, they correspond to k_1, k_3. With the help of this equation, the relation between ship speed and extinction coefficients can be seen in Table 7.

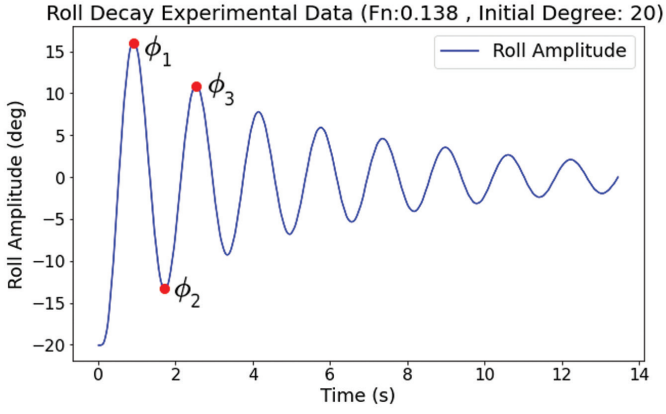

Figure 9. Roll decay curve.

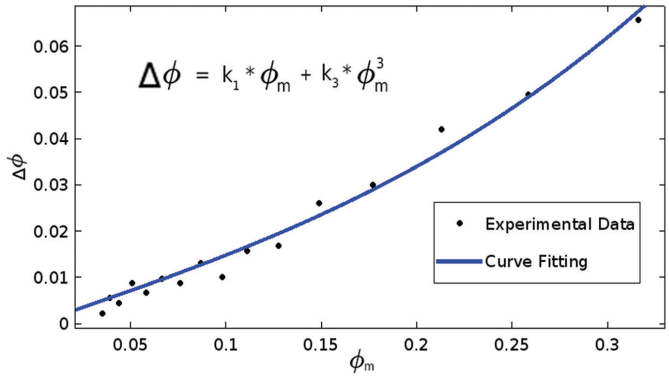

Figure 10. Curve fitting ϕ_m - $\Delta\phi$.

Table 5. An example of peaks determination (Fn: 0.138, initial degree: 20).

i	0	1	2	3	4	5	6	7	8	9	10
Degree	-20.000	16.243	-13.403	10.997	-9.276	7.781	-6.817	5.919	-5.342	4.591	-4.093
Radian	-0.349	0.283	-0.234	0.192	-0.162	0.136	-0.119	0.103	-0.093	0.080	-0.071
ϕ_m	0.316	0.259	0.213	0.177	0.149	0.127	0.111	0.098	0.087	0.076	0.067
$\Delta\phi$	0.066	0.050	0.042	0.030	0.026	0.017	0.016	0.010	0.013	0.009	0.010

Table 6. Froude numbers with k_1 and k_3, B_L and B_{NL} values.

	10 Degrees		15 Degrees		20 Degrees		Mean		Mean	
Fn	k_1	k_3	k_1	k_3	k_1	k_3	k_1	k_3	B_{NL}	B_L
0.069	0.0852	0.7934	0.0925	0.6461	0.0964	0.6273	0.0914	0.6889	0.3124	0.5172
0.096	0.0735	2.4241	0.0865	1.2270	0.0885	1.0079	0.0828	1.5530	0.7041	0.4689
0.138	0.1231	2.3301	0.1266	1.4163	0.1316	1.0453	0.1271	1.5972	0.7242	0.7195
0.190	0.1888	-0.1952	0.1821	0.6285	0.1814	0.6407	0.1841	0.3580	0.1623	1.0421
0.280	0.1912	2.8576	0.2042	1.3570	0.2220	0.4862	0.2058	1.5669	0.7104	1.1649
0.340	0.2178	2.8760	0.2292	1.4073	0.2403	0.8342	0.2291	1.7058	0.7734	1.2968
0.410	0.2980	0.4669	0.2926	0.9056	0.2971	0.4596	0.2959	0.6107	0.2769	1.6750

Table 7. Extinction coefficients.

Fn	γ	κ_a
0.069	470.5244	0.0582
0.096	1060.661	0.0527
0.138	1090.871	0.0809
0.190	244.5051	0.1172
0.280	1070.177	0.1310
0.340	1165.042	0.1458
0.410	417.0930	0.1884

The relationship between decay coefficients, coefficients of the non-linear representation of roll damping, and extinction coefficients can be examined in detail in the ITTC documents [21].

$$a = \frac{\pi}{2}\frac{2\alpha}{\omega_\phi} = \frac{\pi}{2}\kappa_a \tag{14}$$

$$c\left(\frac{180}{\pi}\right)^2 = \frac{3\pi}{8}\omega_\phi\gamma \tag{15}$$

After these calculations, a scatter plot was drawn with speed on the x-axis and linear (B_L) or non-linear (B_{NL}) damping coefficients on the y-axis. As can be seen in Figures 11 and 12, a 2nd order curve fitting was performed for the linear coefficient, while a 1st order curve fitting was performed for the non-linear damping coefficient. Thus, the relationship between the damping coefficients and the forward speed was revealed for DTMB 5512.

3.5. Numerical Analysis Background

Runge-Kutta method was used for numerical analysis. The code was written in Python language to perform the analysis. The algorithm can be seen in Figure 13. The inputs of the algorithm are as follows:

- Speed

Since the ship will be examined with the head and the following waves, therefore $\cos(\varphi_w) = 1$ or $\cos(\varphi_w) = -1$, respectively.

$$\omega_e = \omega - k\,V\cos(\varphi_w) \tag{16}$$

Equation 16 shows how the encounter frequency is calculated for the speed the ship has. φ_w refers to the angle of encounter. Therefore, in Table 8, $i \leq 12$ refers to following waves, while $i > 12$ refers to head waves. The speed coefficients in the table express the ratio with service speed. The service speed of the ship is assumed to be Fn= 0.41. With the help of Equation 17, the ship's service speed at Fn= 0.41 is equal to 2.2434 (m/s).

$$Fn = \frac{V}{\sqrt{g\,L}} \tag{17}$$

$$V_s = 2.2434\ m/s$$

- Wave height

Wave height as an input determines the values of GM_m and GM_a in the equation. More information on wave heights is in section 3.2.

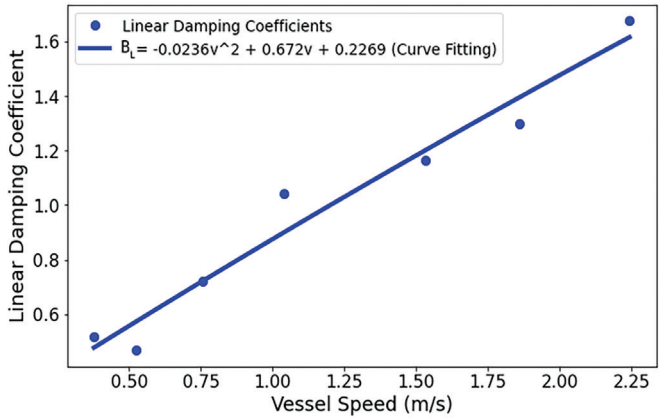

Figure 11. Linear coefficient - ship speed (m/s).

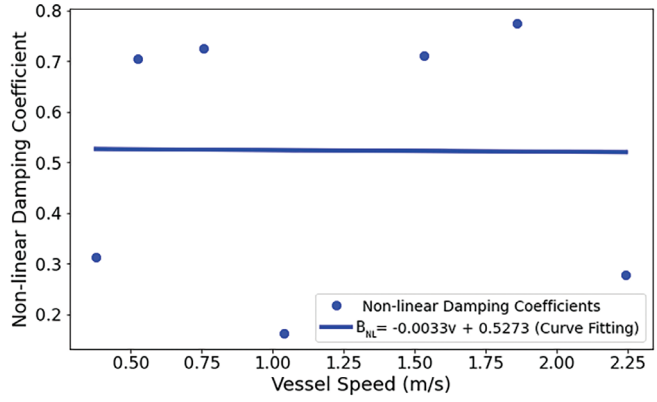

Figure 12. Non-linear coefficient - ship speed (m/s).

Table 8. Speed coefficients.

i	k_i	i	k_i
1	1.000	13	-1.000
2	0.991	14	-0.991
3	0.996	15	-0.996
4	0.924	16	-0.924
5	0.866	17	-0.866
6	0.793	18	-0.793
7	0.707	19	-0.707
8	0.609	20	-0.609
9	0.500	21	-0.500
10	0.383	22	-0.383
11	0.259	23	-0.259
12	0.131	24	-0.131

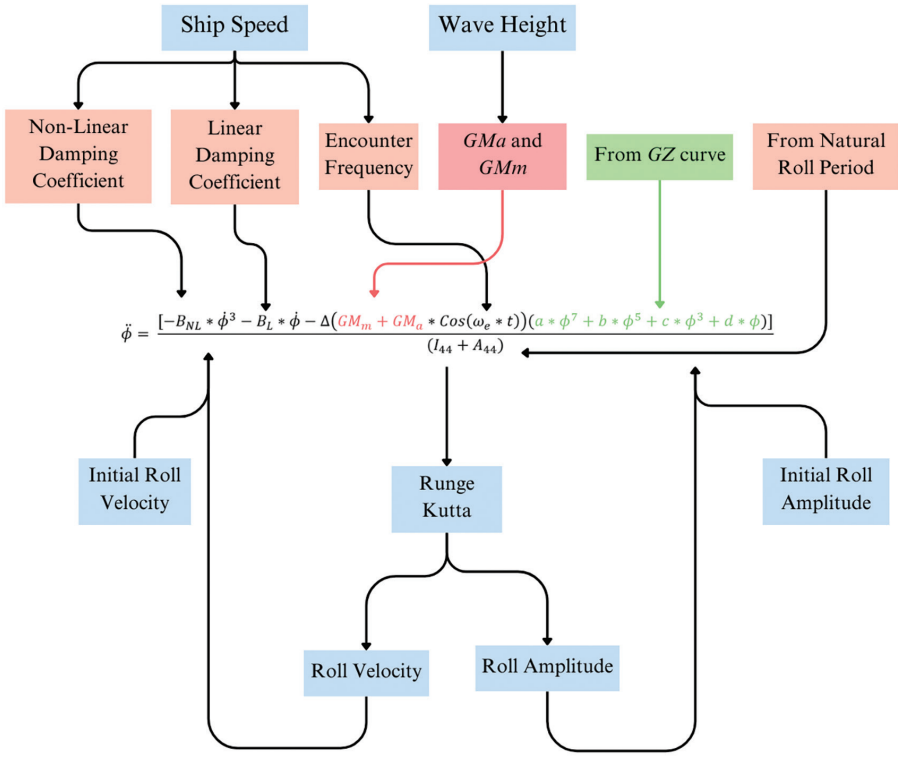

Figure 13. Algorithm of analysis.

- Initial roll amplitude and roll velocity

The initial roll angle and roll velocity for the analysis are as follows:

$\phi(0) = 0.0872\ rd\ (5\text{deg})$

$\dot{\phi}(0) = 0\ rd/s$

- Time

The time interval for numerical analysis was determined as 0.01 seconds.

- Runge-Kutta Method

In the numerical analysis, the 4th-order Runge-Kutta method was used to calculate the instantaneous roll angles and velocities.

4. Results and Discussion

4.1. Validation

The experimental results were compared with those derived from the Runge-Kutta method to assess the proximity of the calculated damping coefficients to experimental values [16]. The equation was structured to depict free-damped motion. The numerical analysis using the Runge-Kutta method was conducted for different initial roll angles and vessel speeds. Figures 14 to 21 show that the numerical results closely match the experimental data obtained under the same initial conditions. This agreement between experimental and numerical results shows that the coded Runge Kutta method gives reliable outcomes.

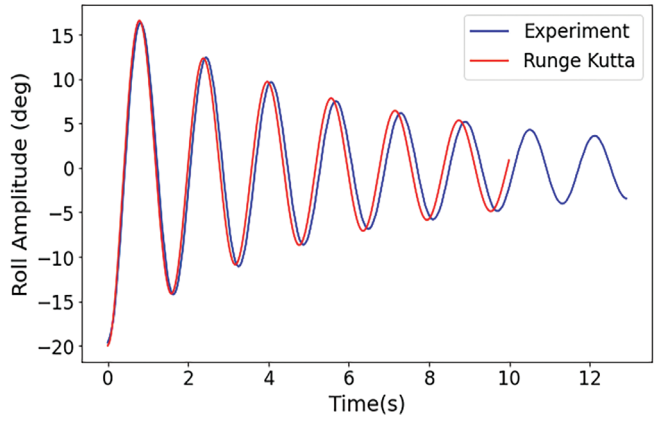

Figure 14. Roll amplitude at Fn=0.069 and initial roll angle=20.

4.2. Results

Table 9 on the subsequent pages displays the wave heights, ship speeds, encounter frequencies, and maximum roll angles (degrees). Additionally, motion graphs depicting these unstable states can be found in from Figure 21 to Figure 26. Please note that following figures show the head sea cases.

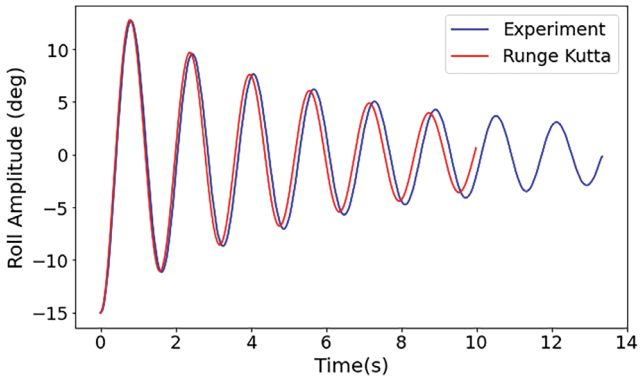

Figure 15. Roll amplitude at Fn=0.096 and initial roll angle=15.

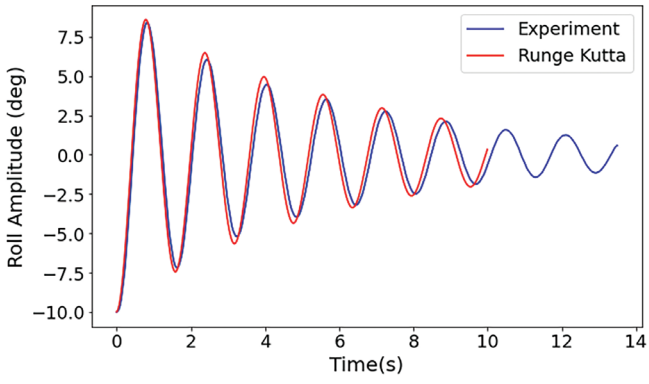

Figure 16. Roll amplitude at Fn=0.138 and initial roll angle=10.

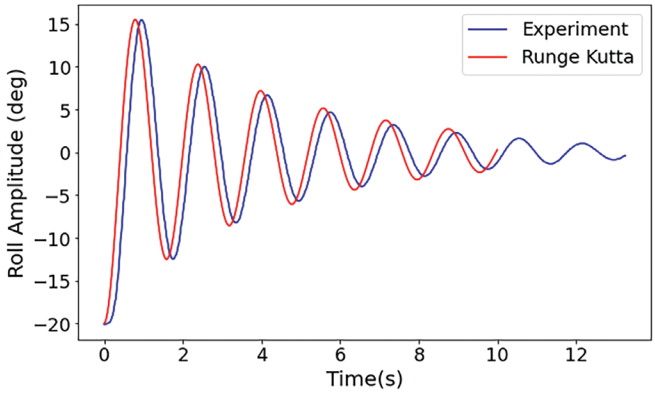

Figure 17. Roll amplitude at Fn=0.190 and initial roll angle=20.

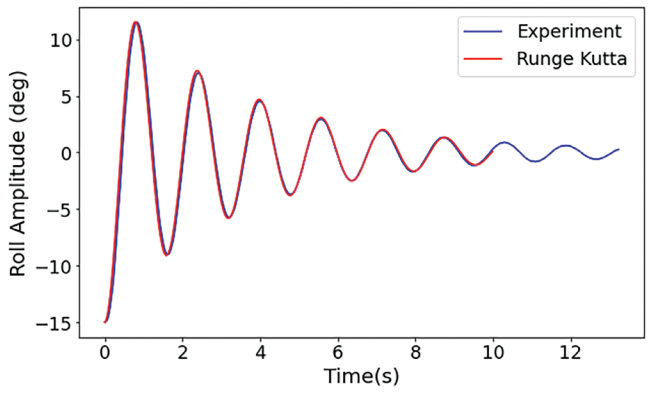

Figure 18. Roll amplitude at Fn=0.280 and initial roll angle=15.

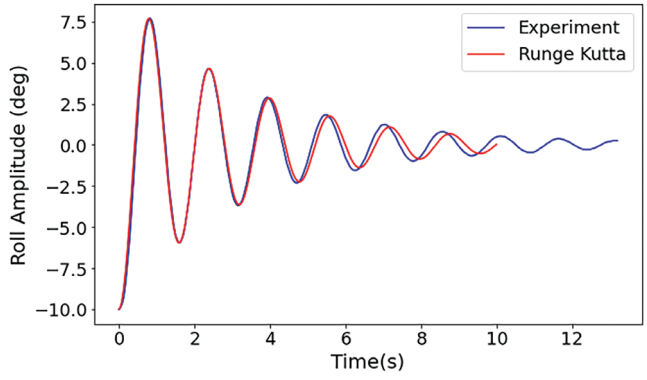

Figure 19. Roll amplitude at Fn=0.340 and initial roll angle=10.

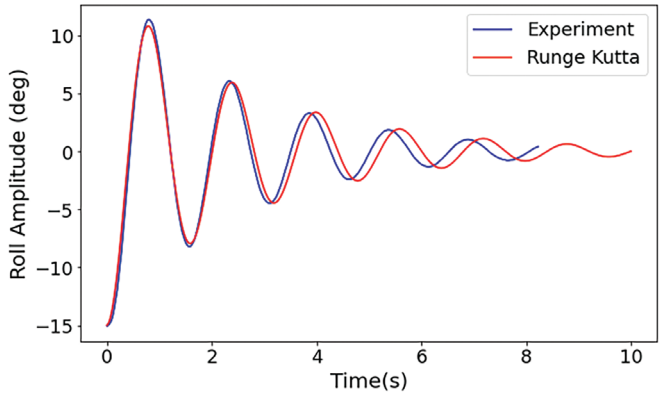

Figure 20. Roll amplitude at Fn=0.410 and initial roll angle=15.

Table 9. Maximum roll angle.

H (m) / Fn (-)	0.024	0.048	0.072	0.096	0.120	0.144	0.168	0.192	0.216	0.240	ω_e	ω_e / ω_Φ
0.054	5.00	5.00	5.00	4.99	4.99	4.99	4.99	4.99	4.99	4.99	3.89	0.865
0.106	5.00	5.00	5.00	4.99	4.99	4.99	4.99	4.99	4.99	4.99	3.30	0.734
0.157	5.00	5.00	5.00	4.99	4.99	4.99	4.99	4.99	4.99	4.99	2.73	0.606
0.205	5.00	5.00	5.00	4.99	4.99	4.99	4.99	4.99	4.99	4.99	2.18	0.486
0.250	5.00	5.00	5.00	4.99	4.99	4.99	4.99	4.99	4.99	4.99	1.68	0.374
0.290	5.00	5.00	5.00	4.99	4.99	4.99	4.99	4.99	4.99	4.99	1.23	0.273
0.325	5.00	5.00	5.00	4.99	4.99	4.99	4.99	4.99	4.99	4.99	0.83	0.185
0.355	5.00	5.00	5.00	4.99	4.99	4.99	4.99	4.99	4.99	4.99	0.49	0.110
0.379	5.00	5.00	5.00	4.99	4.99	4.99	4.99	4.99	4.99	4.99	0.23	0.050
0.396	5.00	5.00	5.00	4.99	4.99	4.99	4.99	4.99	4.99	4.99	0.03	0.007
0.406	5.00	5.00	5.00	4.99	4.99	4.99	4.99	4.99	4.99	4.99	-0.08	0.018
0.410	5.00	5.00	5.00	4.99	4.99	4.99	4.99	4.99	4.99	4.99	-0.12	0.028
0.054	5.00	5.00	5.00	4.99	4.99	4.99	5.09	5.11	5.21	5.21	5.10	1.135
0.106	5.00	5.00	5.00	4.99	5.01	5.18	5.33	5.37	5.51	5.52	5.69	1.266
0.157	5.00	5.00	5.00	4.99	5.03	5.27	5.50	5.59	5.80	5.82	6.26	1.394
0.205	5.00	5.00	5.00	4.99	4.99	5.09	5.38	5.57	5.88	5.93	6.80	1.514
0.250	5.00	5.00	5.00	4.99	4.99	4.99	4.99	5.21	5.60	5.67	7.31	1.626
0.290	5.00	5.00	5.00	4.99	4.99	4.99	4.99	5.16	5.82	5.92	7.76	1.727
0.325	5.00	5.00	5.00	4.99	4.99	4.99	6.96	9.67	13.47	13.49	8.16	1.815
0.355	5.00	5.00	5.00	4.99	4.99	4.99	4.99	6.75	13.68	14.45	8.49	1.890
0.379	5.00	5.00	5.00	4.99	4.99	4.99	4.99	4.99	8.63	10.70	8.76	1.950
0.396	5.00	5.00	5.00	4.99	4.99	4.99	4.99	4.99	4.99	4.99	8.96	1.993
0.406	5.00	5.00	5.00	4.99	4.99	4.99	4.99	4.99	4.99	4.99	9.07	2.018
0.410	5.00	5.00	5.00	4.99	4.99	4.99	4.99	4.99	4.99	4.99	9.11	2.028

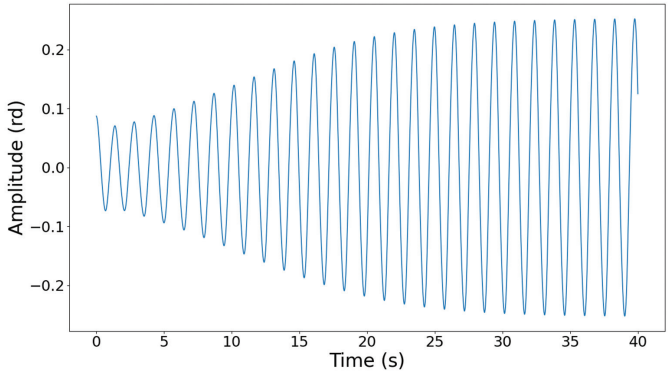

Figure 21. Speed: 1.943 m/s - wave height: 0.240 m.

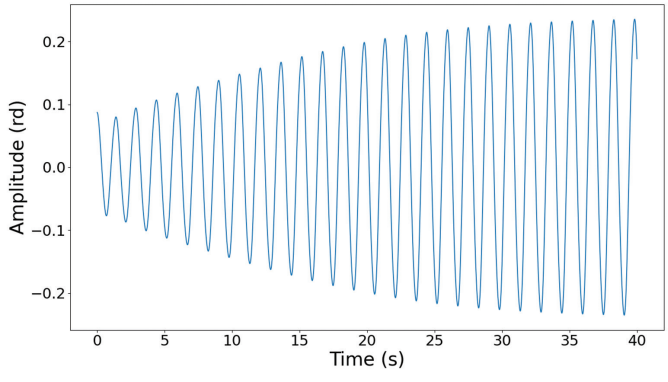

Figure 22. Speed: 1.7789 m/s - wave height: 0.240 m.

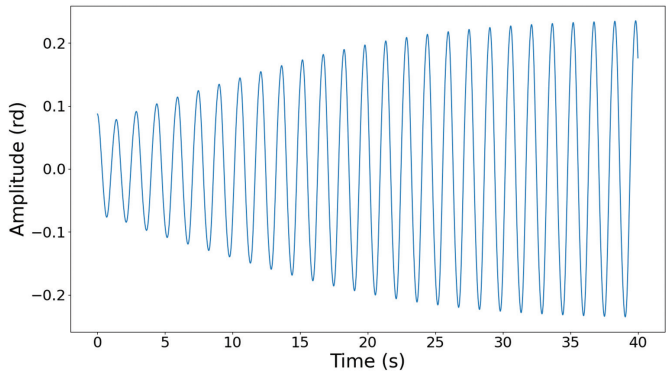

Figure 23. Speed: 1.7789 m/s - wave height: 0.216 m.

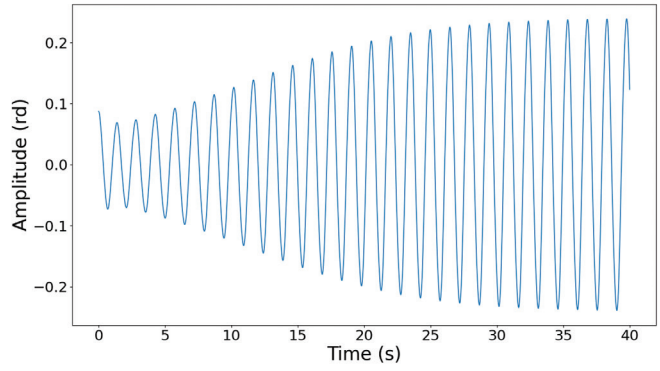

Figure 24. Speed: 1.943 m/s - wave height: 0.216 m.

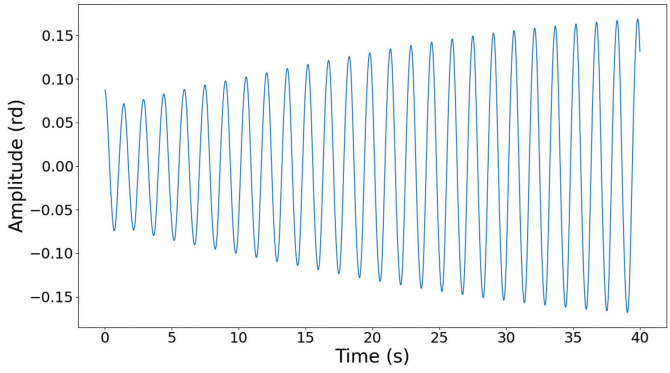

Figure 25. Speed: 1.7789 m/s - wave height: 0.192 m.

5. Conclusion

Parametric roll resonance significantly impacts the operational capabilities of naval combatants. Therefore, in the current study, an analysis of parametric roll resonance was conducted for the DTMB 5512 model. This analysis involved determining both linear and non-linear damping coefficients, as well as extinction coefficients. *GM* values for the restoring term were established based on varying wave heights, and coefficients of *GZ* were also calculated. Using the Runge-Kutta method for analysis, maximum roll angles were observed to reach approximately 14 degrees. Although this angle does not meet the IMO threshold of 25 degrees for considering parametric roll, it is crucial to recognize that such roll angles still pose significant risks and should be carefully evaluated.

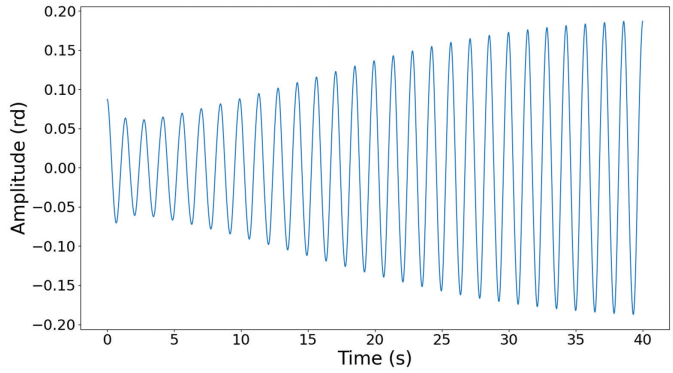

Figure 26. Speed: 2.0727 m/s - wave height: 0.240 m.

NOMENCLATURE

L_{PP} : Length between perpendiculars

L_{WL}: Length of waterline

B_{WL}: Maximum moulded breadth at design waterline

C_B: Block coefficient

T: Draught

KG: Centre of gravity above moulded base or keel

GM: Transverse metacentric height

λ_w: Wave length

Fn: Froude Number

ω_e: Encounter frequency

ω_ϕ : Natural roll frequency

Acknowledgements

This study is supported by project number 123M482 of the Scientific and Technological Research Council of Türkiye (Tübitak).

Footnotes

Authorship Contributions

Concept: F. Dündar, and F. Çakıcı., Design: F. Dündar, and F. Çakıcı., Data Collection or Processing: F. Dündar, and F. Çakıcı., Analysis or Interpretation: F. Dündar, and F. Çakıcı.,

Literature Search: F. Dündar, and F. Çakıcı., Writing: F. Dündar, and F. Çakıcı.

Conflict of Interest: No conflict of interest was declared by the authors.

Financial Disclosure: The authors declared that this study received no financial support.

6. References

[1] Y. Watanabe, "On the dynamic properties of the transverse instability of a ship due to pitching," *Journal of the Society of Naval Architects of Japan*, vol. 53, pp. 51-70, 1934.

[2] G. Kempf, "Die Stabilität Beanspruchung der Schiffe durch Wellen und Schwingungen," *Werft Reederei Hafen*, vol. 19, pp. 200-202, 1938.

[3] J. E. Kerwin, "Note on rolling in longitudinal waves," *International Shipbuilding Progress*, vol. 2, no. 16, pp. 597-614, 1955.

[4] J. R. Paulling and R. M. Rosenberg, "On unstable ship motions resulting from nonlinear coupling," *Journal of Ship Research*, vol. 3, pp. 36-46, 1959.

[5] J. R. Paulling, S. Kastner, and S. Schaffran, "*Experimental studies of capsizing of intact ships in heavy seas*," U.S. Coast Guard Technical Report (also IMO Doc. STAB/7), 1972.

[6] W. L. France, et al., "An investigation of head-sea parametric rolling and its influence on container lashing systems," *Marine Technology*, vol. 40, no. 1, 2003.

[7] G. Bulian, "Approximate analytical response curve for a parametrically excited highly nonlinear 1-DOF system with an application to ship roll motion prediction," *Nonlinear Analysis: Real-World Applications*, vol. 5, no. 4, pp. 725-748, 2004.

[8] N. Umeda, "Current status of second generation intact stability criteria," *Proceedings of the 13th International Ship Stability Workshop*, Brest, pp. 138-157, 2013.

[9] F. Cakici, "A numerical application of ship parametric roll under second generation stability criteria," *Journal of ETA Maritime Science*, vol. 7, no. 3, pp. 242-251, 2019.

[10] H. I. Çopuroğlu, E. Pesman, and M. Taylan, "Assessment of second-generation intact stability criteria and case study for a Ro-Ro ship," *Proceedings of the 19th International Ship Stability Workshop*, Istanbul, Turkiye, 9-11 Sept. 2023, pp. 315-320.

[11] V. Luthy, "Probability of occurrence of parametric roll on a predefined sea state," PhD thesis, HESAM, Paris, 2023.

[12] ClassNK, "Guidelines on preventive measures against parametric rolling (Edition 1.0)," ClassNK, 2023.

[13] ABS, "The assessment of parametric roll resonance in the design of container carriers," 2019.

[14] IMO, "Interim guidelines on the second generation intact stability criteria," International Maritime Organization, London, UK, 2020.

[15] M. Iqbal, et al., "Unsteady RANS CFD simulation on the parametric roll of small fishing boat under different loading conditions," *J. Marine. Sci. Appl.*, vol. 23, pp. 327-351, 2024.

[16] M. Irvine, J. Longo, and F. Stern, "Towing tank tests for surface combatant for free roll decay and coupled pitch and heave motions," in *Proceedings of the 25th ONR Symposium on Naval Hydrodynamics*, St Johns, Canada, 2004.

[17] International Towing Tank Conference (ITTC), "Estimation of roll damping," ITTC Recommended Procedures and Guidelines, 7.5-02-07-04.5, 2021.

[18] V. Belenky, C. Bassler, and K. Spyrou, "Development of second generation intact stability criteria," Hydromechanics Department Report, Naval Surface Warfare Center Carderock Division-50-TR-2011/065, 2011.

[19] Maxsurf Stability, "Windows Version 20 User Manual."

[20] Y. Himeno, "Prediction of ship roll damping: A state of the art," Report No. 239, Department of Naval Architecture and Marine Engineering, The University of Michigan, Ann Arbor, MI, 1981.

[21] International Towing Tank Conference (ITTC), "Numerical Estimation of Roll Damping," ITTC Recommended Procedures and Guidelines, 7.5-02-07-04.5, 2011.

RESEARCH ARTICLE

DOI: 10.54926/jnamt.2024.1476244

J Nav Architect Mar Technol 2024;226(2):12-24

Numerical Analysis of Ship Airwake on a Simplified Frigate Model

Tunahan Şık, Uğur Oral Ünal

Faculty of Naval Architecture and Ocean Engineering, İstanbul Technical University, İstanbul, Türkiye

To cite this article: T. Şık, and U. O. Ünal. Numerical analysis of ship airwake on a simplified frigate model. *J Nav Architect Mar Technol*. 2024;226(2):12-24.

Received: 02.06.2024 - **Revised:** 14.06.2024 - **Accepted:** 27.06.2024 - **Publication Date:** 31.01.2025

Abstract

Modelling ship airwake as well as ship air resistance calculation is of great importance in ships with flight deck. Especially with a flight deck at the stern, the airwake shaped by the superstructure aerodynamics generates a complex, asymmetrical and highly turbulent form in the helicopter operation area. Within the helicopter recovery and launch operations, the turbulent area makes pilot control difficult and can even cause loss of control. It is vital to accurately evaluate the turbulence occurring in the relevant region in order to increase operational efficiency, prevent possible accidents and reduce pilot workload. In this study, the effect of the flow regime in the flight deck airborne on a simple frigate shape has been examined with computational fluid dynamics using scale-resolving simulations. The results have been exhibited a remarkable agreement with the experimental data, and it has been agreed that the solution method could be a priority in ship airwake calculations.

Keywords: Ship aerodynamics, ship airwake, turbulence, computational fluid dynamics (CFD), scale-resolving simulations (SRS), simple frigate shape 2 (SFS2)

1. Introduction

In ship construction, aerodynamic design is often overlooked due to the relatively lower contribution of air resistance to the overall resistance of the vessel. While aerodynamic considerations are more critical for yachts, they are not typically prioritized for commercial and military ships. In modern military ship design, the superstructures are primarily shaped to minimize radar visibility, with less emphasis on aerodynamic efficiency. These enclosed, bluff-body designs significantly impact the ship's air resistance and have a considerable influence on the flow characteristics over the vessel.

In ships with helicopter decks, such as large naval ships, mega yachts, research ships, and drilling platforms; besides considering the air resistance, calculation of the airwake over the flight deck are of great importance. Particularly in ships with stern flight decks, the airflow, shaped by the superstructure, directly influences the flight operations by forming a complex turbulent wake over the deck.

The relative airflow over the flight deck created by the ship's own motion and the external wind flow, is the main factor driving the airwake formation. Additional elements, such as the thermodynamic effects of air temperature and exhaust gases, contribute to the complexity of the airwake. These bluff superstructures, along with various systems and equipment mounted on them (such as antennas, radars, funnels, and weapon systems), further complicate the already asymmetric flow regime. This turbulent environment, characterized by various multi-directional vortices, causes sudden pressure differences at both low and high frequencies, which result in a significant increase in the pilot's workload. Especially within the ratchet frequency range of 2-3 Hz, helicopter control

Address for Correspondence: Tunahan Şık, Faculty of Naval Architecture and Ocean Engineering, İstanbul Technical University, İstanbul, Türkiye
E-mail: sikt21@itu.edu.tr
ORCID ID: orcid.org/0009-0008-7752-2583

becomes difficult [1]. In bad weather and sea conditions, these situations can even lead to crashes. Given the high intensity of flight operations on naval ships and the importance of manoeuvre efficiency and time, it is extremely important to include airwake calculations during the design phase and implement related aerodynamic structural improvements.

Given the presence of high vortices and turbulence over a simple ship form, the resulting airwake becomes complex, and each ship exhibits distinct flow characteristics, making airwake interpretation a challenging task. To date, the interpretation of airwake has been conducted using in situ measurements taken on ships, low-speed wind tunnel experiments, and flow-resolving simulations.

In-situ tests, also known as sea trials, began in the mid-1950s, but due to operational costs, time-consuming processes, and military secrecy, they are rarely mentioned in the literature. Instead, tests verified by wind tunnel experiments have been more common.

In the early 1960s, wind tunnels started to be used alongside the first computational fluid dynamics (CFD) simulations introduced by Mahaffey et al. [2]. It is known that CFD studies verified with experimental data are more practical during the early design stages of a ship. As computational capacity and code capabilities have improved, CFD has become a crucial component for ship-helicopter dynamic interface (SHDI) calculations.

Notable ship forms frequently used in the literature include the Canadian Patrol Frigate (CPF), the UK's Duke-class Type 23 frigate (T23), the simple frigate shape (SFS1) and revised SFS1 (SFS2).

Zan et al. [3], and Zan [4,5] worked on airwake analysis for CPF using both low-speed wind tunnel experiments and CFD at the National Research Council of Canada (NRC) Aerodynamics Laboratory. The numerical results were consistent with the experimental results from the simplified CPF model, providing valuable insights into airwake calculations. Later, Syms [6] conducted time-independent CFD simulations (Reynolds-Averaged Navier-Stokes, RANS) for various wind angles. When compared with experimental results, RANS successfully captured the main flow characteristics but exhibited higher gradients. Similarly, Yuan et al. [7,8] compared their CFD studies using delayed detached-eddy simulation (DDES) models in OpenFOAM with experimental data from CPF, demonstrating the effectiveness of the code in simulating unsteady airflows over ships. Furthermore, to include ship motion, Yuan et al. [9] placed the CPF model on a multi-degree of freedom system in a wind tunnel. They found that OpenFOAM was able to solve the airflows, which became more unstable with ship movements.

In NATO workshops, as part of The Technical Cooperation Program, Cheney and Zan [10] introduced the SFS1 geometry and carried out CFD studies alongside wind tunnel experiments at the NRC. Subsequently, Reddy et al. [11] shared their RANS simulations on SFS1, demonstrating the consistency of the results with experimental data. They observed that vortices dominated the flow field in the region of interest and noted differences in the position of the reattachment point. Similarly, Wakefield et al. [12] developed a CFD model for the combination of a helicopter rotor and SFS1, commenting that the induced velocity gradients around the rotor increased the force required to keep the helicopter in a specific position. Experimentally, Bardera-Mora [13] conducted tests on SFS1 using laser Doppler anemometry (LDA) and particle image velocimetry (PIV) at the National Institute of Aerospace Technology in Spain. They observed a horseshoe-shaped vortex structure forming in front of the hangar. Lindon and Thornber [14] used SFS1 to propose a method for quantifying uncertainties due to rounding and truncation errors caused by the finite-difference approach in CFD. To ensure statistical accuracy in simulation time, they developed a formula for a stopping criterion based on pre-defined requirements. Additionally, Zamiri and Chung [15] conducted a DDES-based study on SFS1, applying flow from seven different wind angles. They reported that as the wind angle increased, the turbulence kinetic energy over the ship increased, and the flow field became more asymmetric.

The first study to compare SFS1 and SFS2 was conducted by Syms [16]. He used the experimental results provided by NRC to validate his study and compared the bodies using the Lattice-Boltzmann flow solver in the PowerFLOW code. The results demonstrated that the Lattice-Boltzmann method could accurately capture the flow topology. He pointed out that SFS2 has more realistic results with its bow shape than SFS1 because it represents a closer geometry to a frigate. There after many studies have focused on the SFS2 body instead of SFS1.

Zhang et al. [17] performed time-dependent simulations on SFS2 using the Cobalt solver with Euler formulation. They also used the NRC data for CFD validation. The computed data showed acceptable agreement with experimental data. Again based on the NRC data, Forrest and Owen [18] conducted a comprehensive study on SFS2 using DDES, examining a simplified T23 frigate model under various wind angles. They observed that DDES could model large-scale turbulent structures in a remarkable manner. Forrest et al. [19,20] further explored the effects of modifications to the vertical hangar edge on airwake characteristics using DDES with ANSYS-Fluent, noting that two out of five modifications provided beneficial effects while the other

three increased the pilot workload. Similarly, Kääriä et al. [21] applied six different modifications to the superstructure corner of a Simple Research Frigate model and tested them in a wind tunnel. Their study showed that the modifications directly impacted the airwake region and that certain modifications reduced turbulence intensity in the helicopter manoeuvring area. For further detailed information on the history of airwake calculations and their analysis, it is worth reviewing the study of Shukla et al. [22]. Turbulence models and simulations commonly used in airwake studies include RANS, unsteady RANS (URANS), scale-adaptive simulation (SAS), detached-eddy simulation (DES), and delayed DDES. Shukla et al. [23] performed CFD analysis using the scale-adaptive simulation (SAS) turbulence model on SFS2, comparing the results with NRC data. Subsequently, they conducted a wind tunnel test, comparing URANS, SAS, and DES models [24,25]. They concluded that DES and SAS closely matched experimental data, with SAS offering solutions for large-scale turbulent structures at lower computational costs.

In consideration of this information, accurately assessing turbulence in the region of interest is essential for improving operational efficiency, reducing pilot workload, and preventing potential accidents and damage. Accordingly, this study focuses on calculating the ship airwake, which represents the initial step in ship-helicopter interaction studies, and aims to establish a foundation for airwake calculations using CFD.

Based on previous research, it has been concluded that scale-resolving simulations (SRS) offer an effective approach to resolving the turbulent structures generated by bluff bodies, such as ship superstructures, which induce significant flow separations. Though, a review of the literature reveals that the critical computational steps necessary for accurately capturing flow structures, particularly turbulence intensity, using different SRS techniques have not been clearly defined. Thus, this study aims to present a comprehensive computational strategy for effectively and reliably conducting ship airwake simulations using advanced SRS methods.

In addition to the commonly employed SRS models, this study incorporates the stress-blended eddy simulation (SBES) model, which has been introduced in recent studies but has not yet been applied to ship airwake calculations. By comparing the computational results with experimental data available in the literature, this study demonstrates the predictive capabilities of these methods for complex separated flows characterized by high levels of vorticity and turbulence. It serves as a roadmap for researchers interested in advancing this field.

2. Scale-Resolving Simulations

Principally, RANS equations can undoubtedly be solved in a time-dependent manner (URANS). However, classic turbulence models, while sufficient for time-step resolution, are insufficient to accurately predict high-vorticity and turbulence levels in complex flows where significant flow separation occurs. SRS, which have been developed to address this deficiency, offer results closer to experimental data.

Commonly used SRS techniques such as large eddy simulation (LES), DES, DDES, and SAS have been further developed over time. These have been followed by improved DDES (IDDES), shielded DES (SDES), and more recently, SBES.

Among these, LES is considered the most effective alternative to direct numerical simulation (DNS) for solving vortex dynamics. Due to its wide applicability and high accuracy, LES is often preferred for industrial applications. However, LES solutions require very small time steps and highly refined mesh grids, significantly increasing computational time and cost. Recent studies have focused on finding more practical and efficient solutions to this phenomenon.

Menter and Egorov [26], Egorov et al. [27] introduced the SAS concept by including the von Kármán length scale in the RANS turbulence equations. The von Kármán length scale enables SAS to dynamically adjust to the unsteady regions of the flow, behaving like LES in regions of high instability. In stable regions, it behaves like standard RANS models, providing a broad range of turbulence solutions for certain types of unsteady flows. The two-equation formulation for SAS, where "L_{vK}" represents the von Kármán length scale, is shown below:

$$\frac{\partial(\rho k)}{\partial t}+\frac{\partial(\rho \bar{U}_j k)}{\partial x_j}=P_k-c_\mu^{3/4}\rho\frac{k}{\Phi^2}+\frac{\partial}{\partial x_j}\left(\frac{\mu_t}{\sigma_k}\frac{\partial k}{\partial x_j}\right) \tag{1}$$

$$\begin{aligned}\frac{\partial(\rho\Phi)}{\partial t}+\frac{\partial(\rho \bar{U}_j \Phi)}{\partial x_j}=&\frac{\Phi}{k}P_k\left(\zeta_1-\zeta_2\left(\frac{L_t}{L_{vK}}\right)^2\right)\\&-\zeta_3\rho k+\frac{\partial}{\partial x_j}\left(\frac{\mu_t}{\sigma_\Phi}\frac{\partial\Phi}{\partial x_j}\right)\end{aligned} \tag{2}$$

In contrast to SAS, a family of hybrid simulation models has been developed, directly benefiting from LES while maintaining RANS efficiency. These simulations, which transition between RANS and LES, include models like DES, DDES, IDDES, SDES, and SBES. Hybrid models are powerful formulations for resolving turbulence in unstable regions, such as those found in flight envelopes. While

applying a standard RANS model in these regions can result in single-frequency vortex formation, hybrid models allow large structures to be broken down into smaller scales. Additionally, they can model smaller vortices near the boundary layers while preventing excessive resolution requirements, allowing RANS solutions in boundary layers.

The first hybrid simulation, DES, developed by Spalart et al. [28], and Spalart [29], enabled a transition between RANS and LES. In this formulation, boundary layers near walls are fully modelled by RANS, while free flows away from the walls are modelled by LES. This relatively simple mathematical formulation can be built on top of any existing RANS turbulence model. DES has garnered significant interest by turbulence communities as the first and highly effective SRS method.

Following the proposal by Menter and Kuntz [30] to protect boundary layer separation near walls, Spalart et al. [31] further developed DES into the DDES. The formulation for DDES includes a protection function that equals "1" inside the boundary layer and "0" outside of it:

$$E_{DES} = \rho \frac{k^{3/2}}{L_t} \max\left(1; \frac{L_t}{C_{DES}\Delta}\right) \longrightarrow$$
$$E_{DDES} = \rho \frac{k^{3/2}}{L_t} \max\left(1; \frac{L_t}{C_{DES}\Delta}\left(1 - F_{DDES}\right)\right) \quad (3)$$

As it became clear that preserving boundary layer solutions near walls led to more effective results in CFD applications, DDES evolved further into the SDES and eventually into SBES, developed by Menter [32]. In SBES, unlike previous models, the protection function is adjusted based on the stress level:

$$\tau_{ij} = \tau_{ij}^{RANS} f_s + \tau_{ij}^{LES}\left(1 - f_s\right) \quad (4)$$

$$\mu_t = \mu_t^{RANS} f_s + \mu_t^{LES}\left(1 - f_s\right) \quad (5)$$

SBES is believed to provide stronger protection of the boundary layer compared to DES/DDES, allowing for a faster transition between RANS and LES models.

The following points stand out regarding the use of SRS models in [32,33]:

1. SAS is considered the most reliable SRS method when dealing with coarse grids where the mesh resolution required for LES cannot be achieved.

2. In cases where SAS is insufficient, increasing the grid resolution and applying DDES provides better results.

3. SBES can be used more broadly for a variety of complex problems.

4. The Courant-Friedrichs-Lewy (CFL) number should be kept around "1" or below for all SRS methods.

3. Computational Study

The validation of the computational analyses was based on the low-speed wind tunnel experimental data of the NRC by Lee [34] in 2007. The experiments examined the effect of the flow regime on the helicopter deck of the commonly used ship geometry, the SFS2 (Figure 1).

The test section of the tunnel has dimensions of 1.9 m × 2.7 m × 5.2 m, with a turbulence intensity of 0.14%. To ensure accuracy in the computational solution, the SFS2 geometry and the flow field were modelled at a 1:100 scale, identical to the experimental setup, and matched to the dimensions of the wind tunnel as seen in Figure 2. Two different wind angles were analysed, one from the bow (0°) and one at 45° from the starboard side, as in the experiment.

The DDES model, commonly used in airwake studies, has shown close agreement with experimental data in prior researches. While there have been limited applications of

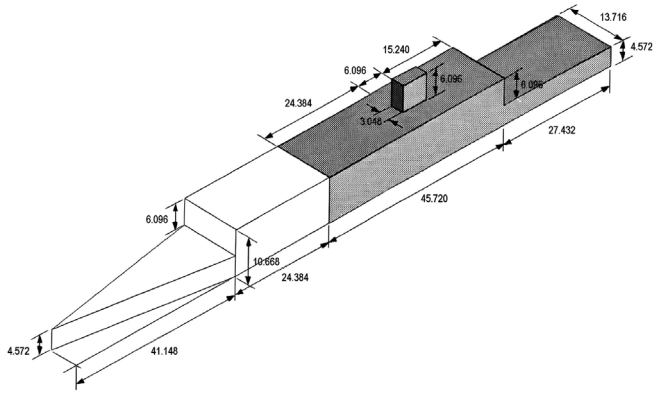

Figure 1. SFS2 Model (Dimensions are in meters; the shaded section represents SFS1) [5].

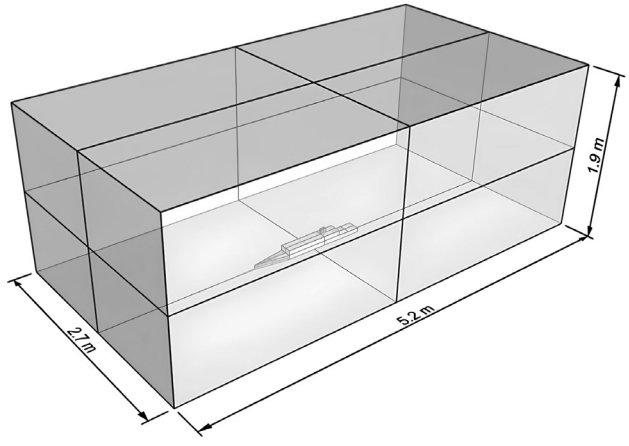

Figure 2. 1:100 scale SFS2 model geometry located in the middle bottom of the flow field.

URANS and SAS, SBES has not yet been used in any ship airwake study. It is known that geometries causing high levels of flow separation, such as the transition between the hangar and helicopter deck, lead to rapid transitions to turbulence from the boundary layer. Therefore, considering the previously mentioned SRS models, it was determined that using SBES, which transitions rapidly between RANS and LES, would be meaningful.

In this survey, a comparison of the URANS, SAS, DDES, and SBES simulation techniques was conducted to establish a baseline for airwake calculations using CFD.

3.1. Mesh and Boundary Layer Approach

A method based on "cutcell", which reduces the cells in size by powers of two, was used for the mesh generation. The mesh structure was refined around the region of interest (the helicopter operation area) where the airwake was examined, as seen in Figure 3, as well as around the funnel where turbulence was expected to increase. A smooth transition was ensured between the hexagonal cells used on the surfaces and the cubic cells used in the flow field. Since cubic and hexagonal cells were used, the aspect ratio was approximately 1:1 in 90% of the total mesh, and below 20 for the rest.

The number of cells required in the boundary layer depends on the type of flow and the accuracy required. In high-Reynolds-number flows, such as in aerospace studies, where high accuracy is needed, the number of cells in the boundary layer perpendicular to the wall is typically around 40-50. However, in many industrial applications, 10 cells are considered sufficient.

Additionally, there are many flow problems where reasonable solutions can be achieved with fewer cells, often only 3-5 layers. The common feature of these problems is that the main flow phenomenon occurs outside the boundary layer due to flow separation. Yuan et al. [8] highlighted that, in airwake studies, the flow is primarily driven by inertial forces, and separation points are more influenced by sharp edges and corners than by boundary layer separation. Accordingly, it was determined that it was not necessary to fully resolve the boundary layer with RANS calculations in this study.

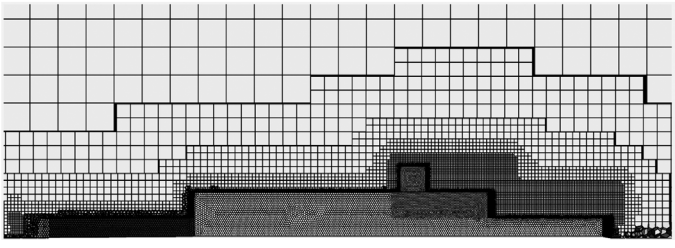

Figure 3. 1:100 scale SFS2 model geometry located in the middle bottom of the flow field.

Therefore, it was concluded that a detailed boundary layer solution over the ship's geometry with discontinuities was unnecessary. However, the CFL number needed to be kept close to 1, especially in target regions. Spectral analysis and detailed problem resolution require both small time steps and high mesh resolution in regions where LES is applied. Thus, the cell aspect ratio was kept close to 1 both inside and outside the boundary layer, and 3 boundary sublayers were used in the direction normal to the wall. For each solution, the y^+ value was kept around 50. Additional studies confirmed that maintaining a y^+ value of 1 did not significantly alter the results for this problem.

3.2. Initial, Boundary Conditions and Timing

At the inlet boundary, a flow speed of 60 m/s was specified for the 0° wind angle and 50 m/s for the 45° wind angle. The turbulence intensity was set to 0.14%, and the turbulence length scale was defined as 4.3b (b, ship's width) according to the reference experimental study. No-slip wall condition was applied for the lateral boundaries, and atmospheric pressure was specified at the outlet boundary.

In the experimental study [34], data were collected at a frequency of 2 kHz. Not to exceed the equivalent time step size (5×10^{-4}) and to keep the CFL number below 1 in the region of interest, the time step sizes for the study used are 1.3×10^{-4}, 1×10^{-4}, 7×10^{-5} s respectively for the meshes A, B and C.

Before the time-dependent solution was initiated, a steady-state solution was performed to achieve early convergence. The results of the steady-state simulation were used as initial conditions for the time-dependent simulation. In terms of pressure-velocity coupling, the equations were solved in the "Coupled" method for the first ~10 time steps, then the "SIMPLE" method was applied in continuation. It was observed that 10 iterations per time step were sufficient. The data acquisition was started after the solutions reached iterative stability at about 5×10^{-2} s, therefore the earlier data was disregarded.

3.3. Data Acquisition

In the experimental wind tunnel test, each measurement lasted for 16.4 s. In this study, the simulation time was extended beyond this duration, with at least 20 s of measurement for each solution. The acquired data were used for the power spectral density (PSD) calculations through Fourier transformation.

Measurements were taken over the flight deck, with data points placed at the "hover" position above the hangar edge, where a helicopter would be during launch or recovery operations. To observe the pressure and velocity distributions, four planes were positioned starting from the ship's stern and extending toward the bow at intervals of one-quarter of

the platform length (L_p) and having a width of 2 times ship beam. These planes were aligned along the ship's centreline from their mid-section and were positioned at a height along the hangar halfway, with a total height equal to 75% of the hangar height (h). The planes were named "0% L_p, 25% L_p, 50% L_p and 75% L_p" respectively towards the bow. Linear data measurements made at the level of the hangar upper edge line on the planes are expressed such as "25% L_p line".

Spectral velocity measurements were acquired from two locations: for the 0° wind angle, from the point which is located at h/4 height from the bottom line of 50% L_p plane, 2b/5 to the starboard side from the centreline and for the 45° wind angle from the point on 25% L_p. Those were named "50% L_p spectrum point" and "25% L_p spectrum point," respectively.

The formula used to calculate turbulence intensity is shown below, where "k" represents turbulence kinetic energy, "U_∞" is the free-stream velocity, and "u', v', w'" represent the Reynolds decomposition components:

$$I(\%) = \frac{100}{U_\infty}\sqrt{\frac{2}{3}k} \tag{6}$$

$$k = \frac{1}{2}((\overline{u'})^2 + (\overline{v'})^2 + (\overline{w'})^2) \tag{7}$$

3.4. Mesh Independence Analysis

The mesh independence study was conducted using the SBES method. Three different mesh densities were used: coarse, medium, and fine, named Grid A, Grid B, and Grid C, respectively. The cell sizes in the region of interest were refined in this order for LES computations, while they were kept constant for outer cells. The smallest cube-shaped cell edge dimensions (Δ_0), which are normalized by the hangar height (h) and reduced in multiples of $\sqrt[3]{2}$, and the total number of cells are presented in Table 1.

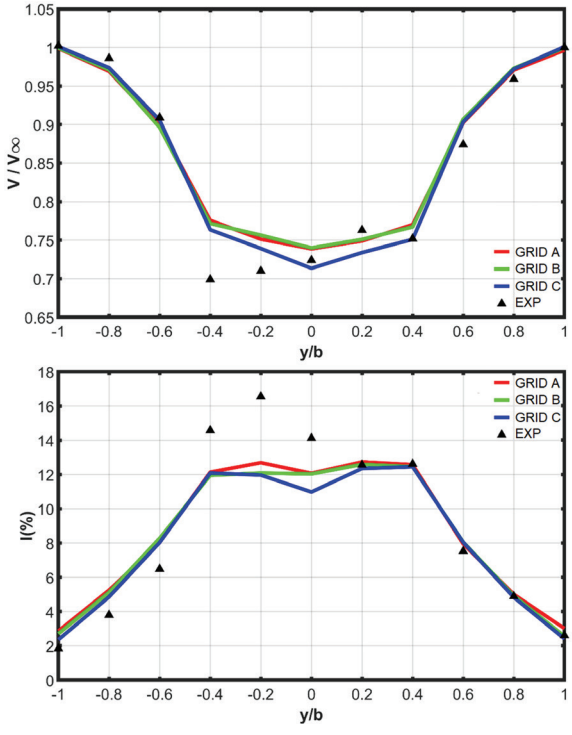

Figure 4. Comparison of mean velocity magnitude (up) and turbulence intensity distribution along the 50% L_p line for the grids.

The results of the simulations in 1 s of duration were considered sufficient for the mesh independence analysis since the solutions had been observed to stabilize after 50 ms. Figure 4 shows the mean velocity magnitude and mean turbulence intensity distributions. The experimental results [34] are labelled as "EXP" in the figure and the comparisons are also presented in Table 1. The relative error values in the table were calculated individually for each point by comparing the computed results with the corresponding experimental data, then the mean error values were taken.

Although both Grid A and Grid B produced nearly identical results for velocity magnitude, Grid C yielded slightly more accurate results. As expected, finer grids provided better results for turbulence intensity. However, given that the total number of cells in Grid C was four times that of Grid B, the ~1% difference in relative error was considered negligible in terms of time and computational efficiency. Therefore, the simulations were continued using Grid B.

4. Results and Discussion

The comparison for the 0° case also included a study conducted by Forrest and Owen [18] at the University of Liverpool using the DDES method, labelled as "LIV". The experimental results [34] are labelled as "EXP". The x-axis denoteas the non-dimensionalized lateral position normalized by the ship's beam in the graphs representing the mean velocity magnitude and turbulence intensity across the section. Both the velocity and turbulence intensity values were non-dimensionalized by the free-stream velocity.

Table 1. Comparison of the grid characteristics and relative error for velocity magnitude and turbulence intensity.

	Grid A	Grid B	Grid C
Δ_0/h (x 10^{-2})	7.2	5.7	4.6
Total cell count (x 10^6)	0.36	0.40	1.3
Relative error in velocity magnitude (%)	2.8	2.8	2.3
Relative error in turbulence intensity (%)	18.0	16.4	15.0

4.1. Comparative Performance Assessments of the Simulations

Table 2 presents the relative error values for velocity magnitude and turbulence intensity distributions seen in Figure 5. These errors were calculated individually for each point by comparing the simulation results with the corresponding experimental data, and the average error for each method was reported.

As shown in Table 2, the URANS method produced the poorest results, particularly for turbulence intensity. While SAS performed relatively better in predicting velocity magnitude, its performance in predicting turbulence intensity was inferior to that of DDES and SBES. Although the results from SAS, DDES, and SBES were relatively close to each other, they significantly outperformed the LIV results in terms of turbulence intensity. Considering the turbulence intensity that forms the basis of ship airwake studies, DDES and SBES have produced results that are closer to experimental data compared to SAS. For velocity magnitude, DDES and SBES yielded nearly identical results. Only minor differences were observed in turbulence intensity predictions of these simulations.

Given the importance of PSD distribution in flight envelope calculations, it is essential to compare the performance of DDES and SBES in spectral analyses. Figure 6 shows the spectral density distributions obtained using Fourier transformation, where the frequency and amplitude are presented on a logarithmic scale. In the spectral analysis, the longitudinal PSD values were closer to the experimental results compared to the lateral PSD values. At low frequencies, the differences between the simulation methods were negligible. However, at higher frequencies, SBES produced results closer to the experimental data. In the longitudinal spectrum, SBES showed a closer match to the experimental data at low frequencies, while following similar pattern at high frequencies, consistent with the lateral spectrum. Although DDES and SBES produced similar results for velocity magnitude and turbulence intensity, their differences become more pronounced in the spectral

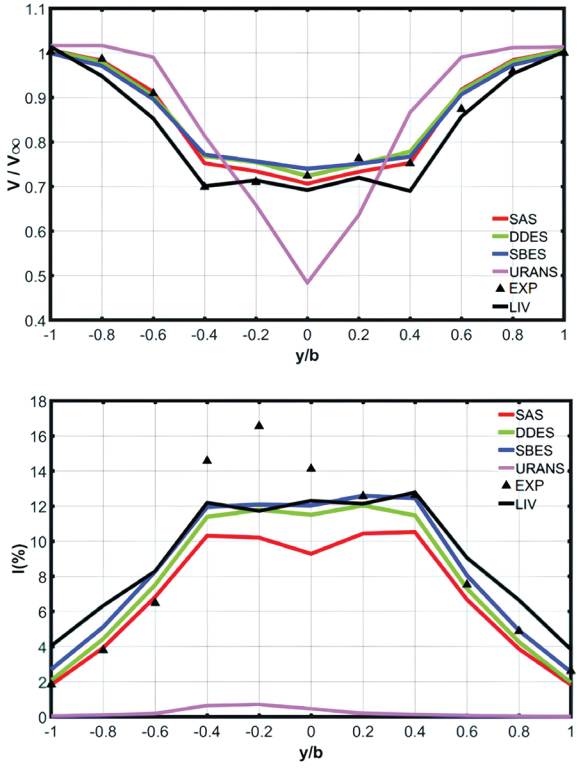

Figure 5. Comparison of mean velocity magnitude (up) and turbulence intensity distribution across the 50% L_p line.

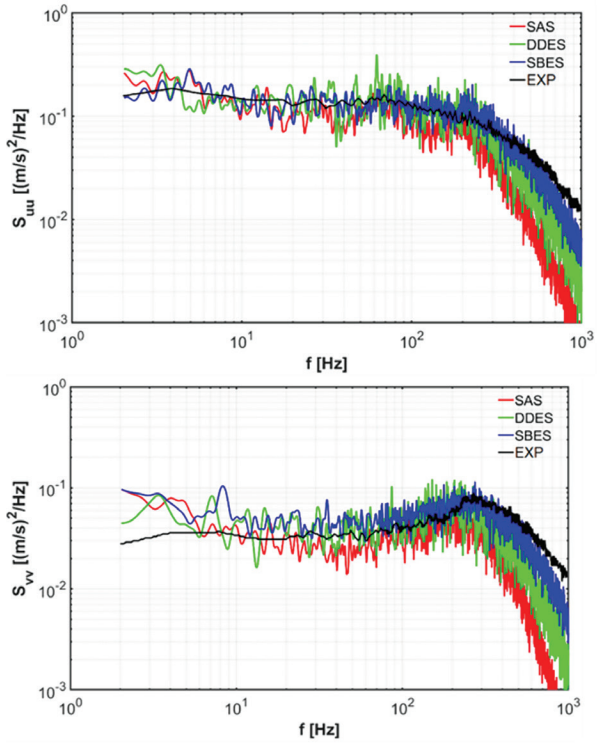

Figure 6. Comparison of longitudinal (up) and lateral PSD on the 50% L_p spectrum point for 0°.

Table 2. Comparison of relative errors in velocity and turbulence intensity.

Relative error (%)	LIV	URANS	SAS	DDES	SBES
Velocity Magnitude	3.0	11.1	2.4	2.8	2.8
Turbulence Intensity	34.7	97.6	18.8	15.1	16.4

analysis. As expected, SBES provided the most accurate results; therefore, the simulations were continued using this method.

Figure 7 illustrates the vortex structures using the Q-criterion [35] at the end of the first second of the solution. The SBES method provided a more detailed and comprehensive solution in the region of interest compared to the other methods.

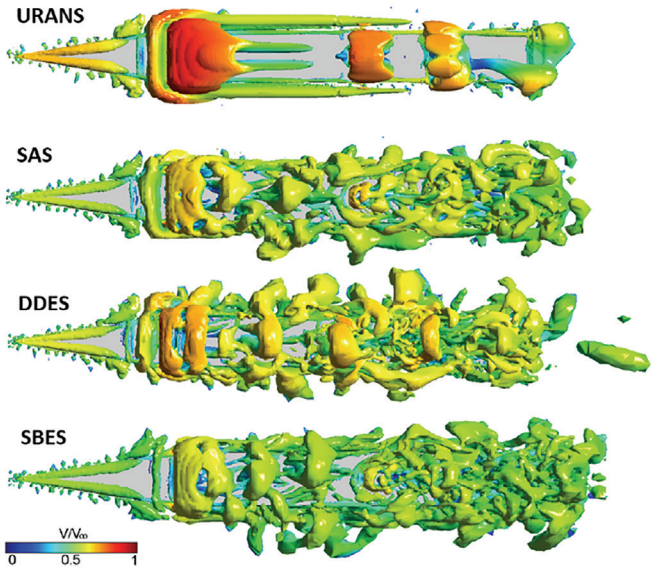

Figure 7. Comparison based on Q criterion (Q=0.1; vortex colorization is based on velocity magnitude).

4.2. SBES Methodology and Comparative Flow Direction Evaluations

4.2.1. 0° flow direction

For all results, experimental data [34] is labelled as "EXP", and the SBES simulation results as "CFD". The colours represent the velocity values non-dimensionalized by the free-stream velocity. The flow field resulting from the head direction flow was compared with the experimental data on the data planes. The longitudinal and lateral velocity distributions are shown in Figure 8. As seen in the comparison of the calculated data along the 50% L_p line in terms of velocity and turbulence intensity above, a similar relative error (15-20%) can also be observed here when looking at the planes they are located on.

The primary factors causing the discrepancies between the experimental and computational results were considered to be experimental measurement errors, computational method limitations, and mesh resolution. As noted in the mesh independence section, the resolution of the mesh impacted the accuracy of the results, with finer meshes providing closer agreement with experimental data.

4.2.2. S45° flow direction

For the 45° flow angle from the starboard side (S45°), the velocity distributions across the data planes were compared with the experimental data [34]. The longitudinal and lateral velocity distributions are presented in Figure 9. The velocity values are non-dimensionalized by the free-stream velocity.

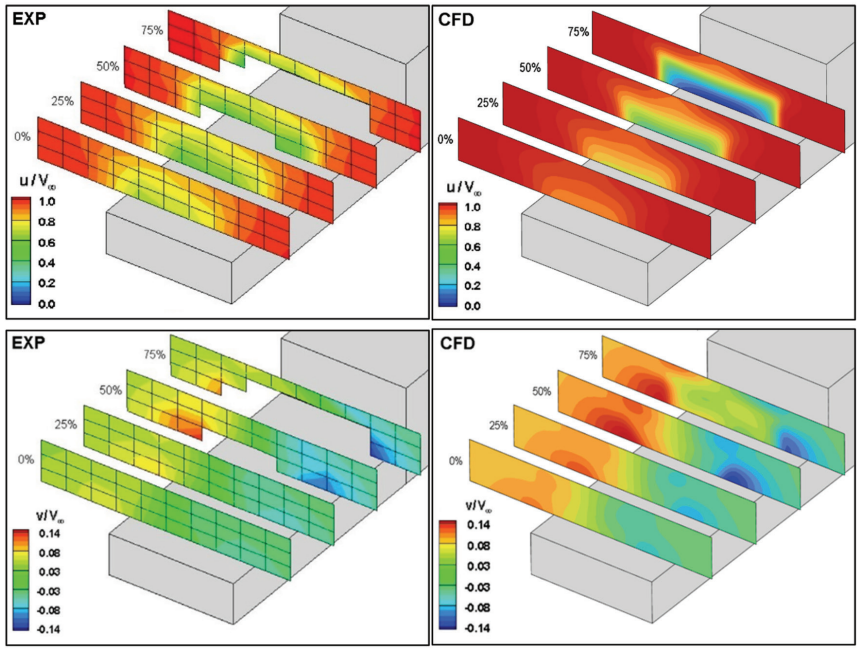

Figure 8. Comparison of longitudinal (up) and lateral velocity distributions on the data planes for 0°.

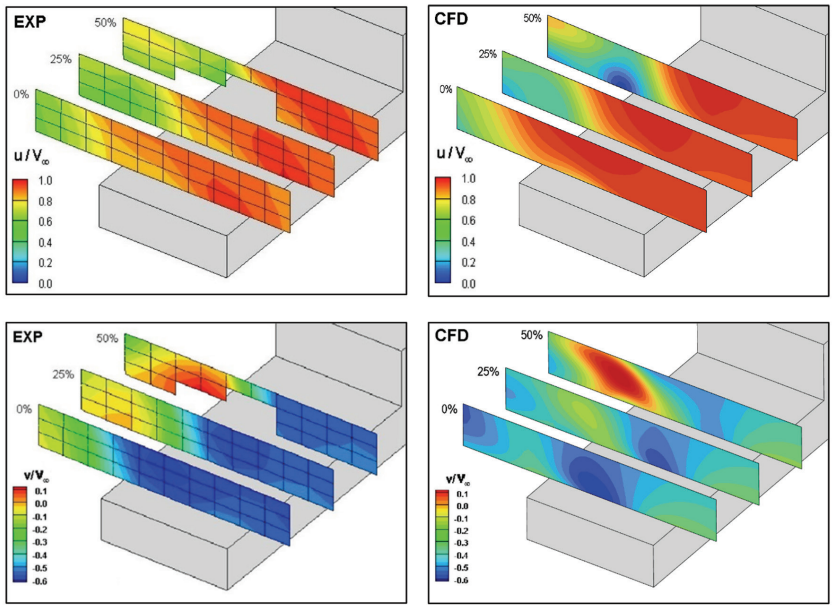

Figure 9. Comparison of longitudinal (up) and lateral velocity distributions on the data planes for S45°.

While the superstructure of the ship interacts with the flow primarily from the bow with the bridge and funnel in the 0° case, the S45° case additionally includes the structure from the starboard side, increasing the cross-sectional area exposed to the flow. As a result, the turbulence kinetic energy over the ship increases, and the flow field becomes much more asymmetric. This makes it more challenging to predict the wake region accurately with computational methods. As seen in the comparison of the calculated data along the 50% L_p line for the S45° case in terms of velocity and turbulence intensity above, a similar relative error (30%) can also be observed here in Figure 9 when looking at the planes they are located on.

4.2.3. 0° and S45° flow directions comparison

A comparison of the average velocity magnitude contours and streamlines for the 0° and S45° cases on a plane located 75% of the hangar height is shown in Figure 10. In the 0° case, the flow decelerates to nearly a complete stop around the bridge region. As the flow accelerates again towards the flight deck, it experiences a reduction in velocity due to the discontinuity in the superstructure. The S45° case presents a more pronounced reduction in velocity on the leeward side of the superstructure. Additionally, the increased complexity of the flow in the wake region of the S45° case is characterized by the presence of multiple independent vortices, which are not observed in the 0° case.

Figure 11 shows the distribution of vortices over the ship for the both cases, visualized using the Q-criterion [35]. The vortex structures formed at the bow and bridge are more pronounced in the S45° case, where the starboard side of the

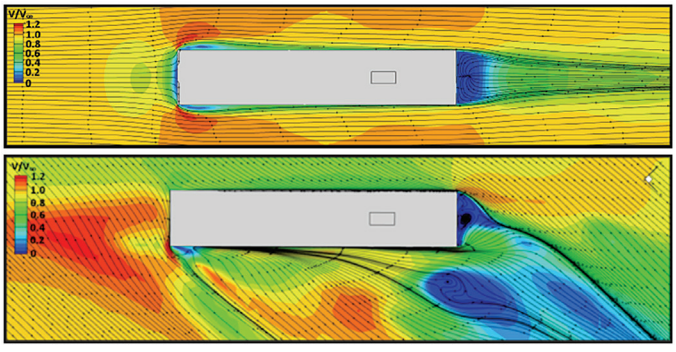

Figure 10. Mean velocity magnitude contours and streamlines for 0° (up) and S45° occurred at 75% of hangar height line (results based on the SBES method).

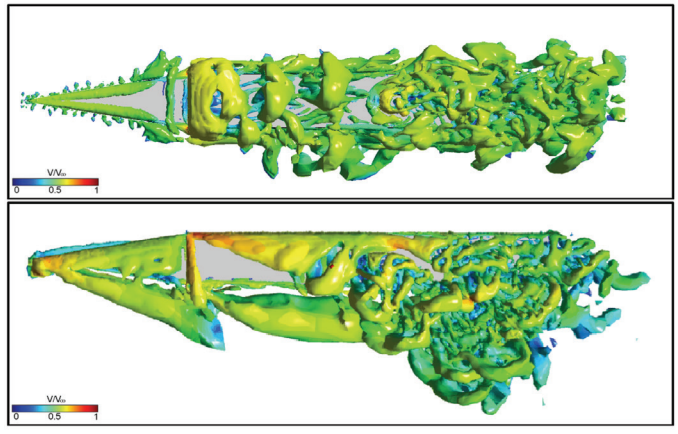

Figure 11. Comparison of the Q-criterion vortex distribution for 0° (up) and 45° flows (Q=0.1, vortex colorization is based on velocity magnitude; results based on the SBES method).

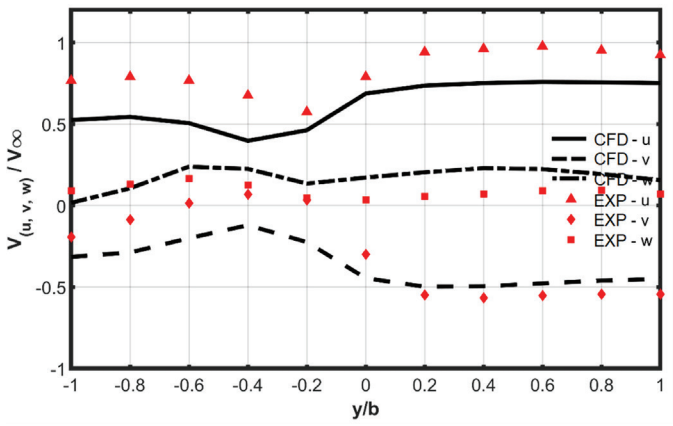

Figure 12. Distribution of velocity components on the 50% L_p line for 0° (up) and S45°

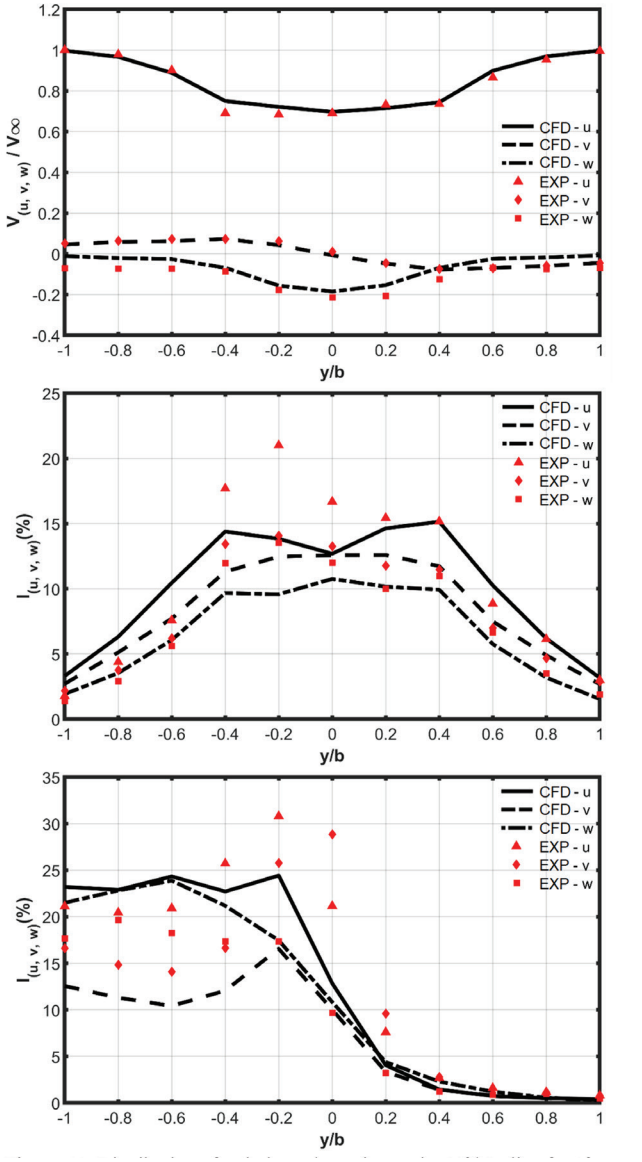

Figure 13. Distribution of turbulence intensity on the 50% L_p line for 0° (up) and S45° flow directions.

superstructure also contributes to the formation of additional vortices. A 30% increase in vorticity is observed in the S45° case compared to the 0° case.

Non-dimensional distributions of mean velocity magnitude and turbulence intensity for the 0° and S45° flow directions are presented in Figures 12 and 13 respectively. As mentioned previously, the results show that while the superstructure interacts with the flow primarily at the bow in the 0° case, the S45° case introduces the starboard side of the superstructure into the flow, making the wake region more complex and difficult to interpret computationally. Consequently, while the simulated results show good agreement with the experimental data in the 0° case, the complexity of the wake region results in a less precise correlation between the simulation and the experimental data in the S45° case. Nevertheless, it can be said that the results follow a similar trend.

Figures 14 and 15 show the longitudinal and lateral PSD distributions for the 0° and S45° flow directions, respectively. The PSD values for the head flow case are in close agreement with the experimental results, while the results for the S45° case exhibit larger discrepancies, particularly at frequencies above approximately 100 Hz for both longitudinal and lateral components.

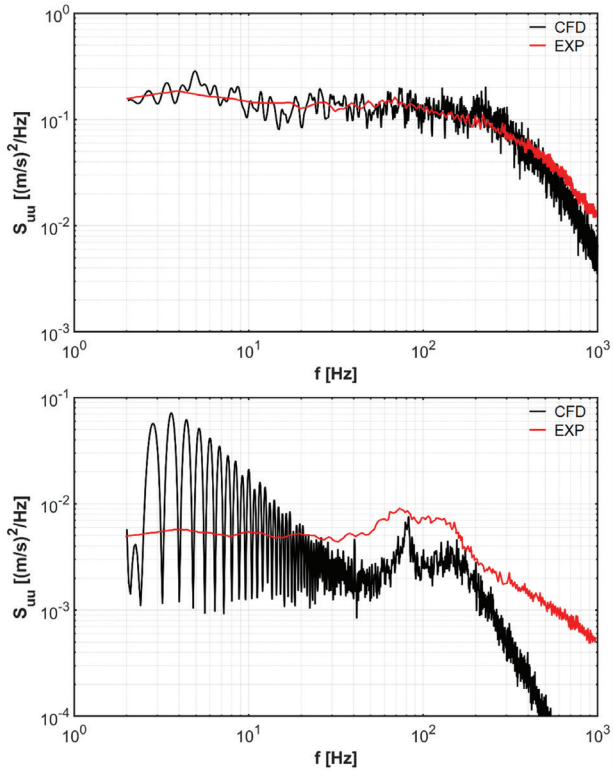

Figure 14. Longitudinal PSD comparison at the 50% L_p spectrum point for 0° (up) and at the 25% L_p for S45°.

5. Conclusions and Future Work

This study presents a comprehensive computational strategy for the effective and accurate calculation of ship airwake. SRS techniques, which have gained popularity in recent years, were applied and compared against experimental data from the literature. The predictive capabilities of these methods were evaluated in detail.

Primarily, all SRS methods demonstrated significantly superior results in terms of velocity magnitudes and turbulence intensity levels compared to URANS. For velocity magnitude, SRS methods yielded results within a ~1% difference from each other. However, predictions of turbulence intensity varied by ~1-4%, depending on the simulation technique employed. Notably, the DDES and SBES models predicted turbulence intensity within ~15% and ~16% of the experimental values, respectively. In spectral analyses, which are crucial for assessing flight envelope characteristics, SBES exhibited greater alignment with experimental results, particularly in the high-frequency ranges, where it demonstrated approximately 50% greater accuracy compared to DDES. This improvement is attributed to SBES' faster transition to LES resolution, leading to better performance in turbulent flow regions.

Key findings from this study are as follows:

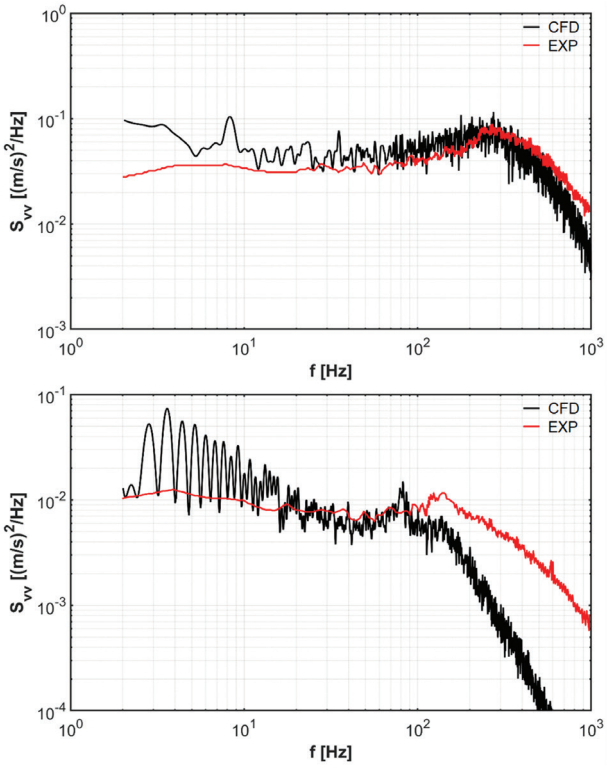

Figure 15. Lateral PSD comparison at the 50% L_p spectrum point for 0° (up) and at the 25% L_p for S45°.

- The detailed comparisons showed that SRS methods are highly effective in modelling turbulence, especially in the regions with high levels of flow separation occurring on discontinuous ship superstructure.

- Increasing the mesh resolution in the helicopter flight zone improved the accuracy of the results. This confirms that grid refinement, particularly in critical flow regions, plays an important role in capturing turbulence structures.

- The computational load was reduced by adopting a simplified boundary layer modelling approach, while conserving the accuracy of the airwake simulations. However, it was seen that ~1% refinement of the solution accuracy in terms of turbulence intensity costed 4 times higher cell count. Thus, there should be a balanced approach while determining the grid for entire solutions as it is a trade-off between solution accuracy and time efficiency.

- Using optimal time step values ensured that there is no need to perform additional time dependence studies.

- The computational strategy resulted in effective and reliable outcomes with relatively less resource usage, making the methods suitable for ship airwake simulations critical to SHDI studies.

- It is concluded that SBES, which has been used in recent studies for different types of analyses, can also be used as a primary method for ship airwake calculations.

For future studies, the focus will be on achieving aerodynamic improvements in the ship's airwake through various design applications, examining the effects of the atmospheric boundary layer, incorporating six degrees of freedom for ship motion, and conducting both numerical and experimental airwake analyses on more detailed ship geometries. By continuing this line of research, it will be possible to further enhance the accuracy of airwake predictions, ultimately contributing to the design of safer and more efficient ship-aircraft interaction systems for future naval and commercial platforms.

Acknowledgement

The authors would like to thank Turkish Naval Forces MILGEM Design Project Office (DPO) to bring the topic in question for research and for their support.

Footnotes

Authorship Contributions

Concept/Design: T. Şık, Data Collection or Processing: T. Şık, Analysis or Interpretation: T. Şık, and U. O. Ünal., Literature Review: T. Şık, Writing, Reviewing and Editing: T. Şık, and U. O. Ünal.

Conflict of Interest: No conflict of interest was declared by the authors.

Financial Disclosure: The authors declared that this study received no financial support.

6. References

[1] D. E. Johnston and D. T. McRuer, "Investigation of interactions between limb-manipulator dynamics and effective vehicle roll control characteristics", *NASA CR-3983*, 1986.

[2] W. Mahaffey, T. Mukerjee and A. Singhal, "Prediction of turbulent ship air-wake characteristics", *Numerical Simulation of Fluid Flow and Heat/Mass Transfer Processes*. Lecture Notes in Engineering, Springer, Berlin, Heidelberg. vol. 18, 1986.

[3] S. J. Zan, J. F. Syms and B. T., Cheney, "Analysis of patrol frigate air wakes", *Fluid Dynamics Problems of Vehicles Operating Near or in the Air-Sea Interface*, RTO-MP-15, Paper 7, RTO/NATO, Amsterdam, 1998.

[4] S. J. Zan, "Experimental determination of rotor thrust in a ship airwake", *American Helicopter Society*, vol. 47, no. 2, pp. 100-108, 2002.

[5] S. J. Zan, "On aerodynamic modelling and simulation of the dynamic interface", *Journal of Aerospace Engineering*, Proc. IMechE Part G, vol. 219, pp. 393-410, 2005.

[6] G. F. Syms, "Numerical simulation of frigate airwakes", *International Journal of Computational Fluid Dynamics*, vol. 18, no. 6, pp. 199-207, 2004.

[7] W. Yuan, R. Lee and A. Wall, "Simulation of unsteady ship airwakes using OpenFOAM", *30th Congress of the International Council of the Aeronautical Sciences*, Daejon, Korea, 2016.

[8] W. Yuan, A. Wall and R. Lee, "Combined numerical and experimental simulations of unsteady ship airwakes", *Computers & Fluids*, vol. 172, pp. 29-53, 2018.

[9] W. Yuan, A. Wall and R. Lee, "Simulations of unsteady airwakes behind ships in motion", *31st Congress International Council of the Aeronautical Sciences*, Belo Horizonte, Brazil, 2018.

[10] B. T. Cheney and S. J. Zan, "CFD code validation data and flow topology for the technical co-operation program AER-TP2 Simple Frigate Shape", *National Research Council*, Canada, Report LTR-A-035, 1999.

[11] K. R. Reddy, R. Toffoletto and K. R. W. Jones, "Numerical simulation of ship airwake", *Computers & Fluids*, vol. 29, pp. 451-465, 2000.

[12] N. H. Wakefield, S. J. Newman and P. A. Wilson, "Helicopter flight around a ship's superstructure", *Journal of Aerospace Engineering*, Proc Instn Mech Engrs, vol. 216, part G, no. 01801, pp. 13-28, 2002.

[13] R. Bardera-Mora, "Experimental investigation of the flow on a Simple Frigate Shape (SFS)", *The Scientific World Journal*, vol. 2014, no. 818132, 2014.

[14] D. Lindon and B. Thornber, "Quantifying uncertainty in turbulence resolving ship airwake simulations", *Ocean Engineering*, vol. 229, no. 108983, 2021.

[15] A. Zamiri and J. T. Chung, "Numerical evaluation of wind direction effects on the turbulence aerodynamics of a ship airwake", *Ocean Engineering*, vol. 284, no. 115104, 2023.

[16] G. F. Syms, "Simulation of simplified-frigate airwakes using a Lattice-Boltzmann method", *Journal of Wind Engineering and Industrial Aerodynamics*, vol. 96, no. 6, pp. 1197-1206, 2008.

[17] F. Zhang, H. Xu and N. Ball, "Numerical simulation of unsteady flow over SFS2 ship model", *AIAA Aerospace Sciences Meeting*, Orlando, Florida, vol. 47, AIAA 2009-81, no. 090081, 2009.

[18] J. S. Forrest and I. Owen, "An investigation of ship airwakes using Detached-Eddy Simulation", *Computers & Fluids*, Vol. 39, pp. 656-673, 2009.

[19] J. S. Forrest, C. H. Kääriä and I. Owen, "Determining the impact of hangar-edge modifications on ship-helicopter operations using offline and piloted helicopter flight simulation", *American Helicopter Society*, 66th Annual Forum & Technology Display, 2010.

[20] J. S. Forrest, C. H. Kääriä and I. Owen, "Evaluating ship superstructure aerodynamics for maritime helicopter operations through CFD and flight simulation", *Aeronautical Journal*, vol. 120, no. 1236, pp. 1578-1603, 2016.

[21] C. H. Kääriä, Y. Wang, M. D. White and I. Owen, "An experimental technique for evaluating the aerodynamic impact of ship superstructures on helicopter operations", *Ocean Engineering*, vol. 61, pp. 97-108, 2013.

[22] S. Shukla, S. S. Sinha and S. N. Singh, "Ship-helo coupled airwake aerodynamics: a comprehensive review", *Prog Aero Sci*, vol.106, pp. 71-107, 2019.

[23] S. Shukla, S. S. Sinha and S. N. Singh, "An investigation of ship airwakes by scale adaptive simulation" the *International Journal on Marine Navigation and Safety of Sea Transportation*, vol.1 4, no. 2, pp. 471-476, 2020.

[24] S. Shukla, S. S. Sinha, S. N. Singh and R. Vijayakumar, "A conceptual method to assess ship-helicopter dynamic interface", *Journal of Aerospace Engineering*, Proc IMechE Part G, vol. 234, no. 5, pp. 1092-1116, 2020.

[25] S. Shukla, S. S. Sinha, S. N. Singh and R. Vijayakumar, "Comparative assessment of URANS, SAS and DES turbulence modeling in the predictions of massively separated ship airwake characteristics", *Ocean Engineering*, vol. 229, no. 108954, 2021.

[26] F. R. Menter and Y. Egorov, "Scale-Adaptive Simulation method for unsteady flow predictions. Part 1: theory and model description", *Journal Flow Turbulence and Combustion*. vol. 85, pp. 113-138, 2010.

[27] Y. Egorov, F. R. Menter and D. Cokljat, "Scale-Adaptive Simulation method for unsteady flow predictions. Part 2: Application to Aerodynamic Flows", *Flow, Turbulence and Combustion*, vol. 85, pp. 139-165, 2010.

[28] P. R. Spalart, W. Jou, M. Strelets and S. Allmaras, "Comments on the feasibility of LES for wings and on a hybrid RANS/LES approach", *1st AFOSR Int. Conf. on DNS/LES*, 1997.

[29] P. R. Spalart, "Strategies for turbulence modelling and simulations", *Int. J. Heat Fluid Flow*, vol. 21, p. 2, 2000.

[30] F. R. Menter and M. Kuntz, "Adaptation of eddy-viscosity turbulence models to unsteady separated flow behind vehicles", *Proc. Conf. The Aerodynamics of Heavy Vehicles: Trucks, Busses and Trains*, Springer, Berlin, Heidelberg, pp. 339-352, 2003.

[31] P. R. Spalart, S. Deck, M. Shur, K. Squires, M. Strelets and A. Travin, "A new version of Detached Eddy Simulation resistant to ambiguous grid densities", *Journal of Theorotical Computational Fluid Dynamics*, vol. 20, pp. 181-195, 2006.

[32] F. R. Menter, "Stress-Blended Eddy Simulation (SBES) - a new paradigm in hybrid RANS-LES modeling", *Notes on Numerical Fluid*

Mechanics and Multidisciplinary Design, Springer International Publishing AG. Ansys Germany GmbH, no. 137, 2018.

[33] F. R. Menter, "Best practice: Scale-Resolving Simulations in ANSYS CFD", *Ansys Germany GmbH*, Version 1.0, 2012.

[34] R. G. Lee, "SFS 2 Code Validation Data Update", *TTCP AER TP 2 Dynamic Interface Workshop, 2003*, Patuxent River, USA, 2007.

[35] J. Jeong and F. Hussain, "On the identification of a vortex", *Journal of Fluid Mechanics*, vol. 285, pp. 69-94, 1995.

RESEARCH ARTICLE

DOI: 10.54926/jnamt.2024.1485025

J Nav Architect Mar Technol 2024;226(2):25-35

Investigation of Optimum Structures at Submarine Pressure Hulls under Hydrostatic Pressure with Finite Element Method

Burak Eyiler[1], Ertekin Bayraktarkatal[2]

[1]Department of Naval Architecture and Marine Engineering, National Defense University, Turkish Naval Academy, İstanbul, Türkiye
[2]Department of Naval Architecture and Marine Engineering, İstanbul Technical University, İstanbul, Türkiye

To cite this article: B. Eyiler, and E. Bayraktarkatal. Investigation of optimum structures at submarine pressure hulls under hydrostatic pressure with finite element method. *J Nav Architect Mar Technol*. 2024;226(2):25-35.

Received: 16.05.2024 - **Revised:** 12.11.2024 - **Accepted:** 12.11.2024 - **Publication Date:** 31.01.2025

Abstract

In this study, the optimum structure of submarine pressure hulls under hydrostatic pressure was investigated by finite element method. The weight/volume ratio, which is considered as the buoyancy factor, and the maximum strength were taken as the basis for structural efficiency in the submarine pressure hull design. The collapse diving depth pressure was used for both the scantling of structural components and the calculation of critical buckling pressures. General instability buckling shape was observed during the analysis and the results were verified by DNV-GL Classification Society rules. Finally, the results of the different structures optimized to give the maximum strength at the same weight were presented in tables.

Keywords: Ultimate strength, finite element method, cylindrical shells, buckling, general instability

1. Introduction

The structural stability of submarines is very important for them to carry out their missions without any problems. Accidents at submarines from the past to the present have made these studies valuable for both the safety of the crews and the survival of the structure. Finally, the accident on the Titan submarine, which was planned to dive to a depth of 3800 meters to see the wreckage of the Titanic and resulted in the death of five people, showed the importance of these studies [1].

Submarines generally have two hulls. The first of these hulls is the pressure hull, which contains the living spaces, weapon control systems, weapons communication and control room, batteries, main and auxiliary machinery and provides the strength of the submarine under hydrostatic pressure. The function of the outer shell covering the submarine pressure hull is to add a hydrodynamic feature to the structure [2,3].

Experimental and numerical studies on the strength of cylindrical shells have been studied in the past. The first theoretical solutions for cylindrical shells of uniform thickness were presented by Von Mises, Windenburg and Trilling and Von Sanden and Gunther in 1929, 1934 and 1952 respectively. These theories are still used because they are relatively simple [4].

Address for Correspondence: Burak Eyiler, Department of Naval Architecture and Marine Engineering, National Defense University, Turkish Naval Academy, İstanbul, Türkiye
E-mail: burak.eyiler@gmail.com
ORCID ID: orcid.org/0000-0003-1723-7605

For the calculation of symmetric buckling of a cylindrical shell between stiffeners, Lunchick [5] presented the report numbered 1393 called "plastic axial symmetric buckling of stiffened cylindrical shell made of strain hardening materials and subjected to external hydrostatic pressure". In this study, Lunchick [5] took the hardening behaviour of the material into the calculation and considered the Poisson ratio as a variable ranging from its elastic value to 1/2, which is the upper limit for an incompressible material. He presented a shell length criterion for long and short cylinders. He said that below this value the shell buckles in only one half-wave [5].

For the asymmetrical buckling calculations of the stiffened cylindrical shell, Reynolds [6] presented the report numbered 1392, named inelastic buckling of the cylindrical shell under hydrostatic pressure. In this report, a solution of Gerard's differential equations for plastic buckling of cylindrical shells was found by Reynolds [6] for asymmetric buckling under hydrostatic pressure. According to this study, the critical buckling pressure was found as a function of the cylindrical shell geometry and the secant and tangent moduli for the shell material according to the stress-strain diagrams [6].

For the calculation of the general instability buckling shape of stiffened cylindrical shells, Bryant [7] presented his report number 306, named buckling of a stiffened cylindrical shell under hydrostatic pressure. In his paper, Bryant [7] solved the general instability problem by using the elastic potential energies of the shell and girders.

Aileni et al. [8] calculated the critical buckling pressure of stiffened cylindrical shells under external pressure using finite element method (FEM). Linear and nonlinear buckling analysis results were compared with experimental results and it was observed that the nonlinear analysis results were closer to the experimental results. The variation of critical buckling pressures was investigated by using reinforcing elements in Z, square, rectangular, C, I and T sections. At the end of the analysis, it was observed that the critical buckling pressure decreased as the distance between the reinforcements increased. In addition, it was found that higher critical buckling pressures occurred in Z and square section reinforcements [8].

Oh and Koo [9] analysed 7 case studies with analytical solutions for the optimum design of submarine pressure hull and validated the study with finite element analysis. As a result of the study, they proposed initial scantling formulas for weight optimization in relation to radius (R), yield strength and design pressure for shell thickness, flange width, flange thickness, web height and web thickness. Using the proposed initial sizing formulas, it was found that the pressure hull weight was reduced between 6% and 19% [9].

Kine [10] aimed to optimize the buckling performance of a pressure hull under hydrostatic pressure. His study was based on the critical buckling pressure and the weight corresponding to this pressure. The optimization includes four design parameters including cylindrical shell thickness, unsupported length between stiffeners, stiffener height and stiffener thickness. The results obtained from this study indicated that the critical buckling pressure increased by 7.09%. It was found that the unsupported length between reinforcements and cylinder thickness have a significant effect on the buckling performance of the pressure hull [10].

Wei et al. [11] investigated the optimization of a trapezoidal reinforced composite cylindrical pressure hull under hydrostatic pressure. The composite cylindrical shell was manufactured with carbon fiber reinforced epoxy, while the stiffeners were made of aluminium alloy. An analytical buckling model was derived for the stiffened composite cylindrical shell under hydrostatic pressure. Then, the FEM was used to verify the accuracy of the analytical solution. After verification, the analytical solution was combined with the genetic algorithm to obtain the maximum buckling pressure and optimize the cross-sectional shape of the stiffeners. It was found that there is a linear relationship between the cross-sectional moments of inertia of the stiffeners and the critical buckling pressure [11].

Rathinam et al. [12] generated finite element models with the help of the Ansys package to predict the shell and general instability damage shapes in stiffened cylindrical shells. Finite element analysis results were compared with analytical and experimental results. As a result, it was found that the minimum critical pressure value determines in which buckling mode the pressure hull will be damaged [12].

Şenol [13] presented a structural optimization based on the FEM for the optimum structural design of a submarine pressure hull. He compared the finite element results with the DNV-GL Classification Society results and observed that they converged. In his studies to determine the optimum geometry, a single ring stiffened geometry with effective shell length was subjected to external hydrostatic pressure using non-linear material properties and large deformations. As a result, an optimum design is defined in a way to obtain the minimum weight and maximum internal volume targets [13].

Fu et al. [14] proposed a pressure hull design method within the limits of outer envelope size and inner space utilization using variable section ribs. The pressure hull bearing mechanism was theoretically and numerically calculated and experimentally verified. They used the energy method to calculate the critical buckling pressure. As a result, it was found that variable cross-section ribs increase the buckling load by about 26.7% by maximizing the space utilization [14].

Shinoka and Netto [15] conducted three different optimization studies to minimize the weight of submarine pressure hulls. The optimization tools used were: Differential Evolution, Particle Swarm and Simulated Annealing. As a result, they found that the Differential Evolution algorithm is the most reliable and consistent in minimizing the objective functions [15].

In this study, the optimum structure was investigated for submarine pressure hulls where different reinforcements are used. The FEM was used to calculate the critical buckling pressure and the Screening optimization method was used to calculate the optimum structure. The results of the analysis were also verified with DNV classification society rules. When these results were analyzed in terms of structural efficiency, it was determined that the structures with Transverse Internal Reinforced Systems were the most effective.

2. Submarine Pressure Hull Design

2.1. Calculation of Safety Factor and Diving Depth Pressures

The pressure hull is the basic structure of a submarine and it constitutes half or more of the total weight of the submarine. A typical pressure hull is produced by welding T-section girders to high-strength axisymmetric shells produced by cold rolling. Since the late 1970s, the typical form of a submarine pressure hull has been a ring stiffened circular cylindrical shell, closed by a parabolic bow and an elliptical stern hatch, as shown in Figure 1 [16,17].

Figure 1. Submarine hull form [18].

The biggest problems faced by the submarine designer are to reduce the weight of the pressure hull and the cost of submarine construction, to increase the payload carrying capacity and the ship's speed.

There are some diving depths that form the basis for submarine pressure hull design. These depths are mainly: Nominal diving depth (NDD) is the diving depth at which the submarine can operate unrestrictedly. Collapse diving depth (CDD) is the theoretical maximum depth at which the submarine can dive. Collapse diving pressure (CDP) is the pressure value at which the pressurized hull can collapse under a 1-minute load. This depth value is used for the scantling of pressure hull structural components [19,20].

The conventional submarine considered in this study was assumed to operate at a NDD of 400 meters. The DNV-GL Classification Society gives the calculation of the hydrostatic pressure depending on the NDD in Equation 1 as follows [19].

$$\text{Nominal Diving Pressure} = \text{Nominal Diving Depth} \cdot 0.101\ (\text{bar}) \quad (1)$$

According to the calculation, it was found that the submarine would be exposed to 40.4 bar a hydrostatic pressure at the NDD, which would be 4.04 MPa because 1 bar pressure corresponds to 0.1 MPa pressure.

Considering the constraints given in Table 1, the safety factors S_1 and S_2 corresponding to the nominal diving pressure of 40.4 bar were found to be 1.20 and 1.7984 respectively. The CDP was found 7.26554 MPa and the Test diving pressure applied to test the tightness and function of the pressure hull and equipment was found 4,848 MPa.

Table 1. Determination of safety factors for test and collapse diving pressure in relation to nominal diving pressure [19].

Nominal diving pressure (bar)	10	20	30	40	50	≥60
S_1 = TDP/NDP (2)	1.40	1.25	1.20	1.20	1.20	1.20
S_2 = CDP/NDP (3)	2.40	2.00	1.87	1.80	1.76	1.73

1. Minimum nominal diving pressure 5 bar
2. In the range NDP = 5 ….. 30 bar: S1 = 3/NDP + 1.1
3. In the range NDP = 5 ….. 60 bar: S2 = 8/NDP + 1.6
4. If Depth>Nominal Diving Depth, the minimum value of S_2 is 2.

2.2. Structure Material

Pressure hull materials must be able to withstand high external pressures and the adverse effects of the environment. The commonly used material for a submarine pressure hull is steel with high yield strength, usually obtained by alloying or heat treatment. HY grade steels are metallurgically quenched and tempered martensitic steels. This martensitic lattice structure is formed as a result of heat treatment with alloying elements such as nickel, chromium, molybdenum and vanadium. Table 2 shows the general physical properties of the materials used in the construction of submarine pressure hulls. In this study, HY100 steel was preferred [21,22].

Table 2. Material properties of HY80, HY100 and HY130 [9].

Property	HY80	HY100	HY130
Young's modulus (E)(GPa)	206	206	206
Poisson's ratio (ν)	0.3	0.3	0.3
Density (ρ, kg/m^3)	7746	7850	7885
Yield Strength ($\sigma_{0.2}$, MPa)	552	686	890
Maximum tensile strength (σ_u, MPa)	611	760	986
Elongation (%)	19	17	14

2.3. Scantling of Structural Components

The strength and stiffness of any structure vary according to the properties of the material used and the geometry of the structure. Without changing the geometry of a structure, the strength and stiffness of the structure can be increased by adding small weight stiffeners to the structure. It has been observed that the buckling strength of the hull is greatly improved by using stiffeners. In pressure hulls, T-section stiffeners are most commonly used and are usually placed inside the hull. In this study, different stiffeners with the same cross-sectional moment of inertia were used for transverse, longitudinal and both transverse and longitudinal (combined) systems [8]. Figure 2 shows the effective length shell with T-section stiffeners.

Oh and Koo [9] proposed initial sizing formulas for shell thickness, flange width, flange thickness, web height and web thickness based on R, yield strength and design pressure in their study on the optimum design of submarine pressure hull. These formulas are given in Table 3. In this study, these formulas were used for the initial sizing.

In this study, the R was defined as 3123 mm, and the length of the pressure hull was specified as 9369 mm.

The structure lengths obtained depending on the input parameters were given in Table 4.

For the scantling of the frame space, the effective length formula in Equation 2 in the fourth chapter of the DNV-GL Classification Society Rulebook was used [19].

$$L_{eff} = \frac{2}{\sqrt[4]{3(1-\nu^2)}}\sqrt{R_m . s} \quad (2)$$

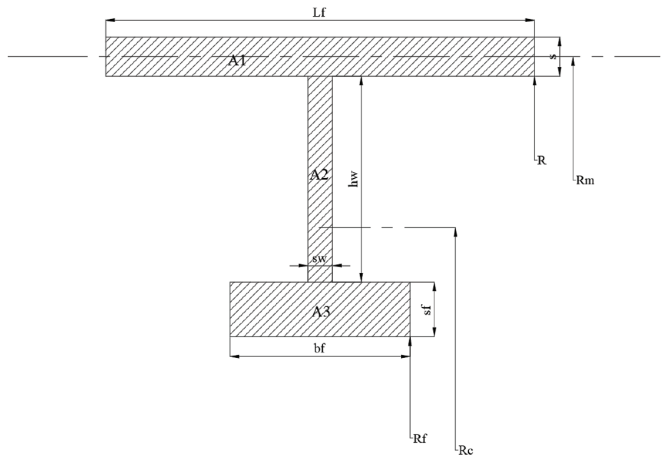

Figure 2. Pressure hull frame geometry [19].

Table 3. Empirical formulas proposed by Oh and Koo [9].

Shell Thickness (h) (mm)	Frame Space (Lfr) (mm)	Web Height (hw) (mm)	
$h = 0.790\frac{pR}{\sigma_{0.2}}$	$L_{fr} = 1{,}557\sqrt{Rh}$	$h_w = 7{,}552h$	$h_w = 5{,}966\frac{pR}{\sigma_{0.2}}$
Web Thickness (sw) (mm)			
$s_w = 0.645h$	$s_w = 0.0866\,h_w$	$s_w = 0.510\frac{pR}{\sigma_{0.2}}$	-
Flange Width (bfl) (mm)			
$b_{fl} = 3{,}827h$	$b_{fl} = 0.507\,h_w$	$b_{fl} = 3{,}025\frac{pR}{\sigma_{0.2}}$	-
Flange Thickness (tfl) (mm)			
$t_{fl} = 1{,}414h$	$t_{fl} = 0.369\,b_{fl}$	$t_{fl} = 1.12\frac{pR}{\sigma_{0.2}}$	-

Table 4. Structural lengths.

Shell Thickness (h) (mm)	Frame Space (Lfr) (mm)	Web Height (hw) (mm)	
$h = 26.13$	$L_{fr} = 444.90$	$h_w = 197.39$	$h_w = 197.38$
Web Thickness (sw) (mm)			
$s_w = 16.85$	$s_w = 17.09$	$s_w = 16.87$	-
Flange Width (bfl) (mm)			
$b_{fl} = 100.02$	$b_{fl} = 100.077$	$b_f = 100.08$	-
Flange Thickness (tfl) (mm)			
$t_{fl} = 36.95$	$t_{fl} = 36.91$	$t_{fl} = 37.05$	-

The structural component lengths chosen as a result of the scantling were given in Table 5.

Table 5. Structural component lengths of the pressure hull.

Pressure hull length	**9,369***
Shell thickness (s)	27
Web height (h_w)	197
Web thickness (s_w)	17
Flange width (b_f)	100
Flange thickness (s_f)	37
Frame space (L_f)	453
*All units in mm.	

The moment of inertia of the singular ring stiffener with reference to the neutral axis was calculated as 7.70536.108 mm^4 (Parallel Axis Theorem).

3. Calculation of Critical Buckling Pressure of Submarine Pressure Hull

When a submarine pressure hull is exposed to a pressure equal to or exceeding the CDD during operation, the hull may experience the following types of damage:

1. Asymmetric Interstiffener Buckling
2. Symmetric Interstiffener Buckling
3. General Instability
4. Tripping of Frames
5. Fore and Aft Buckling [23].

Some of the factors affecting the buckling shape of ring stiffened cylindrical shells are the bending stiffness of the frames and the cylindrical shell, the type of stiffeners such as longitudinal, ring or combination of these two [10].

Buckling shapes for stiffened cylindrical shells can be classified into two main groups. These are interstiffener (local) buckling and general instability of the structure. In local buckling, if the bending stiffness of the frames is such that they will not buckle when subjected to a critical load, the shell will buckle between the frames. This buckling is classified as asymmetric and symmetric interstiffener buckling [10].

Asymmetric buckling is also called lobe buckling and occurs when the sizes of the frames are small and they are located far apart from each other. As shown in Figure 3, the shell buckles in a wave along the circumference between the frames [18].

Symmetrical buckling occurs when the ring stiffeners have large dimensions and are placed very close to each other. As shown in Figure 4, the cylindrical shell buckles in the shape of an accordion [18].

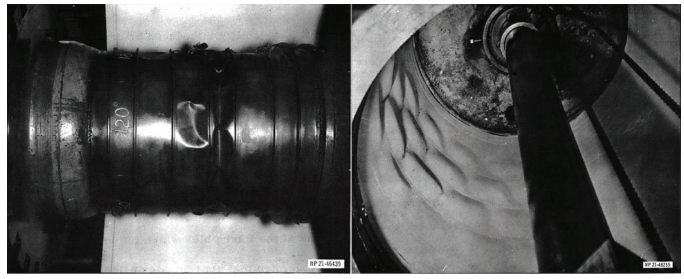

Figure 3. Asymmetric buckling failure [24].

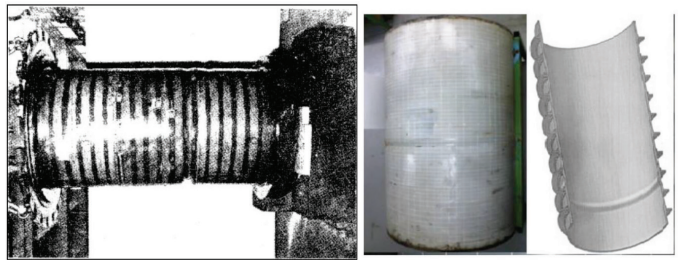

Figure 4. Symmetrical buckling failure [18].

General instability of the structure is described as buckling of the pressure hull between bulkheads, web frames or dished ends. In this buckling mode in order to resist displacements in the shell, there isn't enough bending stiffness in the frames [18].

In our design, general instability buckling mode was found in our finite element analysis. This failure mode is caused by a lack of strength of the material or the submarine diving deeper than the collapse depth [18]. Figure 5 shows the general instability buckling shape.

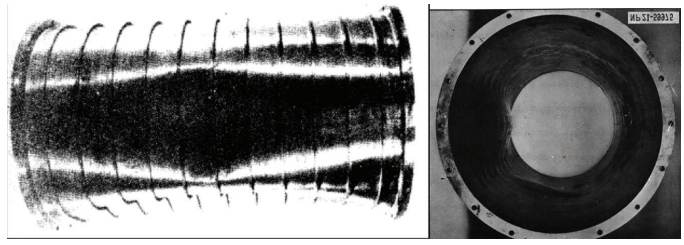

Figure 5. General instability buckling failure [18,24].

DNV-GL Classification Society equations for the calculation of the general instability critical buckling pressure are as follows [19]:

The membrane pressure:

$$P_m = \frac{E.s}{R_m}\cos^3\alpha\frac{\beta^4}{(n^2-1+\beta^2/2)(n^2+\beta^2)^2} \quad (3)$$

The pressure in the web frames:

$$P_D = \frac{2.(n^2-1).E.I_D.\cos^3\alpha}{R_{C,D}^2\left[R_m - 4\left(R_m - R_{C,D}\right)\right]\left(L_D + L_{D,1/r}\right)} \cdot \frac{n^2-1}{n^2-1+\beta_B^2/2} \quad (4)$$

The pressure in the frames:

$$P_F = \frac{(n^2-1).E.I_F}{R_{C,F}^3.L_F}\cos^4\alpha \frac{n^2-1}{n^2-1+\beta^2\frac{1}{2}\frac{P_D}{P_D+P_m}} \quad (5)$$

The pressure in the bulkheads:

$$P_B = \frac{E.s}{R_m}\cos^3\alpha \frac{\beta_B^4}{\left(n^2-1+\beta_B^2/2\right)\left(n^2+\beta_B^2\right)^2} \quad (6)$$

The general instability pressure:

$$P_g^n = P_F + \frac{P_m.P_D}{P_m+P_D} + P_B \quad (7)$$

Table 6 shows the general instability critical buckling pressure and its components.

Table 6. General instability critical buckling pressure results.

Pressures (MPa)	
The membrane pressure:	2.483
The pressure in the frames:	23.8474
The pressure in the bulkheads:	2.483
The pressure in the web frames:	0
General instability pressure:	26.3312

4. Finite Element Analysis and Optimization Method

In this part of the study, the finite element analyses were used to validate the critical buckling pressures found in the previous section and to optimize the structure.

The criteria defined for the optimum design:

$CDP \leq P_{cr\_asym}$

$CDP \leq P_{cr\_sym}$

$CDP \leq P_g$

Minimum Buoyancy Factor

Eigenvalue buckling analysis is used to determine the theoretical critical buckling load of an ideal linear elastic structure. It is assumed that the initial imperfections of the structure are neglected. It is used to predict the bifurcation point using a linearized model of an elastic structure. A full 360 degree model is required for the analysis. Because buckling occurs, the deformation of the structure is no longer axisymmetric [10].

To determine the buckling load factor λ for the structure under pressure P, a linear static analysis is first performed. In the eigenvalue problem given in Equation 8, K is the stiffness and S is the stress matrix of the structure. These are calculated by static analysis with prestressing effects established. The solution of the eigenvalue problem gives the i. eigenvalue λ_i (buckling load factor), where ψi is the i. eigenvector of the displacement corresponding to the eigenvalue. Not all eigenvalues are necessary and the critical buckling load is calculated with the lowest eigenvalue [25].

$$\left(K + \lambda_i S\right)\Psi_i = 0 \quad (8)$$

Depending on the buckling load multiplier obtained at the end of the linear buckling analysis, the critical buckling pressure is calculated as given in Equation 9 [26].

$$\text{Buckling Load Factor} = \frac{\text{Critical Buckling Pressure}}{\text{Applied Load}} \quad (9)$$

The critical load multiplier was calculated here:

If $\lambda_c < 1$, the structure buckles.

If $\lambda_c > 1$, the structure is safe.

4.1. The Geometry Design

The structure was designed as a shell element. Within the scope of the design, 21 frames with a distance of 453 mm between them were used. Figure 6 shows the design process of the structure.

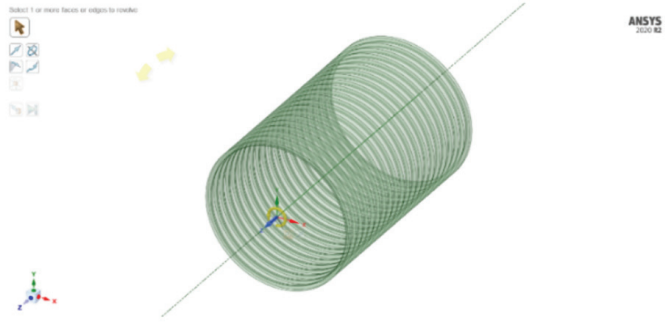

Figure 6. Pressure hull design.

4.2. Mesh Generation

When the convergence analysis was examined in Table 7, the result obtained using a mesh element size of 30 mm was taken as the reference value. According to this value, the deviation amounts from this value for other element sizes were given as percentages. When the average mesh quality, minimum mesh quality and percentage change

Table 7. Mesh convergence analysis.

Element size	Buckling load factor	Critical buckling pressure	Minimum mesh quality	Average mesh quality	% Change
30	3.49725	25.40941	0.988799	0.995736	Reference result
40	3.49901	25.4222	0.911797	0.971807	0.050339
50	**3.50288**	**25.45032**	**0.948748**	**0.989762**	**0.161003**
60	3.504644	25.46313	0.982792	0.991556	0.211425
70	3.506927	25.47972	0.925332	0.971309	0.27671
80	3.509487	25.49832	0.911796	0.972581	0.349917
90	3.513275	25.52584	0.862857	0.965442	0.458238
100	3.514704	25.53622	0.781301	0.917871	0.499084

values generated depending on the mesh element size were examined, it was seen that the most ideal mesh size was 50 mm. Analyses were continued using a mesh size of 50 mm.

The cross-sectional view of the structure as a result of the meshing process was shown in Figure 7.

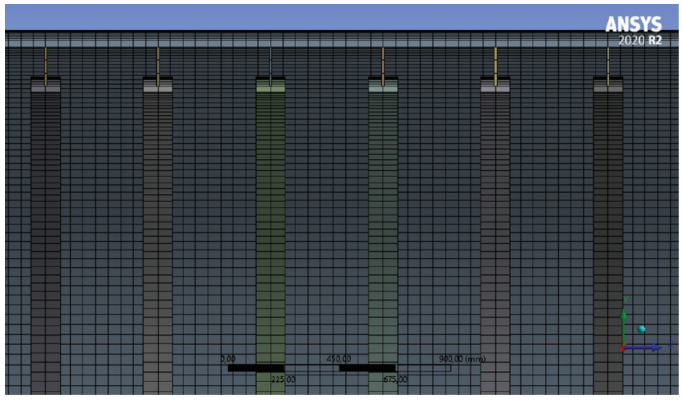

Figure 7. Cross-sectional view of pressure hull.

4.3. Load and Boundary Conditions

The linear buckling analysis of our pressure hull model was analyzed under a collapse buckling pressure of 7.26554 MPa. It was accepted that the pressure hull was constrained by bulkheads and the two ends of the hull are supported by fixed supports.

4.4. Buckling Analysis

After the mesh model of the pressure hull model was designed and the load and boundary conditions were entered into the system, the static analysis was performed first. Following this static analysis, the results obtained were linked to the buckling analysis and the first linear buckling analysis of the structure was done. Figure 8 shows the buckling mode of the structure as a result of buckling analysis.

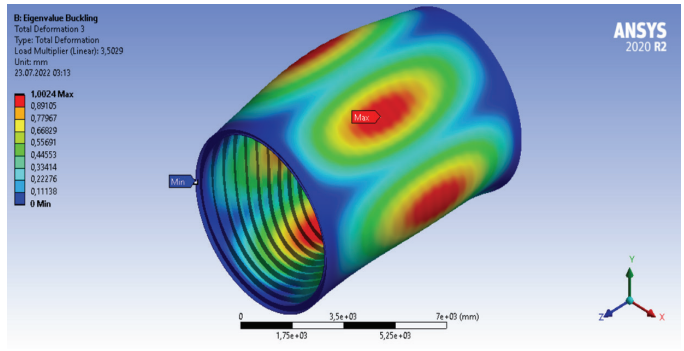

Figure 8. First linear buckling analysis.

5. Investigation of the Optimum Submarine Pressure Hull

In this section, the Screening optimization method was used to determine the ideal design in the model analyzed and to realize the objective functions mentioned in the previous sections. Within the scope of the optimization study, shell, web and flange thicknesses were considered as input parameters, while the pressure hull weight, internal volume and buckling load factor were considered as output parameters. Depending on the changing input parameters in the cylindrical pressure hull geometry, it was desired to resize the structure and recalculate the buckling calculations.

The Screening method can be used for both Response Surface Optimization and Direct Optimization systems. This method enables you to create a new set of samples and order the samples according to the objectives and constraints. This non-iterative method can be used for any type of input parameter. Screening is typically used to find initial candidate points for preliminary design. These candidate points can subsequently serve as initial points for gradient-based methods to refine the solution. Three candidate designs were selected from 9000 samples. The shell, web and flange thicknesses used

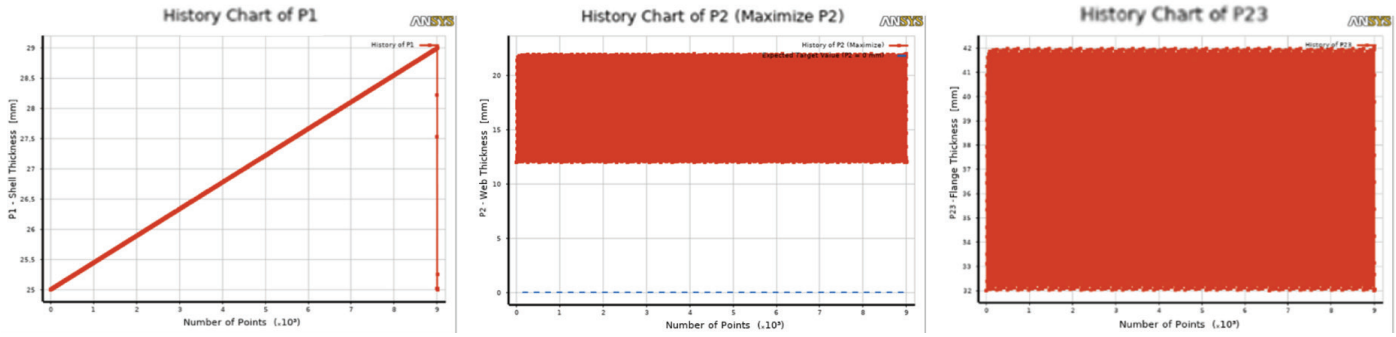

Figure 9. Shell, Web and Flange thickness sample diagram.

in the design scheme created for the optimization study are shown as graphs in Figure 9, respectively [26].

The 9000 sample design points generated within the scope of the optimization and the related output parameters are shown in Figure 10. Here, the points shown in gray are the samples that are out of the targets.

The influence of the input parameters on the output parameters is shown in Figure 11. As can be seen from the graph, the flange thickness has a high sensitivity with the buckling load factor and a much lower sensitivity with the mass of the structure compared to the shell and web thickness.

From the 9000 samples analyzed, 3 design points were identified by Ansys. These 3 candidate design points are shown in Figure 12.

A comparison of the optimized geometry and the initial geometry is given in Table 8.

5.1. Designs Using T-Section Stiffeners

Different designs using T-section stiffeners in the optimization stage are shown in Figures 13, 14, 15, and 16, respectively.

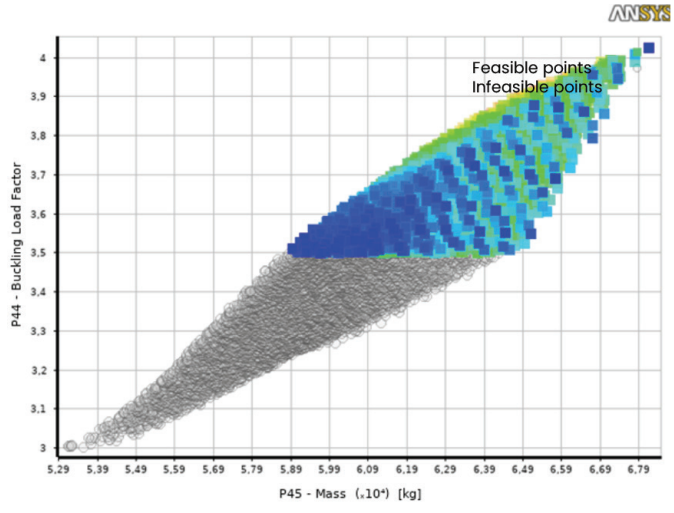

Figure 10. Design points and corresponding output parameters.

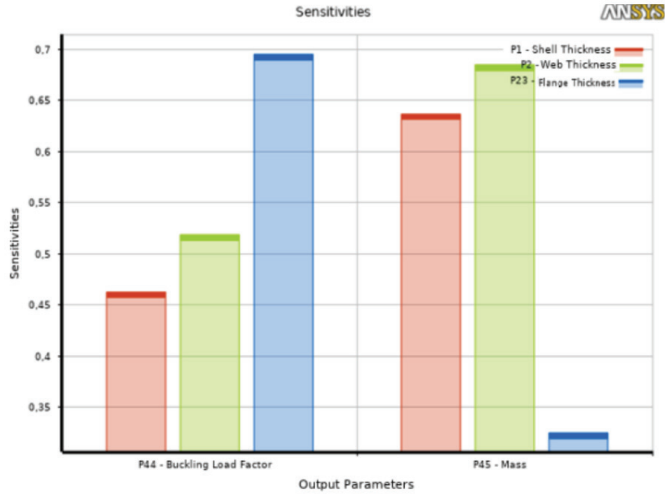

Figure 11. Sensitivity of parameters.

Candidate Points

	Candidate Point 1	Candidate Point 2	Candidate Point 3
P1 - Shell Thickness (mm)	25,092	25,716	26,332
P2 - Web Thickness (mm)	16,493	15,218	13,79
P23 - Flange Thickness (mm)	41,466	41,557	41,883
P44 - Buckling Load Factor	3,5121	3,5034	3,5029
P45 - Mass (kg)	58957	59099	59205

Figure 12. Candidate design points identified by the optimization tool.

Table 8. Comparison of initial buckling analysis and optimized analysis.

Support element	T profile	T profile
Flange thickness	37	41.5
Web thickness	17	16.5
Shell thickness	27	25
Buckling load factor	3.502	3,512
Critical buckling pressure	25.450	25.517
Structure mass (kg)	60670.43	58956.89
Internal volume (m^3)	245.66	244.90

The optimization results for the T-sections stiffened systems are given in Table 9.

5.2. Designs Using Flat Bar Stiffeners

Different from the T-sections stiffened systems, the change of buckling behavior was investigated by using flat bar stiffeners in the structure. The flat bar stiffeners to be used should have an equal moment of inertia with the T-section reinforcing element. The flat bar reinforced systems with different layouts are shown in Figures 17, 18 and 19, respectively.

The optimization results for the flat bars stiffened combined system are given in Table 10.

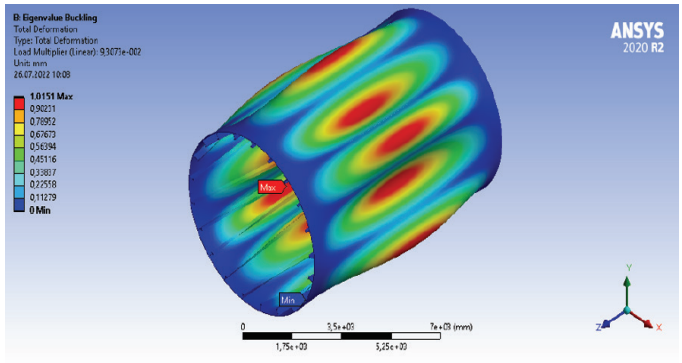

Figure 13. Twenty one T-sections stiffened longitudinal system isometric view.

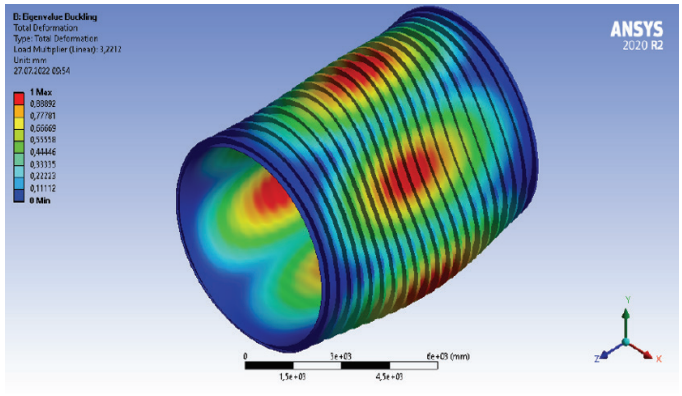

Figure 14. T-sections stiffened externally system isometric view.

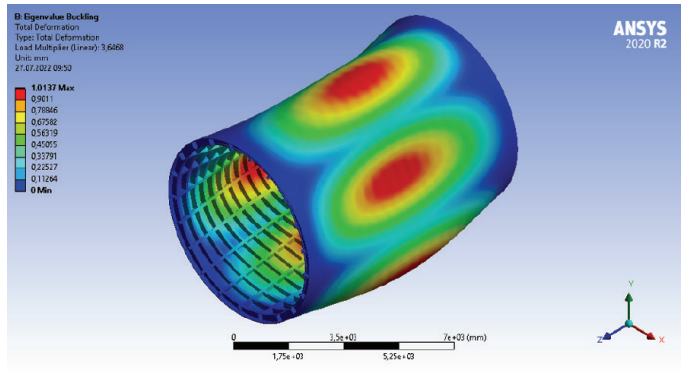

Figure 15. T-sections stiffened combined internally system isometric view.

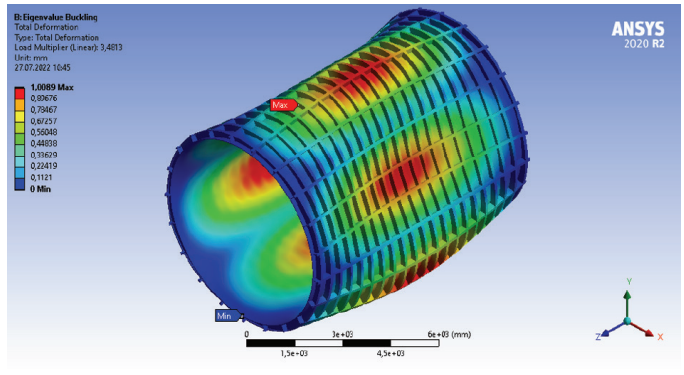

Figure 16. T-sections stiffened combined externally system isometric view.

Table 9. T-reinforced stiffened systems with the same critical buckling pressure produced as a result of optimisation.

Geometry	Transverse internal reinforced system	Longitudinal internal 21 reinforcements system	Transverse external reinforced system	Combined internally reinforced system	Combined external reinforced system
Support element	T Profile	T Profile	T Profile	T Profile	T Profile
Flange thickness (mm)	41.5	32.4	41.9	39.9	39.8
Web thickness (mm)	16.5	12.1	14.8	10.1	14.0
Shell thickness (mm)	25	120.2	28.7	28.0	27.5
Buckling load factor	3.512	3.502	3.502	3.502	3.503
Critical buckling pressure (MPa)	25.517	25.45	25.449	25.447	25.448
Mass (kg)	58956.89	182086.65	66209.12	67942.18	73565.41
Internal volume (m^3)	244.90	246.44	287.06	245.17	287.06
Distance between frames (mm)	453	934.4	453	453	453

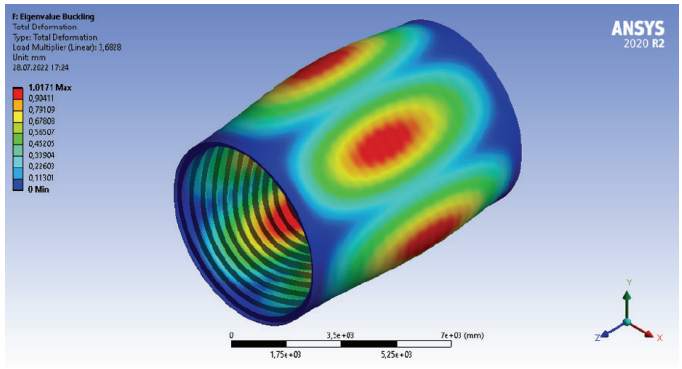

Figure 17. Flat bars stiffened internally system isometric view.

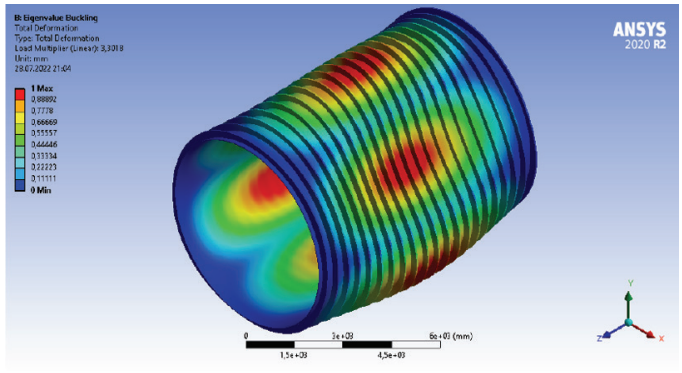

Figure 18. Flat bars stiffened externally system isometric view.

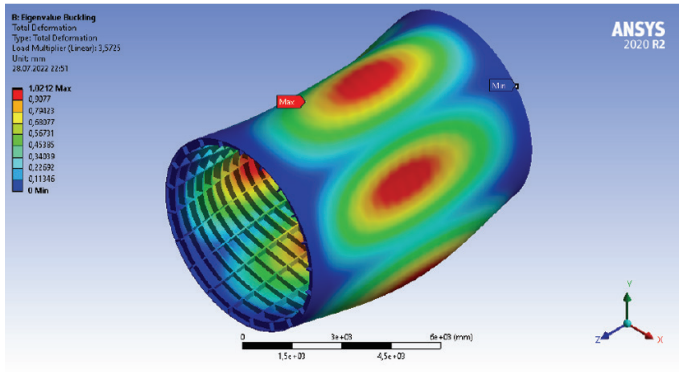

Figure 19. Flat bars stiffened combined system isometric view.

6. Conclusions

Different geometries were investigated for the optimum design of the submarine pressure hull. The objective functions were the lightest structure and the highest internal volume corresponding to the maximum critical buckling pressure. The thicknesses of the structural elements of the pressure hull were the input parameters and the sensitivity of the output parameters on weight and critical buckling pressure were investigated. Different frame profiles were used to investigate the effect of frame geometry on the design. In addition, transverse, longitudinal and combined systems using different frame profiles were investigated and appropriate frames layout was examined. As a result of the optimizations, the minimum weights of the systems with the same critical buckling pressure are given in Table 9. Table 10 shows the flat bar stiffened systems with the same critical buckling pressure. When the results were compared, it is seen that T-sections stiffened systems are more suitable in terms of buckling. When examined in terms of critical buckling pressures at the same weight, transverse internally reinforced system > transverse externally reinforced system > combined internally reinforced system > combined externally reinforced system > longitudinal internally reinforced system.

As can be seen from Table 9, the most ideal design concept in terms of buckling strength is the transverse internal T-sections stiffened system, which is widely used in the construction of many submarine pressure hulls. This system provides the same critical buckling pressure with a lighter weight compared to other systems. Although the Transverse External Reinforced System was advantageous in terms of internal volume, it was disadvantageous compared to the Transverse Internal Reinforced System in terms of weight. The results also indicated that longitudinal reinforcements were insufficient for supporting the submarine pressure hull in terms of buckling strength.

Table 10. Optimization results obtained for flat bar reinforced systems with the same critical buckling pressure.

Geometry	Transverse internal reinforced system	Transverse external reinforced system	Combined internally reinforced system
Support element	Flat bar	Flat bar	Flat bar
Web height (mm)	230	230	230
Web thickness (mm)	49.4	44.2	40.1
Shell thickness (mm)	29.7	34.9	34.3
Buckling load factor	3.502	3.502	3.503
Critical buckling pressure (MPa)	25.443	25.443	25.448
Mass (kg)	78092.40	85201.65	92421.68
Internal volume (m^3)	246.34	287.07	246.34
Distance between frames (mm)	453	453	453

Acknowledgement

This article is extracted from the Master of Science (M.Sc.) thesis, which is entitled "Optimum Structural Design of a Submarine Pressure Hull under Hydrostatic Pressure with Finite Element Method" at the İstanbul Technical University, Institute of Science and Technology, 2022.

Footnotes

Authorship Contributions

Concept: B. Eyiler, and E. Bayraktarkatal., Design: B. Eyiler, and E. Bayraktarkatal., Data Collection or Processing: B. Eyiler, and E. Bayraktarkatal., Analysis or Interpretation:B. Eyiler, and E. Bayraktarkatal., Literature Search: B. Eyiler, and E. Bayraktarkatal., Writing: B. Eyiler, and E. Bayraktarkatal.

Conflict of Interest: No conflict of interest was declared by the authors.

Financial Disclosure: The authors declared that this study received no financial support.

7. References

[1] BBC News Türkçe, "Titanik'i ziyaret ederken iletişimi kesilen denizaltı hakkında neler biliniyor?" Accessed: Nov 28, 2024. [Online]. Available: https://www.bbc.com/turkce/articles/cw0xxl7r9d2o

[2] S. Chakraborty, "Introduction to submarine design," Marine Insight, 2019. [Online]. Available: https://www.marineinsight.com/naval architecture/introduction-to-submarine-design/.

[3] J.R. MacKay, and F.V. Keulen, "Partial safety factor approach to the design of submarine pressure hulls using nonlinear finite element analysis," *Finite Elements in Analysis and Design*, vol. 65, pp. 1-16, 2013.

[4] R. V. Mises, "The critical external pressure of cylindrical tubes under uniform radial and axial load," Report no. 366, The David Taylor Model Basin, Washington, 1933.

[5] M. E. Lunchick, "Plastic axisymemetric buckling of ring-stiffened cylindrical shells fabricated from strain-hardening materials and subject to external hydrostatic pressure," Report No. 1393, The David Taylor Model Basin, Washington, 1961.

[6] T. E. Reynolds, "Inelastic lobar buckling of cylindrical shells under external hydrostatic pressure," Report No. 1392, The David Taylor Model Basin, Washington, 1964.

[7] A. R. Bryant, "Hydrostatic pressure buckling of a ring stiffened tube," Report No. NCRE/306, The David Taylor Model Basin, Washington, 1954.

[8] K. Aileni, P. Prasanna and P. C. Jain, "Buckling analysis of ring stiffened circular cylinders using Ansys," *Int J Res Appl Sci Eng Technol*, vol. 5, pp. 2287-2296, 2017.

[9] D. Oh, and B. Koo, "Empirical initial scantling equations on optimal structural design of submarine pressure hull," *Journal of Advanced Research in Ocean Engineering*, vol. 4, pp. 7-15, 2018.

[10] H. Kine, "Collapse design optimisation of ring-stiffened cylindrical pressure hulls," Master's thesis, University of Stavanger, Stavanger, 2020.

[11] R. Wei, K. Shen and G. Pan, "Optimal design of trapezoid stiffeners of composite cylindrical shells subjected to hydrostatic pressure," *Thin-Walled Structures*, vol. 166. pp.108002.

[12] N. Rathinam, B. Prabu and N. Anbazhaghan, "Buckling analysis of ring stiffened thin cylindrical shell under external pressure," *Journal of Ocean Engineering and Science*, vol 6, pp. 360-366.

[13] S. Şenol, "A structural design approach for submarine resistant hull and structural optimization based on finite element method," Master's thesis, ITU Institute of Science and Technology, Naval Architecture and Marine Engineering Department, İstanbul, Türkiye, 2021.

[14] X. Fu, Z. Mei, S. Wang, X. Bai, E. Zhang, G. Chen and H. Li, "Design method of combined stiffened pressure hulls with variable-curvature characteristic," *Ocean Engineering*, 281. pp. 114685, 2023.

[15] T. K. L. Shinoka and T. A. Netto, "Structural optimization applied to submarine pressure hulls," Elsevier, 2024.

[16] E. Fathallah and M. Helal, "Optimum structural design of deep submarine pressure hull to achieve minimum weight," *The International Conference on Civil and Architecture Engineering*, vol. 11, pp. 1-22, 2016.

[17] R. Burcher and L. Rydill, "Concepts in submarine design," Cambrige Ocean Technology Series, 1995.

[18] S. Chakraborty, "Understanding structure design of a submarine," Marine Insight, 2021. [Online]. Available: https://www.marineinsight.com/naval-architecture/submarine-design-structure-of-a-submarine/.

[19] DNV-GL Rules for Classification: Naval Vessels, Part 4 Sub-surface Ships, Chapter 1 Submarines, 2018.

[20] Bureau Veritas, Rules for the Classification of Naval Submarines, vol. 33, Fransa. 2016.

[21] A. Alogla, "Numerical study and finite element analysis of submerged cylindrical pressure hull," International Journal of Scientific Research in Science, *Engineering and Technology*, pp. 381-388, 2020.

[22] Seyir Defteri, "Denizaltı inşa çeliği-1: HY80, HY100, HY130." Accessed Nov 28, 2024. [Online]. Available:

[23] Türk Loydu, Askeri Gemilere Ait Kurallar, vol E, Sec. 111 - Denizaltılar, İstanbul, 2007.

[24] J. G. Pulos, "Structural analysis and design considerations for cylindrical pressure hulls," Report No. 1639, The David Taylor Model Basin, 1963.

[25] P. Foryś, "Optimization of cylindrical shells stiffened by rings under external pressure including their post-buckling behaviour," *Thin-Walled Structures*, vol. 95, pp. 231-243, 2015.

[26] ANSYS, Mechanical User's Guide 2021-R2, vol. 15317, Canonsburg, 2021.

RESEARCH ARTICLE

DOI: 10.54926/jnamt.2024.243

J Nav Architect Mar Technol 2024;226(2):36-48

Investigating the Impact of Bridge Resource Management on Navigational Safety by Root Cause Analysis

Gizem Kodak[1], Almila Dal[2]

[1]Department of Maritime Transportation and Management Engineering, Faculty of Maritime Studies, University of Kyrenia, Kyrenia, Turkish Republic of Northern Cyprus

[2]Department of Maritime Transportation and Management Engineering, Institute of Graduate Studies, University of Kyrenia, Kyrenia, Turkish Republic of Northern Cyprus

To cite this article: G. Kodak, and A. Dal. Investigating the impact of bridge resource management on navigational safety by root cause analysis. *J Nav Architect Mar Technol*. 2024;226(2):36-48.

Received: 27.09.2024 - **Revised:** 05.11.2024 - **Accepted:** 17.11.2024 - **Publication Date:** 31.01.2025

Abstract

Maritime transportation is a cost-effective and environmentally friendly method of transporting goods between different continents and geographies. It is a more economical means of unit transportation than road transportation. Nevertheless, the growth in maritime traffic and the advent of larger vessels may result in more severe consequences in the event of an accident. At this juncture, the most crucial instrument for averting further potential incidents is to ascertain the underlying causes of recent accidents. In this study, the M/V VITASPIRIT accident is examined through a root cause analysis utilizing the 5 Why technique and a fishbone diagram. The study results demonstrated that communication and awareness, as they pertain to human factors, are the primary dynamics influencing the accident process. Furthermore, it has been observed that effective bridge resource management represents a strategic tool for preventing maritime accidents. With the results obtained, the objective is to raise awareness regarding the prevention of similar accidents that may occur in the region and to create a reference source for policymakers to develop measures to enhance navigational safety.

Keywords: Root cause analysis, 5 Why technique, fishbone diagram, maritime transportation, navigational safety

1. Introduction

First-degree bridge resource management (BRM) is a management concept that ensures the safe and systematic organisation of ship operations. At this juncture, BRM can be defined as the meticulous planning, organisation and effective management of human, information/enformation and equipment resources that converge on the bridge with a view to ensuring the safety of navigation [1]. The conceptual framework of BRM is based on the principle that navigational safety is dependent on a multitude of individual and organisational factors, the prediction and planning of which should occur in advance. Consequently, BRM commences with the pre-voyage planning phase and culminates in the conclusion of the voyage, encompassing information gathering, dissemination and evaluation processes [2]. BRM discussions highlighted emphasise the importance of organising personnel on board in a way that ensures the effective use of bridge resources, with the aim of reducing the risk of accidents [3]. Accordingly, BRM represents an analytical methodology that can be employed

Address for Correspondence: Gizem Kodak, Department of Maritime Transportation and Management Engineering, Faculty of Maritime Studies, University of Kyrenia, Kyrenia, Turkish Republic of Northern Cyprus

E-mail: gizem.kodak@kyrenia.edu.tr

ORCID ID: orcid.org/0000-0002-1845-7901

to predict or avoid the ship encountering difficulties caused by the human factor. For BRM to function effectively, it is essential that the individuals in the team observe and follow each other's actions/inactions and reach the right conclusion by cross-checking. In other words, BRM aims to provide the skills necessary for the effective management of bridge and ship resources, functional task distribution and the ability of personnel to take timely and correct action against all situations that may be encountered at sea [4].

The implementation of BRM facilitates the execution of maritime operations in a safer and more efficient manner. This is achieved by addressing deficiencies and weaknesses within the operational framework, optimising the utilisation of available resources, and enhancing the effectiveness of processes, systems, and procedures. BRM contributes to the implementation of measures designed to minimise or eliminate the potential causes of accidents by preventing the occurrence of errors in decision-making [1]. In addition to the management of operational tasks, BRM places an emphasis on the management of risk, taking into account the emotional, cognitive and behavioural aspects inherent to the human factor. The reduction of stress and the effective functioning of the decision-making mechanism represent key target outputs of BRM. The acquisition of BRM skills by the bridge crew is essential for the efficient performance of their duties, the formulation of appropriate decisions and the safe navigation of the vessel.

The most fundamental element of the decision-making process is the identification of the root causes of the problem. Root cause analysis (RCA) is a methodology designed to diagnose the underlying causes of a problem or event and to prevent similar situations from recurring. Furthermore, this facilitates the formulation of recommendations and solutions [5]. Nevertheless, RCA has been demonstrated to be an effective tool in the context of near-miss scenarios [6]. The process of RCA entails the collection of data, the establishment of a causal table, the identification of the root cause, and the formulation and implementation of recommendations. As it is not feasible to ascertain causal factors in the absence of comprehensive information regarding the circumstances in question, the initial stage of the analysis is the collection of data. Subsequently, a causal factor chart is constructed, which organises the information obtained. A causal factor diagram is, in its most general sense, a series of diagrams that employ logical tests to elucidate the circumstances that precipitated the problem or event and the conditions that surrounded it. The subsequent phase is the identification of the root cause underlying the aforementioned causal factors. At this juncture, decision diagrams, referred to as root cause maps, serve to structure the reasoning process of decision-makers, facilitating the identification of root causes. The final stage of the analysis is the formulation of recommendations and solutions aimed at preventing the recurrence of the problem/incident in accordance with the identified root causes [7].

In recent times, there has been a notable increase in the significance attributed to RCA within the academic literature, particularly in the context of case studies within disciplines such as maritime and aviation. The analysis of actual accidents is essential for the formulation of inferences aimed at accident prevention [8]. In other words, accidents can only be prevented when they are correctly defined and understood [9,10]. At this juncture, the analysis of past accidents is of paramount importance for the development of strategic measures to prevent potential future accidents. In this study, the hypothesis that BRM is an effective tool in preventing maritime accidents is investigated and its impact on the safety of navigation is examined through RCA based on a real maritime accident.

1.1. Literature Review

In the existing literature, BRM was initially designed with the objective of strengthening the relationship between the master and pilot. However, it soon evolved into a safety culture that addresses the human factor in terms of performance and safety [11]. A study on safety culture and hazard risk perception was conducted with the participation of 77 pilots in Australia and New Zealand. The study emphasised that when a pilot is present on the bridge, which is essentially an onboard working environment, there should be a shared sense of purpose between the master, bridge crew and pilot [12]. In a further study examining the role of human factors and BRM in reducing maritime accidents, it was emphasised that crew resource management (CRM) is fundamental to improve and increase the operational efficiency of shipping. Furthermore, CRM/BRM training is now regarded as an essential component of the human error management perspective [13]. In the study on human and organisational factors in maritime accidents, the Human Factors Analysis and Classification System (HFACS) was employed as a methodology for the analysis of collision accidents reported by the UK Marine Accident Investigation Branch (MAIB). The analysis demonstrated that the majority of collisions were attributable to flawed decision-making processes and underscored the influence of environmental factors (restricted visibility, misuse of equipment), operator conditions (loss of situational awareness, lack of attention) and personnel factors (deficiencies in inter-ship communication and BRM). In consequence, the inefficient management of bridge resources is characterised by a lack of coordination among crew members, a deficiency in situational awareness and communication problems. The

study highlighted the significance of BRM in navigational scenarios under pilotage in restricted waters and underscored the pivotal role of the Safety Management System in high-risk situations in offshore navigation [14]. Another study employed the Analytic Hierarchy Process (AHP) to analyse grounding type accidents. Obtained findings indicated that the primary causes of such accidents are deficiencies in communication and coordination within the scope of BRM, position calculation errors, inadequate lookout, errors in interpreting events, ineffective use of charts, inefficient use of bridge equipment and burnout in personnel. The study concluded that improvements should be made to training and education, with a particular focus on ECDIS training, which should be made compulsory and improved. Additionally, the regulation of the crew's working and resting hours, as specified in the STCW Code, should be given greater consideration [15]. Another study defined the maritime accident phenomenon as a problem in a holistic framework and proposed a RCA approach for solution [9]. A Fuzzy FTA has been conducted for marine accidents in the Arctic between 1993 and 2011. In this context, analysing 65 reported accidents/incidents based on the MAIB report. The results of the study showed that personal injury was the most frequently observed incident, while injury due to personal negligence had the highest priority among the main causes of marine accidents [16]. HFACS-Fuzzy Cognitive Mapping was used for fire prevention modeling on ships. The study drew attention to the creation of a proactive fire safety model, the importance of consistent prediction of root causes, the production of intelligent fire systems and the human factor [17]. SHip Accident Root cause Evaluation (SHARE) technique was used for RCA of ship accidents. As a result of this study, a taxonomy that provides standardization in the expression of root causes was developed and a reference methodology was obtained by applying the fuzzy SWOT (strengths, weaknesses, opportunities, and threats) / AHP method in SHARE. The research provides a model for standardizing the existing ship accident investigation and investigation reports [18]. The role of accident analysis methods on accident causation was investigated and presented a systematic review of applications between 1990 and 2018 [19]. Qualitative and quantitative syntheses of the study results were performed for Accimap, HFACS, Systems Theoretic Accident Model and Processes (STAMP) - Causal Analysis based on STAMP and functional resonance analysis method (FRAM). The results highlighted the need to develop new accident analysis approaches in the context of safety science. In another study focusing on BRM based on safety of navigation, a risk assessment of the human error factor in oil tanker collisions using Fault Tree Analysis and Cognitive Reliability Error Analysis method was proposed. Thirty nine experts participated in the study and provided their expert opinions, especially for the navigation of oil tankers around Taiwan waters. The results of the study showed that lack of communication in BRM, lack of communication between ships, fatigue, and violation of navigation rules increase the likelihood of collision-type accidents on oil tankers [20]. HFACS and FTA model were used for collision risk factors analysis of icebreaker assistance in ice-covered waters. Within the scope of the study, the collision risk factors were classified according to the HFACS-SIBCI (ship collision accidents between assisted ships and icebreakers in ice-covered waters) model and the fault tree model was proposed to analyze the collision risk factors under icebreaker assistance [21]. A dynamic Bayesian Network (BN) model was proposed for ship-ice collision risk in Arctic waters. The results of the study pointed out that the main risk factors in the region are location, weather, icing and speed [22]. Another study have highlighted the importance of BRM to avoid maritime accidents caused by human error and emphasized that dysfunctional BRM is an influential factor in the joint errors of pilot/bridge personnel. The results of the study showed that pilot errors are mostly caused by poor communication and pointed out that passage planning should be discussed in pilotage waters before the pilot joins the ship [23]. Other study have evaluated whether applying BRM to simulator-based maritime training is effective in improving non-technical skills and navigational performance. Non-technical skills were evaluated as team communication, decision-making, situational awareness, leadership and management skills for effective utilization of all available technical and personal resources during routine operations and emergencies. As a result of the study, it was observed that the BRM trainings improved the attitudes, behaviors and performance of the training participants regarding BRM [24]. Another study examined Arctic shipping in terms of risk management. In this context, navigational factors affecting accident risk were investigated using bibliometric and systematic perspectives. The results of the study showed that the risk models and their underlying evidence were explained by linear accident causality models such as HFACS, FTA and BN [25]. FRAM was used in a real maritime accident and analyzed the M/T PRESTIGE ship accident as a case study. The obtained results provided a comprehensive analysis of marine accidents, focusing on the functions and variabilities of the systems, and provided a functional tool to analyze the ship operations that cause accidents. However, it is recommended to integrate FRAM with other methods to obtain higher resolution results [26]. A BN-based emergency decision-making model was developed for collision-type accidents in the Yangtze River. Offering intuitive representation, easy implementation, and

the ability to deal with incomplete and updated information, the study presented a practical and novel decision-making method for conflict-type accidents [27]. A framework was proposed for quantitative analysis of the causality of grounding accidents in Arctic shipping. Within the scope of the study, the potential risk factors of grounding type accidents were identified and the interrelationship of these factors was reflected using the AcciMap model. Critical risk factors were identified for quantitative analysis using the BN model and risk control options-*RCOs* were proposed to reduce the risk of grounding of ships in Arctic shipping [28]. Collision type accidents were analyzed using by FTA and multiple correspondence analysis. In this context, 513 collision accidents for all ship types between 1977 and 2022 were analyzed and importance and probability values were calculated for the primary causes of accidents. With the results of the study, the most violated COLREG Rules were determined and recommendations were made to reduce potential collision type accidents [29]. A risk assessment of ship steering gear failures was conducted using by Fuzzy BN. The study results depicted a valid probabilistic effect of root causes and emphasized the importance of line components in mechanical/electrical failures [30]. A data-driven BN for risk analysis of global marine accidents was developed. The results showed that the six most important risk factors affecting maritime accidents are ship type, ship operation, voyage region, deadweight, ship length and machinery power [8].

According to the data of the European Maritime Safety Agency, the biggest share in maritime accidents occurring between 2014 and 2021 was determined as the human factor with 81.1% [31]. Considering that 80% of the world's trade is carried out by sea [32], the importance of measures to increase the safety of navigation emerges [33,34]. Determining the root causes of recent maritime accidents is critical for developing effective measures to prevent possible accidents with a similar profile. At this point, BRM becomes a strategic tool in terms of increasing navigational safety by organizing ship employees to take the right actions at the right time both individually and as a team member. BRM, which refers to the effective management of bridge resources in terms of people, information and equipment, evaluates the main elements of human error within the framework of safety of navigation within the scope of miscommunication / inadequate English, over fatigue (burnout syndrome) and situational awareness. In this study, the effect of BRM on navigational safety has been investigated and the M/V VITASPRIT accident has been analyzed by using the 5 Why technique and fishbone diagram within the scope of RCA. It is aimed to provide a holistic perspective to the reader by schematizing the accident and its possible causes in a single location and providing a visual tool that structures the solution process with cause and effect relationships. In addition, it is thought that the root causes obtained will also be a reference source for policy makers to develop measures to increase the safety of navigation in order to prevent accidents with a similar profile that may occur in the region.

2. Materials and Methods

This study employed a RCA utilising the 5 Why technique and fishbone diagram to investigate the M/V VITASPIRIT accident that occurred in the İstanbul Strait. In the course of this research, the final investigation report of the Ministry of Transport and Infrastructure of the Republic of Türkiye Transportation Safety Investigation Center for serious maritime accidents was taken as a reference, and the findings of the accident were evaluated in terms of the impact of BRM on the safety of navigation. This evaluation was conducted using the structured interview technique, with the participation of six masters and three chief engineers.

The 5 Why technique, initially conceptualised by Sakichi Toyoda in 1958, entails a progressive questioning process whereby the "why" question is repeatedly posed [35-37]. In other words, the 5 Why technique, which is based on repeatedly asking the question "Why?" to the problem, involves asking and answering the question as many times as necessary to identify the root cause or the end of the causal chain [38]. The objective of the 5 Why technique is to identify the root cause by elucidating the cause-and-effect relationships associated with the problem. Once the potential causes of the problem have been identified, the "why" question can be posed five times in succession to create a strategic roadmap to the root cause. The number of repetitions may vary, depending on the nature of the problem [39]. The technique is illustrated in Figure 1.

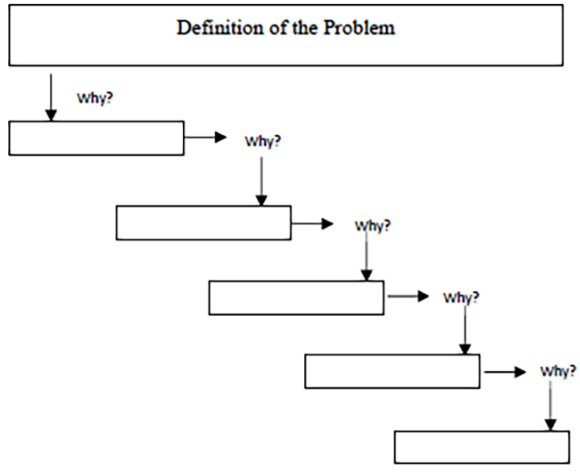

Figure 1. 5 Why technique process [40].

Another frequently utilised RCA technique in the literature is the fishbone diagram, also known as cause and effect analysis. This is often employed in conjunction with the 5 Why technique. The fishbone diagram, developed by Kaoru Ishikawa in 1942, is a technique for classifying factors affecting a problem by defining the relationships between causes and effects [36,37].

A fishbone diagram is a decision-making technique that is used to identify the potential causes of a specific event, situation, or problem. It is based on the principle of revealing the factors that contribute to the problem and identifying and improving the factor that has the most significant impact on the result [41-43]. The diagram offers the advantage of visually representing multiple causes of a problem, facilitating the identification of the factors contributing to the problem and their categorisation according to thematic similarities. The initial stage of the process is to identify the issue and delineate the boundaries of the diagram. In the second stage, the potential sub-causes of the problem are categorised and grouped under main headings [42]. In the initial phase, the diagram assumes the configuration depicted in Figure 2.

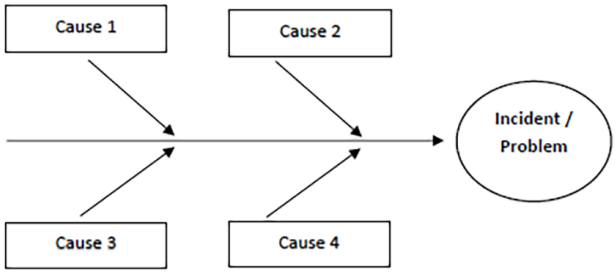

Figure 2. Fishbone diagram: identifying the problem and classifying the main causes.

In the subsequent phase, the sub-causes of the categorised primary causes are identified and each sub-cause is delineated by a distinct branch drawn on the stem of the related primary cause. In other words, for each identified cause, the question "Why?" is posed once more, thereby creating deeper levels of cause [39]. Consequently, the diagram assumes the configuration depicted in Figure 3.

In the final stage of the process, all participants in the research evaluate the sub-causes and identify the root cause of the problem [42]. The benefits of identifying the root cause by progressively deepening the research question, categorising the factors influencing the problem and visualising the established cause-and-effect networks make the fishbone diagram an effective tool for case analysis. It is anticipated that the integration of the fishbone diagram with the 5 Why technique will facilitate the identification of the root causes of accidents. Furthermore, the findings obtained will be instrumental in understanding the role of BRM on navigation safety. The findings obtained within the scope of the study were evaluated through structured interviews with six masters and three chief engineers, with the objective of determining the root and sub-causes of the accidents. The participants were selected on the basis of their expertise in interpreting accident dynamics and in providing a dual perspective from both the deck and engine, as outlined in Table 1.

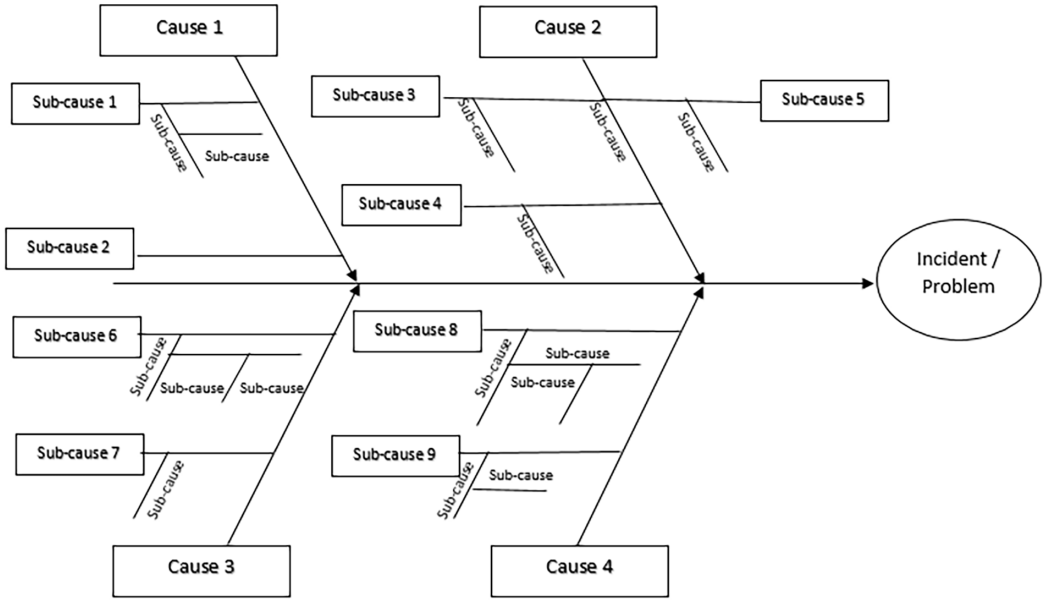

Figure 3. Fishbone diagram: identification of sub-causes.

3. Findings

In the context of the study, accident records were gathered from Republic of Türkiye Ministry of Transport and Infrastructure Transportation Safety Investigation Center [44]. These records were contained a number of sources, including ship technical information, navigational information, accident information, personnel information and environmental factor information. The findings are presented in Figure 4.

As illustrated in Figure 4, the findings are classified into five distinct categories. These are classified as follows: technical information (including full length, width, type, flag, tonnage and class); navigational information (including departure/arrival, cargo and pilot status); accident information (including accident location, time, type, fatalities/injuries and pollution information); personnel information (including number and nationality of personnel); and environmental factors (including current, wind and visibility conditions). The accident summary analysis, created in accordance with the findings obtained, is presented in Figure 5.

Table 1. Personal and professional characteristics of the participants.

Participants	Gender	Age	Professional experience	Profession
K1	Male	64	35	Oceangoing Master
K2	Male	62	31	Oceangoing Master
K3	Male	62	17	Oceangoing Master
K4	Male	57	28	Oceangoing Master
K5	Male	65	42	Oceangoing Master
K6	Male	67	43	Chief Engineer
K7	Male	42	24	Chief Engineer
K8	Male	45	21	Oceangoing Master
K9	Male	40	18	Chief Engineer

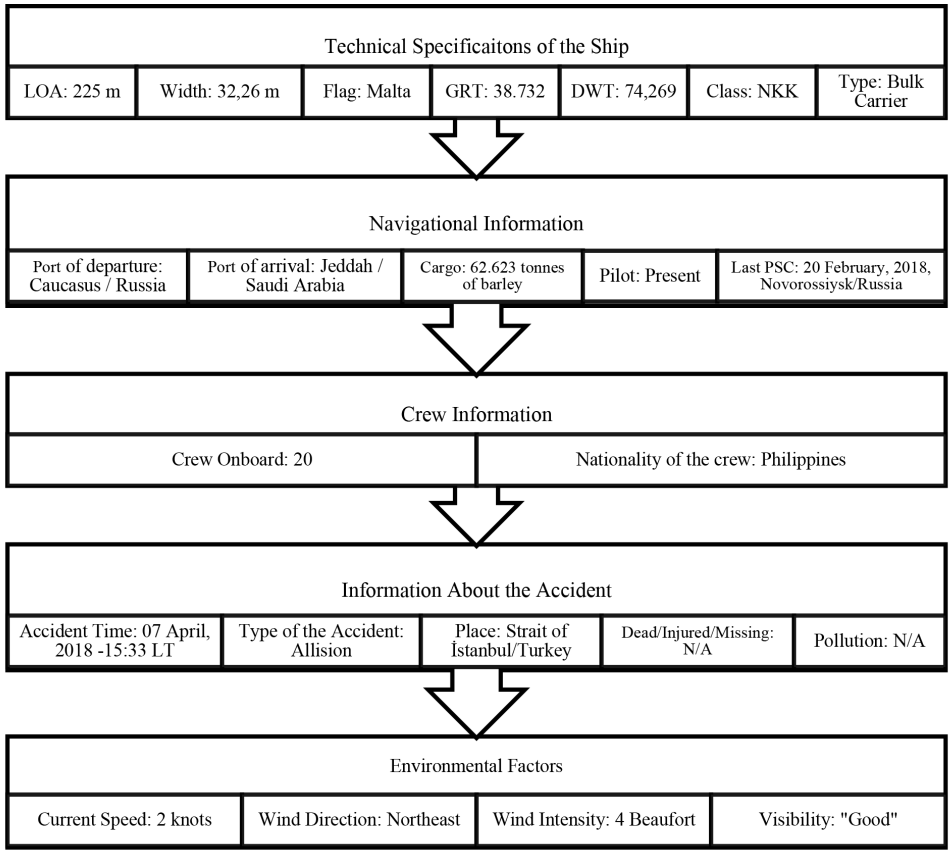

Figure 4. Classification of accident information.

The results of the 5 Why technique, which identify potential underlying causes of the MV VITASPIRIT accident in the İstanbul Strait, are presented in Figure 6.

When the accident findings evaluated by the participants were analyzed within the scope of the 5 Why technique, it was seen that the root causes of accidents were grouped under five categories. The first category is analyzed in terms of equipment maintenance and materials. According to this, the most superficial reason why the ship allided to the mansion is that no effective maneuver could be made to avoid the accident. Under the 5 Why technique, the question of why no effective maneuver could be performed is explained by the loss of the ship's steering ability. When the question of why was asked for the second time, it was found that the reason was that the main engine shutdown. The question asked about why the main engine shutdown is explained by the drop in RPM. The fourth why question indicated that the reason for the drop in RPM was the sudden loss of cooling

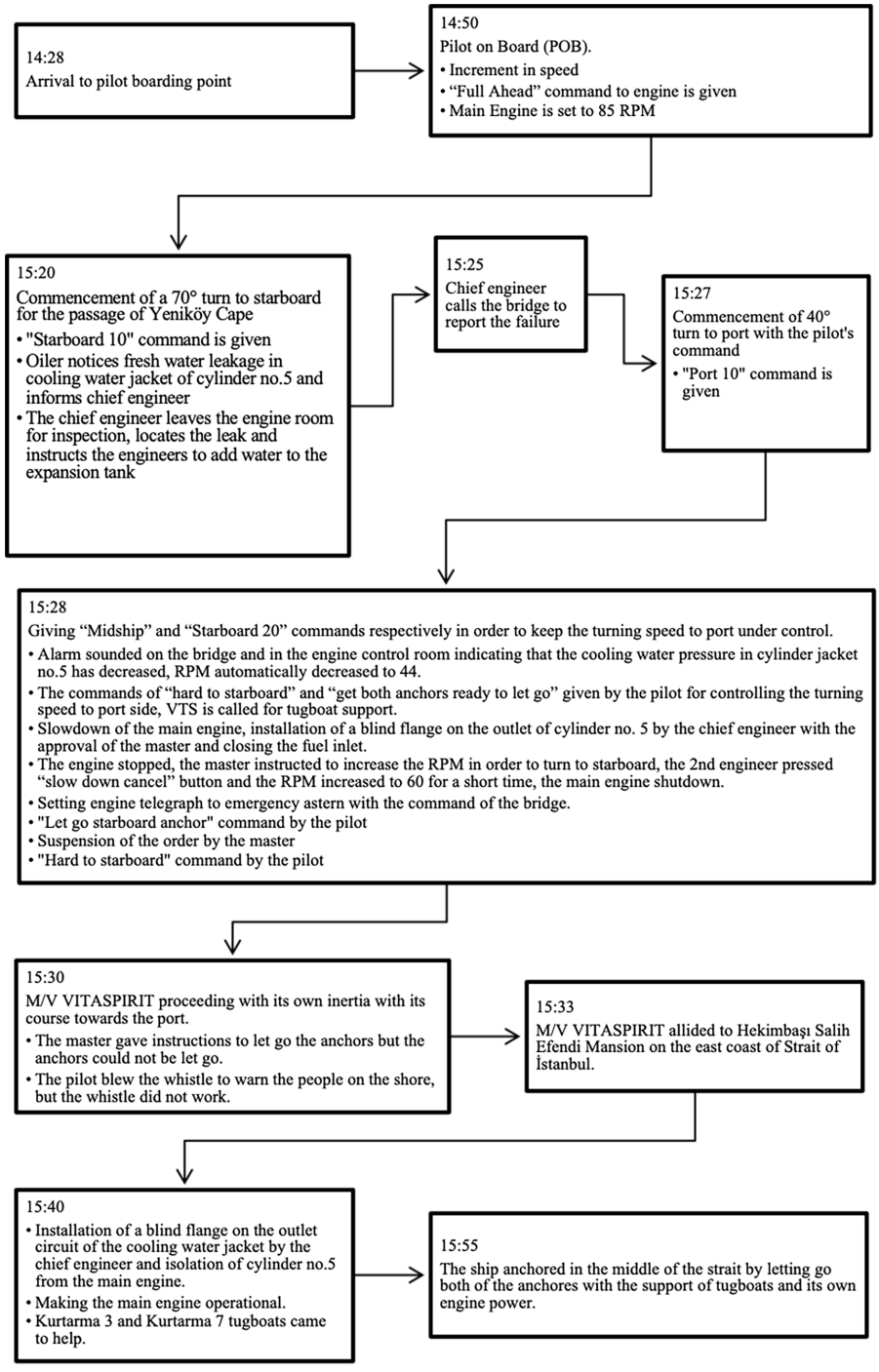

Figure 5. Accident summary review [33].

water. When the question was asked for the fifth time, it was discovered that this situation was due to a water leak in the cylinder jacket number 5. So at the end of the process of the 5 Why technique, it was concluded that one of the root causes of the accident was the material and the equipment. The corresponding process is shown in Figure 7.

It is considered that miscommunication due to inadequate English within the scope of BRM was another main factor that caused the accident. Accordingly, in the process that started with the problem at cylinder jacket number 5 and turned into an accident when the necessary action could not be taken at the right time; it is considered that one of

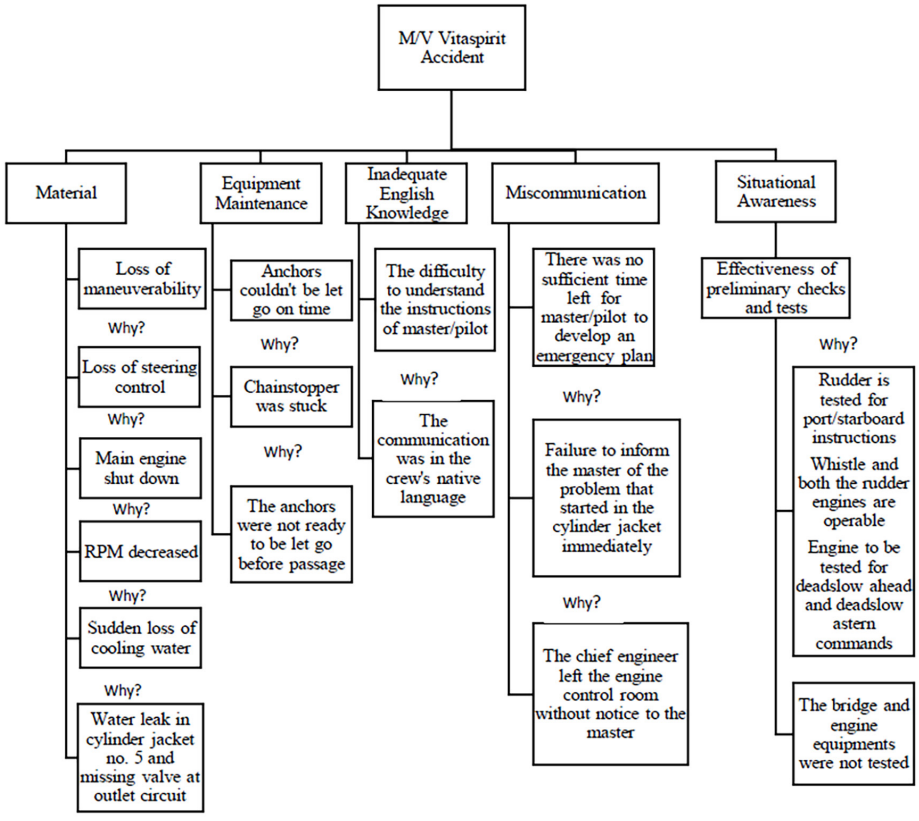

Figure 6. 5 Why technique findings for the M/V VITASPIRIT accident.

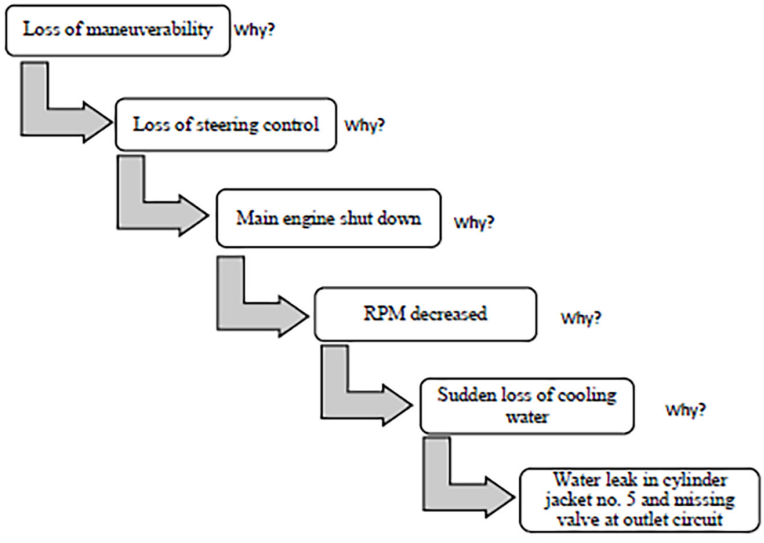

Figure 7. Identification of sub-causes: Material.

the possible main causes of the accident was the difficulty encountered by the crew in understanding the pilot's orders. The "why" question asked for this problem is explained by the fact that communication on board is mostly done in the native language of the crew. The re-asked why question leads to the conclusion that the root cause of the communication difficulty is inadequate English. The related process is shown in Figure 8 below.

Within the scope of BRM, the lack of effective management of the information source created another miscommunication between the master / pilot and master / chief engineer. It is considered that this situation changed the course of the accident by missing the opportunity to call vessel traffic service and tugboats for help earlier. The findings obtained within the scope of the 5 Why technique regarding the process are shown in Figure 9.

Situational awareness, which is the most important element of human factor within the framework of resource management, is considered to be one of the root causes of the accident. The fact that there were only 7 minutes between the reporting of the engine failure to the bridge and the accident left no time for the master/pilot to develop an emergency plan. However, according to ISM, any change in speed due to engine/rudder failures should be reported immediately to the bridge by the engineers [44]. Failure to inform the master immediately about the problem that started in the engine caused a maneuvering disagreement between the master and the pilot and did not leave time to develop an effective accident preventive strategy. It is considered that the chief engineer's leaving the engine control room to solve the problem without informing the master caused time loss. The findings obtained within the scope of 5 Why technique regarding situational awareness are given in Figure 10.

The results obtained showed that the lack of situational awareness, which is evaluated within the scope of BRM, is both a root cause in itself and a sub-cause that triggers other factors. As a result of the 5 Why technique, situational

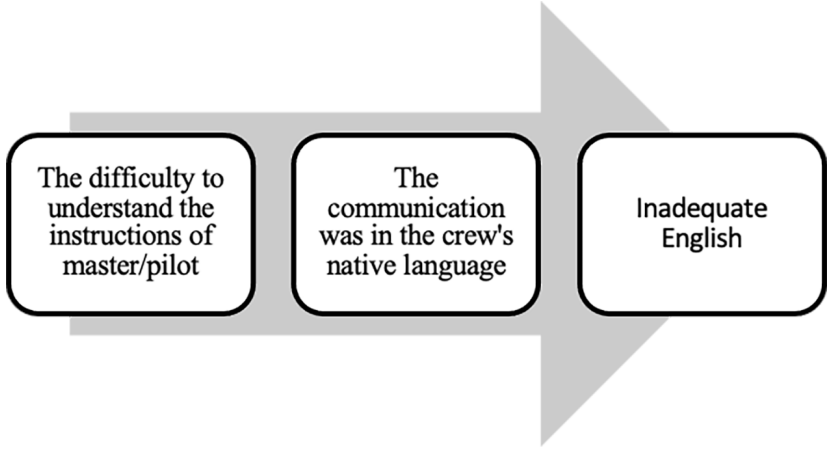

Figure 8. Identification of sub-causes: Miscommunication/insufficient English.

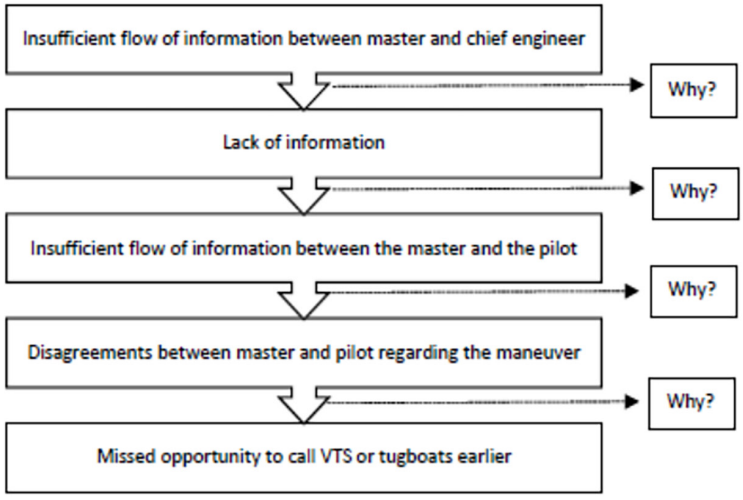

Figure 9. Identification of sub-causes: Miscommunication - lack of information flow.

awareness categorized under the human factor also plays a decisive role in material maintenance attitude and equipment testing/drills. The findings of the accident indicate that the anchors could not be let go in time because the chainstopper could not be moved after the "let go" command. This situation draws attention to the lack of preparation and reveals the importance of adopting routine checks and preparations on board as a safety culture rather than a procedure. The results obtained within the scope of the 5 Why technique formed the main categories of the fishbone diagram. Within the scope of the study, the root causes of the accident were categorized within the framework of "Management (BRM), Equipment, Material, Human and Communication" and the results of the fishbone diagram integrated with the 5 Cause Technique are given in Figure 11.

Within the scope of the fishbone diagram, the root and sub-causes of the accident were determined as follows.

Management: Ineffective management of human, information and equipment resources. It is thought that the following vulnerabilities observed during the preliminary controls of the bridge and engine equipments weakened the safety of navigation and paved the way for the accident.

- Preliminary check of rudder's responsiveness with hard to port/starboard commands.

- Preliminary check that the dual rudder engines are operational.

- Testing the main engine including deadslow ahead and deadslow astern commands.

- Not keeping both anchors ready to let go before the strait passage.

- Preliminary check that the whistle is operational.

Equipment: Due to the water leakage that started in cylinder jacket number 5, the engine power and speed decreased, resulting in the shutdown of the main engine. This situation has weakened the steering ability of the ship and eliminated the maneuvering capability.

Material: Age, material and equipment were considered to be the determining factors in terms of performance on

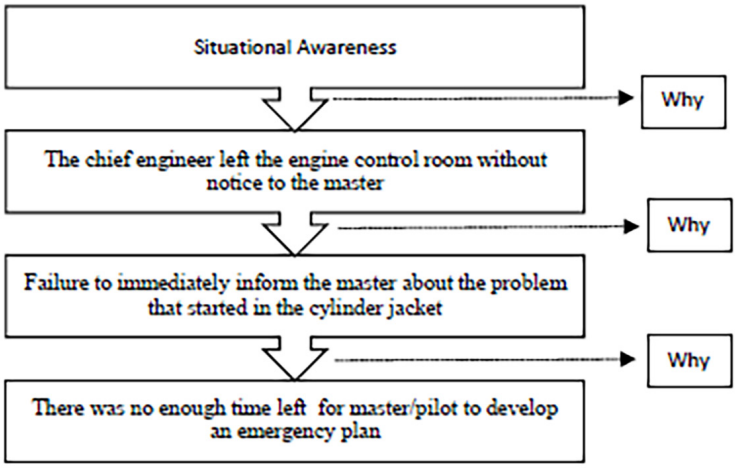

Figure 10. Identifying sub-causes: Situational awareness.

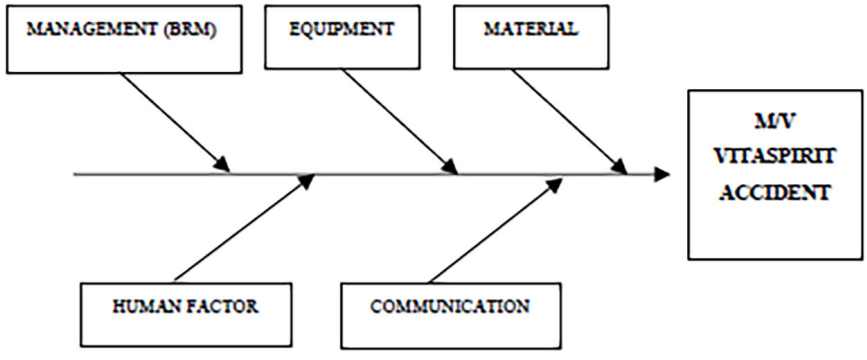

Figure 11. Fishbone diagram classification of main causes.

the ship, which was the subject of the accident. The water leak in the cylinder jacket, the inability to release the chain stopper running over the anchor chain as commanded let go and consequently the inability to let go the anchors in time to counter the forward motion of the ship, as well as the observation that the ship's whistle did not work when instructed, indicate the lack of maintenance and preparation of the ship's components/parts.

Human Factor: The results of the research draw attention to the fact that the human factor is determinant on the accident, especially within the framework of situational awareness. In this respect, the chief engineer's leaving the engine control room without informing the master in order to intervene in the water leakage that took place in the number 5-cylinder jacket is considered to be one of the critical factors affecting the course of the accident. This situation caused the master to be unaware of the need to isolate the leaking cylinder and revealed the lack of preparedness for emergency situations on the bridge. The time loss in this process also left no time for the master and pilot to develop an emergency plan.

Communication: The results obtained within the scope of the study support the conclusion that the lack of effective communication between the master and the chief engineer and between the master and the pilot were the factors that paved the way for the accident. The chief engineer's failure to provide immediate information resulted in the master not being aware that the propulsion power might be lost or that he would have to stop the engine to isolate the damaged cylinder jacket [44]. This situation also triggered a disagreement about maneuver between the master and the pilot. However, it was found that inadequate English was a critical factor in the accident. Although the working language onboard was English, the fact that the vessel's crew communicated in their native language made it difficult for the pilot to follow the engine-related conversations and for the crew to understand and implement the emergency instructions given by the pilot in a timely manner. The fishbone diagram formed according to the findings is shown in Figure 12.

4. Discussion

Within the scope of the RCA conducted regarding the M/V VITASPIRIT accident, it was observed that the root causes of the accident were the building blocks within the BRM. The results of the study showed that the failure to manage human, information and equipment resources correctly and effectively could be the possible main causes of the accident and drew attention the importance of the preliminary preparations needed to be carried out and controls within the scope of BRM. At this point, it has been observed that communication and awareness, which separate the human factor from the technical elements, are the main dynamics affecting the accident process. Also, the findings of the accident point to the critical importance of equipment-based maintenance activities. The fact that a small problem in the cylinder jacket can pave the way to a major accident has drawn attention to the importance of daily checks carried out

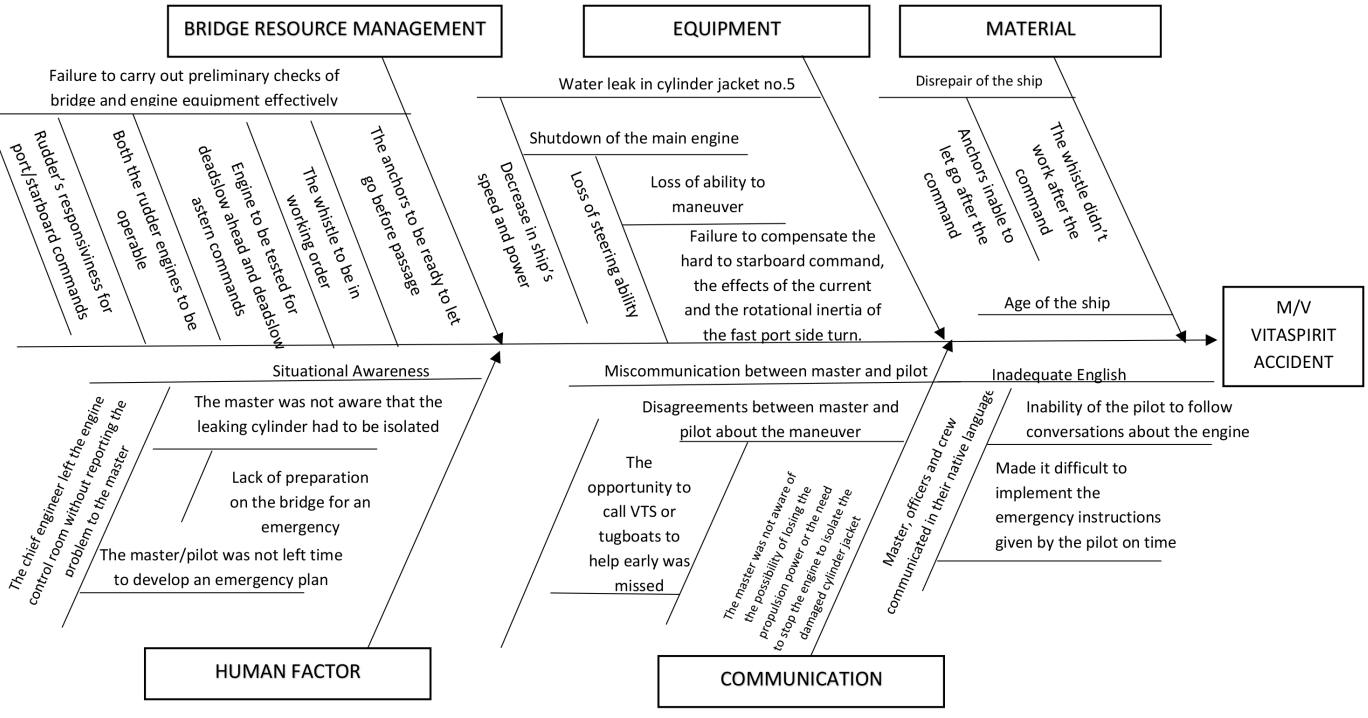

Figure 12. Fishbone Diagram of the root causes of the M/V VITASPIRIT accident.

with situational awareness apart from the inspection period. In this respect, one of the biggest advantages of BRM has emerged as that it creates awareness for equipment-based controls in relevant areas and transforms self-inspection into a safety culture. At this point, the results of the study confirmed the hypothesis that efficient resource management is an effective tool to prevent accidents and that BRM needs to be strengthened to improve safety of navigation.

5. Conclusions

This research is a case study on the M/V VITASPIRIT accident in order to observe the impact of BRM on navigational safety. The in-depth analysis of this accident has provided concrete outputs to the literature on BRM. It is important to examine accidents with similar profiles in order to verify, strengthen and generalize the results obtained in this accident. The common findings obtained by analyzing different accidents will serve as a reference for updating the existing legal practices and regulations within the scope of BRM in a way to increase the safety of navigation. At this point, it is suggested that future studies should carry the research further and produce a road map for policy makers in line with the common findings.

Footnotes

Authorship Contributions

Concept/Design: G. Kodak, Data Collection or Processing: G. Kodak, Analysis or Interpretation: G. Kodak, Literature Review: G. Kodak, and A. Dal., Writing, Reviewing and Editing: G. Kodak, and A. Dal.

Conflict of Interest: No conflict of interest was declared by the authors.

Financial Disclosure: The authors declared that this study received no financial support.

6. References

[1] KAİK: Republic of Turkey Ministry of Transport, Maritime Affairs and Communications, Accident Investigation and Investigation Board, 2017. [Online]. Available: https://ulasimemniyeti.uab.gov.tr/deniz. [Accessed: Dec. 30, 2023].

[2] Oways Online. Merchant Navy MMD Exam Book Store, Bridge resource management on ships, Bridge resource management & bridge team management, 2021. [Online]. Available: https://owaysonline.com/bridge-resource-management-on-ships/. [Accessed: Nov. 12, 2023].

[3] S. Campaniço Cavaleiro, C. Gomes, and M. P. Lopes, "Bridge Resource Management: Training for the Minimisation of Human Error in the Military Naval Context," *Journal of Navigation*, vol. 73, no. 5, pp. 1146-1158, 2020.

[4] IMO. International Maritime Organization, 2024. [Online]. Available: https://www.imo.org/en/OurWork/HumanElement/Pages/STCW-Convention.aspx. [Accessed: Sept. 20, 2024].

[5] M. F. Peerally, S. Carr, J. Waring, and M. D. Woods, "The problem with root cause analysis," *BMJ Quality & Safety*, vol. 25, no. 7, pp. 1-6, 2016.

[6] S. H. Sakdiyah, N. Eltivia, and A. Afandi, "Root cause analysis using fishbone diagram: company management decision making," *Journal of Applied Business, Taxation and Economics Research (JABTER)*, vol. 1, no. 6, pp. 566-576, 2022.

[7] J.J. Rooney and L.N.V. Heuvel, "Root Cause Analysis for beginners," Quality Basics, 2004. [Online]. Available: https://edisciplinas.usp.br/pluginfile.php/4603298/mod_resource/content/1/Quality%20progress%20Root_Cause.pdf [Accessed: Nov. 12, 2023].

[8] Y. Liu, X. Ma, W. Quao, L. Ma, and B. Han, "A novel methodology to model disruption propagation for resilient maritime transportation systems-a case study of the Arctic maritime transportation system," *Reliability Engineering & System Safety*, vol. 241(2024), pp. 109620, 2023.

[9] T. Keçeci, Proposal for a root cause analysis approach for the investigation of the ship accident complex problem, Ph.D. Thesis, Istanbul Technical University, Istanbul Institute of Science and Technology, İstanbul, 2015.

[10] E. Hollnagel, Barriers and accident prevention. Aldershot, UK: Ashgate, 2004.

[11] P. O'Connor, "Assessing the Effectiveness of Bridge Resource Management Training," *International Journal of Aviation Psychology*, vol. 21(2011), pp. 357-374, 2011.

[12] R.M. Darbra, J.F.E. Crawford, C. W. Haley and R. J. Morrison. "Safety culture and hazard risk perception of Australian and New Zealand maritime pilots," *Marine Policy*, vol. 31(6), pp. 736-745, 2007.

[13] H. Yousefi and R. Seyedjavadin, "Crew Resource Management: The Role of Human Factors and Bridge Resource Management in Reducing Maritime Casualties," *TRANSNAV*, vol. 6, pp. 391-396, 2012.

[14] C. Chauvin, S. Lardjane, G. Morel, J.P. Clostermann and B. Langard, "Human and organizational factors in maritime accidents: Analysis of collisions at sea using the HFACS," *Accident Analysis & Prevention*, vol. 59, pp. 26-37, 2013.

[15] Ö. Uğurlu, "Application of Fuzzy Extended AHP methodology for selection of ideal ship for oceangoing watchkeeping officers," *International Journal of Industrial Ergonomics*, vol. 47, 132-140, 2015.

[16] S. Kum and B. Şahin, "A root cause analysis for Arctic Marine accidents from 1993 to 2011," *Safety Science*, vol. 74, pp. 206-220, 2015.

[17] O. Soner, U. Asan and M. Celik, "Use of HFACS-FCM in fire prevention modeling on board ships," *Safety Science*, vol. 77, pp. 25-41, 2015.

[18] T. Keçeci and O. Arslan, "SHARE technique: A novel approach to root cause analysis of ship accidents," *Safety Science*, vol. 96(2017),1-21, 2017.

[19] A. Hulme, N. A. Stanton, G. H. Walker, P. Waterson and P. M. Salmon, "What do applications of systems thinking accident analysis methods tell us about accident causation? A systematic review of applications between 1990 and 2018," *Safety Science*, vol. 117, pp. 164-183, 2019.

[20] S. T. Ung, "Evaluation of human error contribution to oil tanker collision using fault tree analysis and modified fuzzy Bayesian Network based CREAM," *Ocean Engineering*, vol. 179, pp. 159-172, 2019.

[21] M. Zhang, D. Zhang, F. Goerlandt, X. Yan and P. Kujala, "Use of HFACS and fault tree model for collision risk factors analysis of icebreaker assistance in ice-covered waters," *Safety Science*, vol. 111, pp. 128-143, 2019.

[22] B. Khan, F. Khan and B. Veitch, "A Dynamic Bayesian Network model for ship-ice collision risk in the Arctic waters," *Safety Science*, vol. 130, pp. 104858, 2020.

[23] J. Sánchez-Beaskoetxea, I. Basterretxea-Iribar, I. Sotés, and M. M. M. Machado, "Human error in marine accidents: Is the crew normally to blame?" *Maritime Transport Research*, vol. 2, pp. 100016, 2021.

[24] S. Röttger and H. Krey, "Experimental study on the effects of a single simulator-based bridge resource management unit on attitudes, behaviour and performance," *Journal of Navigation*, vol. 74, pp. 1127-1141, 2021.

[25] S. Fu, F. Goerlandt and Y. Xi, "Arctic shipping risk management: A bibliometric analysis and a systematic review of risk influencing factors of navigational accidents," *Safety Science*, vol. 139, pp. 105254, 2021.

[26] E. Salihoglu and E. B. Besikçi, "The use of Functional Resonance Analysis Method (FRAM) in a maritime accident: A case study of Prestige," *Ocean Engineering*, vol. 219, pp. 108223, 2021.

[27] B. Wu, C. Zhao, T.L.Yip, "A novel emergency decision making model for collision accidents in the Yangtze River," *Ocean Engineering*, vol. 223, pp. 108622, 2021.

[28] S. Fu, Y. Yu, J. Chen, Y. Xi, M. Zhang, "A framework for quantitative analysis of the causation of grounding accidents in arctic shipping," *Reliability Engineering & System Safety*, vol. 226, pp. 108706, 2022.

[29] H. Uğurlu and İ. Çiçek, "Analysis and assessment of ship collision accidents using Fault Tree and Multiple Correspondence Analysis," *Ocean Engineering*, vol. 245, pp. 110514, 2022.

[30] B. Goksu, O. Yuksel, C. Sakar, "Risk assessment of the Ship steering gear failures using fuzzy-Bayesian networks," *Ocean Engineering*, vol. 274, pp. 114064, 2023.

[31] EMSA. European Maritime Safety Agency, 2022. [Online]. Available: https://www.emsa.europa.eu/damage-stability-study/items.html?cid=77&id=4980. [Accessed: Oct. 15, 2022].

[32] UNCTAD. United Nations Conference on Trade and Development, 2022. [Online]. Available: https://unctad.org/rmt2022. [Accessed: Oct. 13, 2023]

[33] G. Kodak, G. Kodak, "Implementation of the six thinking hats technique to the maritime field: Ship accident case study," *Trafik Ve Ulaşım Araştırmaları Dergisi*, vol. 7, pp. 31-43, 2024.

[34] G. Kodak and C. İstikbal, "A suggestion to improve navigational safety in the Strait of Istanbul (Bosphorus): Patrol tugs," *Journal of Black Sea / Mediterranean Environment*, vol. 27, pp. 294-316, 2021.

[35] O. Serrat, "The Five Whys Technique". In: Knowledge Solutions. Springer, Singapore. 2017.

[36] H. S. Çelik, "Root Cause Analysis Methods for The Design of Aviation Parts," *J Aviat*, vol. 4, pp. 1-9, 2020.

[37] M. Lillywhite and P. Dyer, "Root Cause Analysis, Publication of Civil Aviation Authority Publications," pp. 1-35, 2016.

[38] AHRQ. Root Cause Analysis, Agency for Healthcare Research and Quality, 2019. [Online]. Available: https://psnet.ahrq.gov/primer/root-cause-analysis. [Accessed: Dec, 10, 2023].

[39] AHRQ. Whys and Fishbone Diagrams, Agency for Healthcare Research and Quality, Primary Care Practice Facilitator Training Series. [Online]. Available: https://www.ahrq.gov/sites/default/files/wysiwyg/ncepcr/resources/job-aid-5-whys.pdf. [Accessed: Jan 01, 2024].

[40] M. Chen, Y. Wu, K. Wang, H. Guo and W. Ke, "An explosion accident analysis of the laboratory in university," *Proc Safety Prog*, vol. 39, pp. 1-10, 2019.

[41] K. Ishikawa, "Guide to Quality Control, Asian Productivity Organization," Japan. 1991.

[42] O. Atalay and Ö. Kılıç, "Investigation of Possible Causes of Mobile Crane Accidents with Fishbone Method," Çukurova University *Journal of the Faculty of Engineering and Architecture*, vol. 30, pp. 73-78, 2015.

[43] T. Romo, N. Vick, L. Quializapa, (n.d.). Fishbone diagram & the 5 whys, County of Los Angeles Public Health, [Online]. Available: http://publichealth.lacounty.gov/qiap/docs/Topic3-Fishbone.pdf. [Accessed: Dec. 15, 2023].

[44] Republic of Turkey Ministry of Transport and Infrastructure Transportation Safety Investigation Center, [Online]. Available: https://ulasimemniyeti.uab.gov.tr/uploads/pages/publishing-of-final-investigation-report-on-seriou/vitaspirit-final-report-31-10-2019.pdf. [Accessed: May. 15, 2023].

RESEARCH ARTICLE

DOI: 10.54926/jnamt.2024.244

J Nav Architect Mar Technol 2024;226(2):49-64

Comprehensive Evaluation of Naval Architecture and Marine Engineering Curricula in Relation to Sustainable Development Goals and IMO Agenda Topics

Çağlar Dere[1], Sertaç Bulut[2]

[1]İzmir Katip Çelebi University Faculty of Naval Architecture and Maritime, Department of Marine Engineering, İzmir, Türkiye
[2]İzmir Katip Çelebi University Faculty of Naval Architecture and Maritime, Department of Naval Architecture and Marine Engineering, İzmir, Türkiye

To cite this article: Ç. Dere, and S. Bulut. Comprehensive Evaluation of Naval Architecture and Marine Engineering Curricula in Relation to Sustainable Development Goals and IMO Agenda Topics. *J Nav Architect Mar Technol*. 2024;226(2):49-64.

Received: 30.09.2024 - **Revised:** 14.11.2024 - **Accepted:** 18.12.2024 - **Publication Date:** 31.01.2025

Abstract

The contribution of engineering education is quite significant in achieving the Sustainable Development Goals (SDGs) set by the United Nations, which are planned to be accomplished by 2030. To this end, the evaluation of the engineering curriculum regarding SDGs provides an insightful resource. Determining the alignment of the engineering education with the SDGs involves examining the curricula of institutions that have international engineering accreditation. Naval Architecture and Marine Engineering is inherently a global engineering field, addressing contemporary issues such as sustainability, advanced materials, automation, and safety. It proposes innovative solutions to evolving challenges in maritime transport, offshore energy, and marine environmental protection. Analyzing the relationship between the curriculum and the SDGs, identifying the challenges in aligning the curriculum with these goals, and gathering information to promote engineering education towards achieving the SDGs are all essential aspects of this process. In this study, two Naval Architecture and Marine Engineering curricula, which have ABET accreditation since 2009 and MÜDEK accreditation since 2012, are evaluated with regard to the SDGs. The study presents and discusses the strong SDG 4-7-8-9-12 and weak SDG 1-2-3-13-14-15 areas of the curricula and promotes Naval Architecture and Marine Engineering education for sustainable development.

Keywords: Education for sustainable development, naval architecture and marine engineering curriculum, sustainable development goals, engineering education

1. Introduction

United Nations (UN) adopted 17 Sustainable Development Goals (SDGs) in 2015 as 2030 Agenda for Sustainable Development. The Agenda mainly involves action plans about people, planet and prosperity considering the harmony between the economic, social and environmental aspects with 17 SDGs and their 169 targets. The three fundamental components, environmental protection, economic growth and social equity underpin the sustainable development, seen in Figure 1. The notion of SDGs aims to maintain the main theme of fulfilling contemporary requirements while ensuring that future generations retain the capacity to fulfil their own needs [1]. Furthermore, addressing these issues with transformative steps is crucial for progressive solutions.

Address for Correspondence: Çağlar Dere, İzmir Katip Çelebi University Faculty of Naval Architecture and Maritime, Department of Marine Engineering, İzmir, Türkiye
E-mail: caglar.dere@ikc.edu.tr
ORCID ID: orcid.org/0000-0003-1670-1998

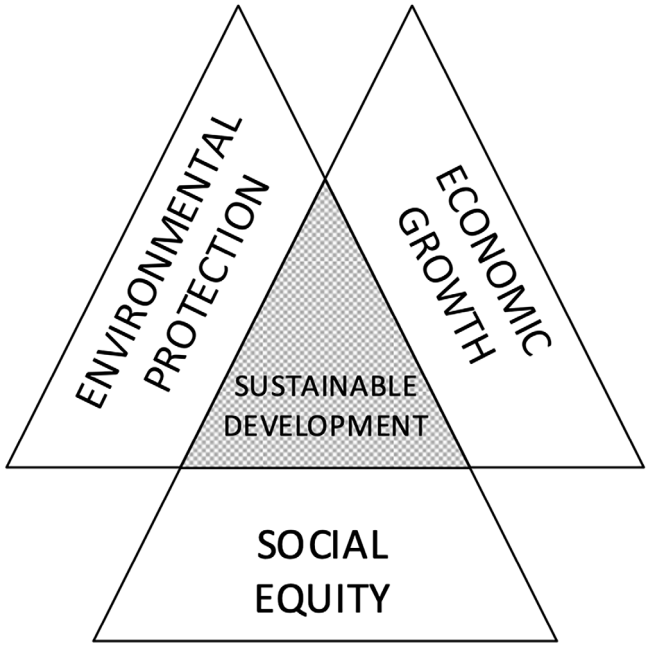

Figure 1. Three fundamental tenets of sustainable development.

UN encourage all member states to expeditiously devise and implement national strategies to ensure the comprehensive execution of this Agenda [2].

Since the concept of sustainable development was first introduced, education has consistently played a key role in supporting the successful realization of its goals [3]. It was also a vital component in the Millennium Development Goals (MDGs), implemented from 2000 to 2015 and later superseded by the SDGs.

The concept of education for sustainable development is an essential pathway to achieving sustainable development, provided that quality education is delivered to transform society by improving the knowledge, skills, values, and behaviors needed for sustainability [4].

Achieving the SDGs in a sustainable manner requires the integration of sustainability principles into all development activities, with a particular focus on higher education (HE). By adopting the SDGs not only in daily life but also the educational framework, and taking into account their long-term impacts, the progress towards these objectives can be created more meaningful and sustainable. The educational goal of the SDGs, as SDG4, largely focuses on the elementary education and literacy fields, and enhancing the notion towards the university level will improve the other SDGs implementation [5]. Given that sustainability is not adequately embedded in the curricula of HE institutions, it poses a significant challenge to the goal of achieving sustainable development [6]. Therefore, the universities are the essential partners in the fulfilment of the 2030 Agenda.

On the other hand, engineers play a crucial role in achieving the UN's SDGs for 2030. Engineering proposes solutions to meet current problems and contribute to economic development by utilizing mathematics, natural sciences, engineering knowledge, and technology. To minimize potential adverse outcomes of these solutions, it must prioritize ethics, economic viability, environmental sustainability, health and safety, and risk management. There is a significant relevancy between the engineering graduate attributes (GAs) and SDGs. In this regard, universities are responsible for fostering an engineering community that is more aware of people, the environment, and equality.

In the 21st-century business environment, engineers are expected not only to offer solutions to current issues using their professional knowledge but also to demonstrate skills that, while different from the disciplinary expertise, contribute to their business. These abilities, attitudes, and understandings, known as GAs, are acquired during students' time at educational institutions.

In professional life, engineers' awareness of their responsibilities develops in line with the skills acquired in basic engineering education. Therefore, receiving education from an accredited education system in the engineering education is quite important. The primary goal of engineering education is to equip engineering candidates not only with engineering capabilities but also competencies that understand and respond to the requirements of the era. In support of this perspective, it can be observed in the report by International Engineering Alliance (IEA) [7] states the World Federation of Engineering Organizations-WFEO-IEA working group established by UNESCO [8] has made improvements under the title "Engineer and the World" to ensure that the GAs and professional competencies (PCs) resulting from engineering education outcomes can contribute to the goals aimed at in the UN SDGs.

As the world moves towards economically, socially and environmentally responsible practices, naval architects play a crucial role in designing eco&human friendly ships and offshore structures. 90% of the products are carried with marine transportation [9]. Education in naval architecture and marine engineering focuses on sustainable design principles, alternative fuels, and reducing emissions, ensuring that future engineers can contribute to a more sustainable maritime industry. Additionally, to protect the lives of crew members and passengers on board the education also comprises the safety standards and risk management. The maritime industry is inherently global, requiring collaboration across countries and cultures so as to understand diverse market needs, and adapt to different regulatory environments. Furthermore, the maritime sector

faces contemporary challenges such as climate change, maritime security, and the need for innovative marine energy solutions. By addressing these areas, naval architecture and marine engineering education ensures that graduates are well-equipped to meet the demands of the modern maritime industry and contribute to its sustainable and innovative future.

In the study carried out in World Maritime University [3] about Maritime Education and Training (MET) with the perspective of sustainable development it is emphasized that the foundation for the successful implementation of the sustainable development strategy lies in education, and it was suggested that the MET curriculum should be analyzed in this perspective and that courses to be introduced. The study focuses on the education of future maritime professionals to support sustainable practices, ensuring the industry meets environmental, economic, and social challenges. In another study carried out in Istanbul Technical University [10] the Marine Engineering curriculum have been analyzed so as to determine the relevancy between curriculum and SGSs and strong and weak sides of the curriculum considering 17 SDGs of UN. It is found that there is a need a modernization to achieve sustainable development-based curriculum. In another study, considering MET [4] found out that the education evolving to have a more academic perspective, which helps incorporate SDGs into education, and these educational institutions are becoming more inclined to integrate SDGs into their curricula. There are very limited studies with maritime education strongly based on marine engineering and not existing study about naval architecture and marine engineering to the best of author's knowledge. On the other hand, there are some investigations about SDG integration into universities curriculum as architecture education or nursing [11,12]. It is an anticipated result for different university curricula to prioritize different SDGs; for instance, while SDG 11 (Sustainable Cities and Communities) stands out as the most adapted SDG for the architecture curriculum [11], nursing curriculum prioritizes SDG 3 (Good Health and Well-being) together with SDG 16 (Peace and Justice Strong Intuitions) [12]. Additionally, there are studies that broadly examine the SDG tendencies of HE institutions. The study about universities efforts on integrating SDGs demonstrated that SDG 3 (Good Health and Well-being), SDG 4 (Quality Education), SDG 5 (Gender Equality), SDG 8 (Decent Work and Economic Growth), SDG 9 (Industry, Innovation and Infrastructure), and SDG 16 (Peace, Justice and Strong Institutions) take precedence [13]. Which seems the areas which the social and economic dimensions are prioritized in [14]. One of the major obstacles to integrating the SDGs into the curriculum is the limited support provided by top management and the reliance on academic staff development for the integration workload [15]. Therefore, conducting an analysis of the existing curriculum is crucial to ensure that valuable efforts are allocated in the most efficient manner for successful integration of SDGs into the curriculum.

In the context of sustainability, understanding the expectations that can be gained from the naval architecture and marine engineering education requires first analyzing the current state of curriculum within the framework of the SDGs, in order to progressive improve and design. Additionally, technological advancements and industrial requirements are parameters that guide the education system.

The main aim of this study is to determine to what extent the naval architecture and marine engineering curriculum includes SDGs. Further motivation is to identify the areas for improvement to increase scope of curriculum regarding SDGs. As an engineering program, it is crucial to determine to what extend the GAs developed by naval architecture and marine engineering students will contribute themselves regarding SDGs. Separately, the results are also expected to contribute to the establishment of quantitative targets for IMO's strategic direction performance indicators that were not clearly defined [16] for activities contributing to the SDGs by IMO.

It must be mentioned that, although the agenda, which is fundamentally focused on the 2030 SDGs, pertains more to the governmental level and was not created for implementation in HE institutions, it is essential for engineering programs to adopt and incorporate this concept and its goals, especially when seeking accreditation from a signatory agency of the Washington Accord [14] which is Represented by Association for Evaluation and Accreditation of Engineering Programs (MÜDEK) in Türkiye. The "Accords" are Mutual Recognition Agreements (MRA) that accredit academic programs and ensure equivalent program outcomes, standards and processes in a certain extent. In the field of engineering science, there are two widely recognized accredited programs: ABET and the Washington Accord. To the best of authors knowledge, the study is antecedent study that analyses the two accredited (ABET and MÜDEK) [17,18]-naval architecture and marine engineering curriculum of a university from the perspective of SDGs.

The curricula used in the study is designed considering ABET and MÜDEK requirements that is a body in IEA. The IEA has made some revisions in recent years to emphasize the contribution of PCs and GAs of engineering education which are already related to SGS, to the SDGs within engineering education. The study evaluates the existing accredited curricula through five main steps, which are detailed in the

next section as follows: assessing the connection between the engineering field and the SDGs through a review of relevant literature, systematically evaluating the alignment of both curricula with the IEA's WK topics, mapping each course to the corresponding knowledge and attitude domains, mapping courses to the SDGs, evaluating the curricula in relation to IMO topics, and conducting an overall analysis.

2. Materials and Methods

2.1. The Methodology Outline

This study provides a comprehensive assessment of the undergraduate curricula in Naval Architecture and Marine Engineering at Istanbul Technical University (ITU) and Yıldız Technical University (YTU), considering the UN SDGs, the International Maritime Organization (IMO) agenda topics and the engineering education output perspective. The methodology involves five main steps. Each research step is presented in the flowchart that outlines the procedure in Figure 2.

The first section, Connecting UN SGDs and Naval Architecture, explores the connection between each SDG and the field of Naval Architecture and Marine Engineering, utilizing Carpenter's framework as a reference [19] The second section, Evaluation Curriculum Courses, systematically assesses the alignment of the ITU and YTU curricula with the IEA's WK topics, mapping each course to the relevant knowledge and attitude domains. In Mapping Courses to SDGs, the study examines the extent to which the curricula at ITU and YTU align with the SDGs, highlighting their integration of sustainability principles. The section Assessing IMO Topics further examines the curricula by evaluating the alignment between course content and critical IMO topics, thus determining their adequacy in meeting maritime industry requirements. Finally, in Overall Analysis and Curriculum Recommendations, the study synthesizes the findings, identifying both the strengths and areas for improvement in the ITU and YTU curricula, and offering strategic recommendations for future curriculum enhancements.

2.2. Understanding of SDGs and Connecting with Naval Architecture and Marine Engineering Curriculum

Understanding of the SDGs and their sub targets together with keywords is a crucial step to begin. Table 1 comprises the SDGs and corresponding keywords. SDG1, with the given keywords, encompasses activities aimed at encouraging investments to achieve the goal of reducing humanity's susceptibility to poverty, or contributing to the development of incentive policies. The achieving food security as in the SDG 2 aims to eliminate hunger and achieve food security by 2030 through improved nutrition and sustainable agriculture. It prioritizes access to safe and sufficient food for all. The goal also seeks to boost the productivity of small-scale farmers, protect agricultural biodiversity, and stabilize food markets through enhanced international cooperation and investment. SDG3 covers the well-being and good health and aims to provide universal health coverage and strengthen countries' capacities to manage health risks. SDG 4 seeks to provide inclusive, equitable quality education for all, enhance skills and literacy, promote sustainable development, improve education facilities, expand scholarships for developing countries, and increase the number of qualified teachers. Another complementary SDG for the goal 4 is gender equality as the SDG 5 focuses on achieving gender equality and empowering women and girls by eliminating discrimination, violence, and harmful practices, ensuring equal opportunities and rights. SDG 6, considering ecology, environment and disaster keywords aims to ensure universal access to clean water and sanitation, improve quality, and efficiency in water use by 2030. Additionally, focuses on protecting water ecosystems and improving local participation in water management. SGD 7, comprises clean energy generation, affordable and sustainable energy sources. SDG 8 aims to make economic growth sustainable and inclusive, ensure full utilization of the workforce, and increase quality job opportunities. In order to create increased employment opportunities, as the aim of SDG 8, SDG 9 aims to promote robust economic foundation through infrastructure development and industrial growth, which

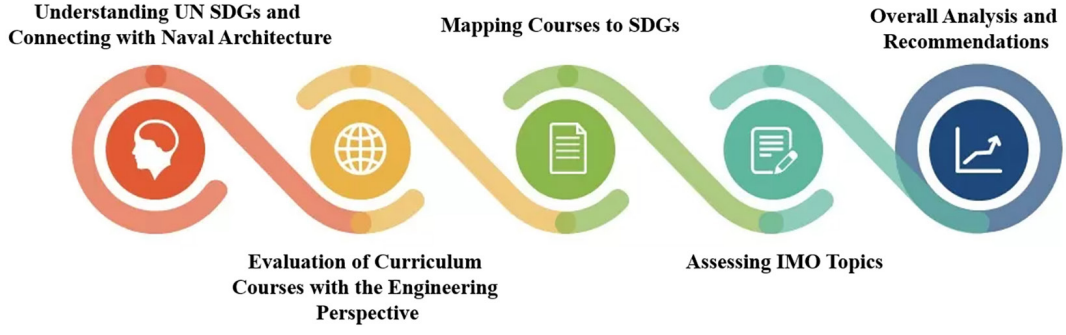

Figure 2. The methodology overview.

Table 1. UN sustainable development goals.

SDG no	SDGs	Keywords
SDG 1	No poverty	Economy, social security, disasters
SDG 2	Zero hunger	Social security, disasters
SDG 3	Good health and well-being	Safety, physical education, health, disaster
SDG 4	Quality education	Practical skill, manual skill, language skill, academic skill
SDG 5	Gender equality	Rules, regulations, law, ethics
SDG 6	Clean water and sanitation	Water, sea, sanitation, ecology, environment, disasters
SDG 7	Affordable and clean energy	Energy, energy generation, energy efficiency
SDG 8	Decent work and economic growth	Ethics, safety, advising, rules, regulations, law, economy, finance, human resource
SDG 9	Industry, innovation and infrastructure	Industry, innovation, infrastructure
SDG 10	Reduced inequalities	Reduced inequalities
SDG 11	Sustainable cities and communities	Law, environment, society, safety, quality
SDG 12	Responsible consumption and production	Energy efficiency, consumption theory, design
SDG 13	Climate action	Environment, disasters, innovative technologies, clean energy
SDG 14	Life below water	Disasters, rules, regulations, environment, ecology
SDG 15	Life on land	Environment, disasters
SDG 16	Peace, justice and strong institutions	Advising, rules, regulations, law, economy, ethics, disasters
SDG 17	Partnerships for the goals	Advising

supports and drives overall economic progress. Goal 10 aims to reduce inequality within and among countries through income growth, social inclusion, and less discrimination. Supporting the reduction of inequalities within countries and ensuring inclusive urbanization of human settlements are also key aspects of SDG 11. Additionally, SDG 11 aims to make habitats safe and sustainable. SDG 12 encompasses the sustainable management of natural resources, the efficient use of these resources, and the reduction of consumption, while also promoting practices in this domain. Sustainable consumption and production models undoubtedly contribute to slow down climate change. Climate action is addressed under SDG 13 as set forth by the UN. This goal encompasses educating, encouraging, and planning for individuals in this field. While SDG 14 covers the sustainable management and protection of marine and coastal ecosystems, as well as the regulation of fishing activities, SDG 15 addresses preventing the degradation of terrestrial ecosystems and improving ecosystem and biodiversity. Institutional reliability addressed by SDG16 is a necessary element for monitoring the mechanisms of the SDGs and implementing supportive policies and besides SDG 17 addresses global partnership to achieve the all SDGs.

In the last part of step 1 the relevance of the Naval Architecture and Marine Engineering field to the UN SDGs is addressed. The relevance is assessed using four different levels: “directly”, “partially/directly”, “partially”, and “non-directly”. Table 2 presents the relevance level of each UN SDG in relation to the field of Naval Architecture and Marine Engineering. It has been determined that SDG 3, 4, 5, 6, 7, 8, 12, 13, 14, 16, 17 are directly relevant UN SDGs in relation to the field of Naval Architecture and Marine Engineering. SDG 3 (Good Health and Well-being) is directly relevant to Naval Architecture and Marine Engineering due to its focus on healthcare for seafarers [20] and reducing ship-related pollution [21], with the IMO’s role in mitigating health impacts from marine pollution [22] further reinforcing this connection. SDG 4 (Quality Education) is relevant to Naval Architecture and Marine Engineering due to its emphasis on access to quality technical education, which is vital for a skilled workforce, particularly in training for AI and Robotics [23]. The maritime industry is inherently a global sector, and the qualified engineers trained for this global sector are educated in qualified maritime faculties. SDG 5 (Gender Equality) is directly relevant to Naval Architecture due to its focus on eliminating discrimination and increasing women’s leadership roles, where the sector has low female representation [24,25]. SDG 7 (Affordable and clean energy) is directly relevant to Naval Architecture as it promotes the use of sustainable energy sources, such as renewable fuels and port electrification, as well as offshore energy generation technologies like wind and tidal power [25]. SDG 8 (Decent work and economic growth) is directly relevant to Naval Architecture due to its emphasis on protecting labor rights and ensuring safe working conditions, especially in ports where many jobs involve low-skilled manual labor, often under

Table 2. SDGs and their relevancy with Naval Architecture and Marine Engineering.

SDG no	SDGs	Description [8]	Relevancy [19]
1	No poverty	End poverty in all its forms everywhere	Partially/Directly
2	Zero hunger	End hunger, achieve food security and improved nutrition and promote sustainable agriculture	Partially
3	Good health and well-being	Ensure healthy lives and promote well-being for all at all ages	Directly
4	Quality education	Ensure inclusive and equitable quality education and promote lifelong learning opportunities for all	Directly
5	Gender equality	Achieve gender equality and empower all woman and girls	Directly
6	Clean water and sanitation	Ensure availability and sustainable management of water and sanitation for all	Partially/Directly
7	Affordable and clean energy	Ensure access to affordable, reliable, sustainable and modern energy for all	Directly
8	Decent work and economic growth	Promote sustained, inclusive and sustainable economic growth, full and productive employment and decent work for all	Directly
9	Industry, innovation and infrastructure	Build resilient infrastructure, promote inclusive and sustainable industrialization and foster innovation	Directly
10	Reduced inequalities	Reduce inequality within and among countries	Non
11	Sustainable cities and communities	Make cities and human settlements inclusive, safe, resilient and sustainable	Partially/Directly
12	Responsible consumption and production	Ensure sustainable consumption and production patterns	Directly
13	Climate action	Take urgent action to combat climate change and its impacts	Directly
14	Life below water	Conserve and sustainably use the oceans, seas and marine resources for sustainable development	Directly
15	Life on land	Protect, restore and promote sustainable use of terrestrial ecosystems, sustainably manage forests, combat desertification, and halt and reverse land degradation and halt biodiversity loss	Partially
16	Peace, justice and strong institutions	Promote peaceful and inclusive societies for sustainable development, provide access to justice for all and build effective, accountable and inclusive institutions at all levels	Directly
17	Partnerships for the goals	Strengthen the means of implementation and revitalize the global partnership for sustainable development	Directly

unsafe conditions [26]. The need for improved labor rights and secure environments, particularly for migrant and low-wage workers, highlights the importance of this SDG in the Naval Architecture sector. SDG 9 (Industry, Innovation, and Infrastructure) is directly relevant to the Naval Architecture sector as it focuses on investments in infrastructure such as transport, energy, and communication technologies to achieve sustainable development and empower communities [25]. SDG 12 (Responsible Consumption and Production) is directly relevant to the Naval Architecture sector as it promotes sustainable practices across the lifecycle of production and consumption, including the adoption of energy-efficient and environmentally sound technologies in shipping and port operations, which is crucial given that 90% of global trade is transported by sea [9,27,28]. SDG 13 (Climate action) is directly relevant to shipbuilding because the sector plays a crucial role in reducing global carbon emissions through the development of energy-efficient and low-emission vessels, thereby combating climate change [25]. SDG 14 (Life below water) is directly relevant to naval architecture because it emphasizes the conservation of oceans and sustainable use of marine resources, which are critical for designing ships that minimize environmental impact [25]. SDG 16 (Peace, justice and strong institutions) is directly relevant to shipbuilding because it involves ensuring ethical practices, legal compliance, and strong institutions in the maritime industry, which are essential for maintaining peace, justice, and security in global trade and ocean governance. SDG 17 (Partnerships for the goals) known as Partnership for the goals, is relevant to naval architecture because it emphasizes the need for global partnerships that support the exchange of knowledge, technology, and resources, which are essential

for advancing sustainable practices and innovations in shipbuilding [25]. It has been identified that SDGs 1, 6, and 11 are partially/directly relevant, SDGs 2 and 15 are partially relevant, and SDG 10 is non-directly relevant to the field of Naval Architecture and Marine Engineering.

3. The Findings of Mapping the Courses and Discussions

3.1. Evaluation of the Curriculum with the Engineering Perspective

This section provides a detailed evaluation of the curricula for the Naval Architecture and Marine Engineering departments at ITU and YTU. Table 3 presents the courses offered in the ITU and YTU curricula on a semester basis. The curricula provided for both universities are the most recent ones, implemented in the year 2024.

The ITU and YTU curricula have been assessed from various perspectives based on the IEA's Knowledge and Attitude Profiles (WKs) to provide a more comprehensive understanding of their characteristics, as shown in Tables 4 and 5. The WKs, or Knowledge and Attitude Profiles, are defined by the IEA as a set of comprehensive criteria that reflect the essential knowledge, skills, and professional attitudes expected of engineering graduates [7]. Each WK represents a specific domain of expertise that is crucial for the effective practice of engineering. These include a systematic understanding of natural and social sciences (WK1), proficiency in mathematics and computational methods (WK2), core engineering fundamentals (WK3), specialized engineering knowledge (WK4), and considerations for sustainable and efficient resource use (WK5). Additionally, they encompass practical engineering skills (WK6), the role of engineering in society (WK7), engagement with current research (WK8), and adherence to ethical standards and inclusive practices (WK9).

Evaluating the first-year courses of the ITU and YTU curricula reveals that the ITU curriculum is focused on natural and social sciences (WK1), whereas the YTU curriculum is heavily centered on mathematics and computational methods (WK2). The ITU curriculum consists of 12% WK1-based courses and 10% WK2-based courses, while the YTU curriculum comprises 14% WK2-based courses and 6% WK1-based courses. In terms of the second-year courses, both universities have a curriculum that predominantly composed of core engineering fundamentals (WK3) courses. In the ITU curriculum, WK3-based courses distributed over the first two years constitute 16% of the all curriculum, while in the YTU curriculum, WK3-based courses covering the first three years represent 18% of the all curriculum. In the third year of study, both curricula are primarily composed

Table 3. Naval architecture and marine engineering curriculum of ITU and YTU.

Istanbul Technical University	Yıldız Technical University
1st Semester	
-Physics I	-Physics I
-Physics I Laboratory	-Int. to Naval Architecture and Marine Eng.
-Int. to Naval Arch. and Marine Eng. and Ethics	-Descriptive Geometry and Technical Geometry
-General Chemistry I	-General Chemistry
-General Chemistry I Laboratory	-Mathematics I
-Mathematics I	-Advanced English I
-English for Academic Purposes	
2nd Semester	
-Physics II	-Physics II
-Physics II Laboratory	-Ship Geometry
-Ship Geometry	-Basic Computer Science
-Int. to Programming Language (PYTHON)	-Mathematics II
-Mathematics II	-Linear Algebra
-Basics of Academic Writing	-Advanced English II
-Entrepreneurship and Career Advising	-Mechanical Workshop
	-Statistics and Probability
3rd Semester	
-Numerical Methods	-Numerical Methods
-Engineering Mathematics	-Differential Equations
-Dynamics	-Mechanics
-Materials and Manufacturing Processes	-Material and Ship Building Materials
-Strength of Materials I	-Computer Aided Design
	-Occupational Health and Safety
	-Technical Thermodynamics I
	-Turkish Language 1
4th Semester	
-Fluid Mechanics	-Fluid Mechanics
-Strength of Materials II	-Strength of Materials
-Thermodynamics	-Technical Thermodynamics II
-Essentials of Research Paper Writing	-Research Project
-Probability and Statistics	-Elective Internship 1
-Technical Elective Course	-Manufacturing Processes
	-Ship Design
	-Turkish language 2
5th Semester	

Table 3. Continued

Istanbul Technical University	Yıldız Technical University
-Marine Engines	-Ship Machinery I
-Ship Theory	-Ship Structural Elements
-Ship Construction	-Machine Elements
-Ship Hydrodynamics (Resistance)	-Heat Transfer
-Maritime and Labor Law	-Ship Hydrostatics and Stability
-Non-Technical Elective Course	-Princp. of Atatürk & Hist. of Modern Türkiye 2
	-Technical Elective Course (x2)
6th Semester	
-Marine Auxiliary Machinery	-Ship Machinery II
-Ship Hydrodynamics (Propulsion)	-Ship Resistance and Propulsion
-Strength of Ships	-Ship Movements
-Ship Design	-Ship Theory
-Electrical Systems in Ships	-Princp. of Atatürk & Hist. of Modern Türkiye 2
-Work Safety & Health Training in Shipbuilding Industry	-Elective Internship 2
-Turkish I	-Technical Elective Course (x^2)
	-Non-Technical Elective Course
7th Semester	
-History of Turkish Revolution I	-Marine Auxiliary Engines
-Naval Architecture & Marine Eng. Design I	-Naval Architecture and Marine Eng. Lab
-Ship Motions and Maneuvering	-Ship Strength
-Methods of Ship Production	-Electrotechnique and Ship Electricity
-Shipping Economics	-Operation and Maintenance of Marine Machinery
-Ship Vibration	-Technical Elective Course (x4)
-Technical Elective Course (x2)	
8th Semester	
-Shipyard Organization	-Shipyard Management and Organization
-History of Turkish Revolution II	-Graduation Thesis
-Naval Architecture & Marine Eng. Design II	-Technical Elective Course (x6)
-Turkish II	
-Computational Fluid Mechanics	
-Technical Elective Course (x2)	

of courses based on engineering knowledge (WK4). These WK4-based courses are supported by sustainable and efficient resource use (WK5) and practical engineering skills (WK6)-based courses. WK4-based courses constitute 29% of the ITU curriculum and 27% of the YTU curriculum. WK5-based courses account for 18% of the ITU curriculum and 16% of the YTU curriculum. In the fourth year, the ITU curriculum is evenly distributed among engineering knowledge (WK4), practical engineering skills (WK6), and engineering in society (WK7)-based courses. For YTU, the curriculum is balanced between WK4 and WK6-based courses. WK6-based courses and WK7-based courses each constitute 18% of both curricula. Research literature (WK8) and ethical standards and inclusive practices (WK9) courses constitute comparatively smaller parts of both curricula.

3.2. Evaluation of the Curriculum with the SDGs

After the understanding of SDGs with a comprehensive approach, as a first step, the curriculum content and SDGs relevancy are to be determined for the study. In order to mapping curriculum courses to the SGDs, firstly the process contains the analyzing the weekly course plan of the all courses in the curricula. The matching the content of the SDGs with the content of naval architecture and marine engineering curriculum is the main body of the study which is carried out meticulously with an annual based approach. The relevancy analysis of the course content with SDGs is determined using the keywords of the SDGs together with their aims and through the studies carried out in literature [9,20-28] on respective areas. The courses may include in their contents one or more SDGs. Therefore, a course name can be represented in multi SDGs in each curriculum analysis. In the evaluation of ITU and YTU curricula, the lecture breakdown structures within the scope of SDG are indicated in Tables 6 and 7.

As seen in the tables, both of the universities' curricula significantly align. There are some differences in the diversity of courses, and what extend differences in the curriculum will affect the SDG evaluation will be presented in the next section. Both curricula include technical and non-technical elective courses. It is expected that these courses will contribute to each SDG, assuming they will be chosen by students from the university's elective lesson pool according to their preferences. It must be emphasized that technical elective courses contribute to all SDGs and will not be specifically mentioned within this statement. To begin with shipping economics have a contribution to SDG 1 in curriculum of ITU. The lectures in YTU; Occupational Health and Safety, Naval Architecture and Marine Eng. Lab contributes to SDG 3 on the other hand, Work Safety & Health Training in Shipbuilding Industry is identified as a supportive lecture at ITU curriculum for this SDG. SDG 4, namely quality education, that is compared to other SDGs, supported by many courses as; Physics I Laboratory, General Chemistry Laboratory, English for Academic Purposes,

Table 4. ITU curriculum breakdown structure regarding to engineering knowledges.	
WKs	ITU- Naval Architecture and Marine Engineering Courses
WK1- Natural sciences and awareness of relevant social sciences	Physics I, Physics I Laboratory, General Chemistry, General Chemistry Laboratory, Physics II, Physics II Laboratory
WK2- Mathematics & computing	Mathematics I, Int. to Programming Language (PYTHON), Mathematics II, Numerical Methods, Probability and Statistics
WK3- Engineering fundamentals	Int. to Naval Arch. and Marine Eng. and Ethics, Engineering Mathematics, Dynamics, Materials and Manufacturing Processes, Strength of Materials I, Fluid Mechanics, Strength of Materials II, Thermodynamics
WK4- Engineering specialist knowledge	Marine Engines, Ship Theory, Ship Construction, Ship Resistance, Marine Auxiliary Machinery, Ship Propulsion, Strength of Ships, Ship Design, Electrical Systems in Ships, Ship Motions and Maneuvering, Methods of Ship Production, Ship Vibration, Shipyard Organization, Technical Elective Course
WK5- Engineering design and operations	Ship Theory, Ship Construction, Ship Resistance, Ship Propulsion, Strength of Ships, Ship Design, Naval Architecture & Marine Eng. Design I, Naval Architecture & Marine Eng. Design II, Computational Fluid Mechanics
WK6- Engineering practice	Physics I Laboratory, General Chemistry Laboratory, Physics II Laboratory, Ship Geometry, Naval Architecture & Marine Eng. Design I, Methods of Ship Production, Shipyard Organization, Naval Architecture & Marine Eng. Design II, Computational Fluid Mechanics
WK7- Engineering in Society	Entrepreneurship and Career Advising, Maritime and Labor Law, Nontechnical Elective Course, Work Safety & Health Training in Shipbuilding Industry, Turkish I, History of Turkish Revolution I, Shipping Economics, History of Turkish Revolution II, Turkish II
WK8- Research literature	English for Academic Purposes, Basics of Academic Writing, Essentials of Research Paper Writing
WK9- Ethics, inclusive behaviour and conduct	Int. to Naval Arch. and Marine Eng. and Ethics, Maritime and Labor Law, Work Safety & Health Training in Shipbuilding Industry

Table 5. YTU curriculum breakdown structure regarding to engineering knowledges.	
WKs	YTU- Naval Architecture and Marine Engineering Courses
WK1- Natural sciences and awareness of relevant social sciences	Physics I, General Chemistry, Physics II
WK2- Mathematics & computing	Mathematics I, Physics II, Basic Computer Science, Mathematics II, Linear Algebra, Statistics and Probability, Numerical Methods
WK3- Engineering fundamentals	Int. to Naval Architecture and Marine Eng., Differential Equations, Mechanics, Material and Ship Building Materials, Technical Thermodynamics I, Fluid Mechanics, Strength of Materials, Technical Thermodynamics II, Heat Transfer
WK4- Engineering specialist knowledge	Ship Design, Ship Machinery I, Ship Structural Elements, Machine Elements, Ship Hydrostatics and Stability, Ship Machinery II, Ship Resistance and Propulsion, Ship Movements, Ship Theory, Marine Auxiliary Engines, Ship Strength, Electrotechnique and Ship Electricity, Shipyard Management and Organization, Technical Elective Course
WK5- Engineering design and operations	Computer Aided Design, Ship Design, Ship Hydrostatics and Stability, Ship Resistance and Propulsion, Ship Theory, Ship Strength, Operation and Maintenance of Marine Machinery, Graduation Thesis
WK6- Engineering practice	Descriptive Geometry and Technical Geometry, Ship Geometry, Mechanical Workshop, Elective Internship I, Elective Internship II, Naval Architecture and Marine Eng. Lab, Operation and Maintenance of Marine Machinery, Shipyard Management and Organization, Graduation Thesis
WK7- Engineering in Society	Advanced English I, Advanced English II, Occupational Health and Safety, Turkish Language I, Manufacturing Processes, Turkish language II, Princp. of Atatürk & Hist. of Modern Türkiye I, Princp. of Atatürk & Hist. of Modern Türkiye II, Nontechnical Elective Course
WK8- Research literature	Research Project
WK9- Ethics, inclusive behavior and conduct	Int. to Naval Architecture and Marine Eng., Occupational Health and Safety

Table 6. The course breakdown structure of ITU regarding SDGs.

SDGs	ITU- Naval Architecture and Marine Engineering Courses
SDG 1	Shipping Economics, Technical Elective Course
SDG 2	Technical Elective Course
SDG 3	Technical Elective Course, Work Safety & Health Training in Shipbuilding Industry
SDG 4	Physics I Laboratory, General Chemistry Laboratory, English for Academic Purposes, Physics II Laboratory, Ship Geometry, Int. to Programming Language, Basics of Academic Writing, Entrepreneurship and Career Advising, Dynamics, Essentials of Research Paper Writing, Ship Theory, Ship Construction, Strength of Ships, Ship Design, Work Safety & Health Training in Shipbuilding Industry, Naval Architecture & Marine Eng. Design I, Naval Architecture & Marine Eng. Design II, Computational Fluid Mechanics, Elective Internship, Technical Elective Course
SDG 5	Entrepreneurship and Career Advising, Work Safety & Health Training in Shipbuilding Industry, Technical Elective Course
SDG 6	Marine Auxiliary Machinery, Technical Elective Course
SDG 7	Thermodynamics, Marine Engines, Ship Resistance, Marine Auxiliary Machinery, Ship Propulsion, Electrical Systems in Ships, Naval Architecture & Marine Eng. Design I, Naval Architecture & Marine Eng. Design II, Computational Fluid Mechanics, Technical Elective Course
SDG 8	Int. to Naval Arch. and Marine Eng. and Ethics, Entrepreneurship and Career Advising, Ship Theory, Ship Construction, Maritime and Labor Law, Work Safety & Health Training in Shipbuilding Industry, Naval Architecture & Marine Eng. Design I, Methods of Ship Production, Shipping Economics, Shipyard Organization, Ship Vibration, Naval Architecture & Marine Eng. Design II, Elective Internship, Technical Elective Course
SDG 9	Materials and Manufacturing Processes, Ship Design, Methods of Ship Production, Shipyard Organization, Elective Internship, Technical Elective Course
SDG 10	-
SDG 11	Ship Theory, Ship Motions and Maneuvering, Maritime and Labor Law Technical Elective Course
SDG 12	Dynamics, Materials and Manufacturing Processes, Fluid Mechanics, Thermodynamics, Marine Engines, Ship Resistance, Marine Auxiliary Machinery, Ship Propulsion, Ship Design, Electrical Systems in Ships, Naval Architecture & Marine Eng. Design I, Naval Architecture & Marine Eng. Design II, Computational Fluid Mechanics, Technical Elective Course
SDG 13	Marine Engines, Technical Elective Course
SDG 14	Technical Elective Course
SDG 15	Technical Elective Course
SDG 16	Int. to Naval Arch. and Marine Eng. and Ethics, Entrepreneurship and Career Advising, Maritime and Labor Law, Work Safety & Health Training in Shipbuilding Industry, Technical Elective Course
SDG 17	English for Academic Purposes, Essentials of Research Paper Writing, Technical Elective Course

Physics II Laboratory, Ship Geometry, Int. to Programming Language, Basics of Academic Writing, Entrepreneurship and Career Advising, Dynamics, Essentials of Research Paper Writing, Ship Theory, Ship Construction, Strength of Ships, Ship Design, Work Safety & Health Training in Shipbuilding Industry, Naval Architecture & Marine Eng. Design I, Naval Architecture & Marine Eng. Design II, Computational Fluid Mechanics, Elective Internship for ITU and Descriptive Geometry and Technical Geometry, Advanced English I, Ship Geometry, Basic Computer Science, Advanced English II, Mechanical Workshop, Mechanics, Computer Aided Design, Research Project, Elective Internship, Ship Design, Ship Structural Elements, Machine Elements, Ship Hydrostatics and Stability, Technical Elective Course, Ship Theory, Naval Architecture and Marine Eng. Lab, Ship Strength, Operation and Maintenance of Marine Machinery, Graduation Thesis for YTU. For the SDG5; Entrepreneurship and Career Advising, Work Safety & Health Training in Shipbuilding Industry have contribution in ITU curricula, however apart from the contribution of technical electives, no course has been identified at YTU. Marine Auxiliary Machinery is the only course supports SDG 6 in both. The SDG 7, affordable and clean energy, is an important goal in today's context where environmental issues are prominent. Contributions from both curricula in this area are provided through mutual courses such as Marine Auxiliary Engines (Marine Auxiliary Machinery in ITU) and Electrical Systems in Ships (Electrotechnique and Ship Electricity in YTU), as well as through additional courses like Thermodynamics, Marine Engines, Ship Resistance, Ship Propulsion, Naval Architecture & Marine Eng. Design I and II, and Computational Fluid Mechanics at ITU; and Ship Machinery I and II, Heat Transfer, Ship Resistance and Propulsion, and Graduation Thesis at YTU. For SDG

Table 7. The course breakdown structure of YTU regarding SDGs

SDGs	YTU- Naval Architecture and Marine Engineering Courses
SDG 1	Technical Elective Course
SDG 2	Technical Elective Course
SDG 3	Technical Elective Course, Occupational Health and Safety, Naval Architecture and Marine Eng. Lab
SDG 4	Descriptive Geometry and Technical Geometry, Advanced English I, Ship Geometry, Basic Computer Science, Advanced English II, Mechanical Workshop, Mechanics, Computer Aided Design, Research Project, Elective Internship, Ship Design, Ship Structural Elements, Machine Elements, Ship Hydrostatics and Stability, Technical Elective Course, Ship Theory, Naval Architecture and Marine Eng. Lab, Ship Strength, Operation and Maintenance of Marine Machinery, Graduation Thesis
SDG 5	Technical Elective Course, Occupational Health and Safety
SDG 6	Technical Elective Course, Marine Auxiliary Engines
SDG 7	Ship Machinery I, Heat Transfer, Technical Elective Course, Ship Machinery II, Ship Resistance and Propulsion, Marine Auxiliary Engines, Electrotechnique and Ship Electricity, Graduation Thesis
SDG 8	Int. to Naval Architecture and Marine Eng., Mechanical Workshop, Occupational Health and Safety, Technical Thermodynamics I, Technical Thermodynamics II, Research Project, Elective Internship, Ship Hydrostatics and Stability, Technical Elective Course, Ship Theory, Shipyard Management and Organization, Graduation Thesis
SDG 9	Mechanical Workshop, Material and Ship Building Materials, Elective Internship, Manufacturing Processes, Ship Design, Machine Elements, Technical Elective Course, Operation and Maintenance of Marine Machinery, Shipyard Management and Organization, Graduation Thesis
SDG 10	-
SDG 11	Occupational Health and Safety, Ship Hydrostatics and Stability, Technical Elective Course, Ship Movements, Ship Theory
SDG 12	Mechanics, Material and Ship Building Materials, Technical Thermodynamics I, Fluid Mechanics, Technical Thermodynamics II, Manufacturing Processes, Ship Design, Ship Machinery I, Heat Transfer, Technical Elective Course, Ship Machinery II, Marine Auxiliary Engines, Electrotechnique and Ship Electricity, Operation and Maintenance of Marine Machinery, Graduation Thesis
SDG 13	Ship Machinery I, Technical Elective Course, Ship Machinery II, Ship Resistance and Propulsion
SDG 14	Technical Elective Course
SDG 15	Technical Elective Course
SDG 16	Int. to Naval Architecture and Marine Eng., Technical Elective Course
SDG 17	Advanced English I, Advanced English II, English for Academic Purposes, Essentials of Research Paper Writing Technical Elective Course

8, Elective Internship holds a significant weight in both curricula. Additionally, courses such as Introduction to Naval Architecture and Marine Engineering, Ship Theory, and Shipyard Organization and Management may contribute to SDG 8 in both curricula. Additionally, in the ITU curriculum, courses such as Entrepreneurship and Career Advising, Ship Construction, Maritime and Labor Law, Work Safety & Health Training in Shipbuilding Industry, Naval Architecture & Marine Engineering Design I and II, Methods of Ship Production, and Shipping Economics contribute to this area. On the other hand, the YTU curriculum, contributions come from Mechanical Workshop, Technical Thermodynamics I and II, Research Project, Ship Hydrostatics and Stability, and Graduation Thesis. The engineering programs significantly have impact on ship building industry. As an SDG focusing on industry innovation and infrastructure, the SDG 9 finds a foothold from the lectures as Materials and Manufacturing Processes, Ship Design, Shipyard Organization, Elective Internship. Furthermore, Methods of Ship Production in ITU; Mechanical Workshop, Machine Elements, Operation and Maintenance of Marine Machinery, Graduation Thesis lectures in YTU have impact on the SDG. While naval architecture curricula have no contribution to the SDG 10, SDG 11 find support with the lectures as Occupational Health and Safety, Ship Hydrostatics and Stability, Ship Movements, Ship Theory. The lectures as; Dynamics (Mechanics), Materials and Manufacturing Processes, Fluid Mechanics, Thermodynamics (I and II), Marine Engines, Operation and Maintenance of Marine Machinery, Ship Resistance, Marine Auxiliary Engines, Ship Propulsion, Ship Design, Electrical Systems in Ships, Naval Architecture & Marine Eng. Design I, Naval Architecture & Marine Eng. Design II, Computational Fluid Mechanics, Heat Transfer, Graduation Thesis have relevancy with another significant

SDG, as responsible consumption and production SDG12. Marine Engines and Ship Machinery, Ship Resistance and Propulsion lessons have relevancy with SDG 13. SDG 14 and 15 are not supported noteworthy by curricula. SDG 16 has relevancy with the lessons Int. to Naval Arch. and Marine Eng. and Ethics, Entrepreneurship and Career Advising, Maritime and Labor Law, Work Safety & Health Training in Shipbuilding Industry and SDG 17 has relevancy with English for Academic Purposes, Essentials of Research Paper Writing courses.

3.3. Mutual Aspect Between IMO Topics and SDGs

Table 8 presents the IMO Agenda for the years 2020-2022 and the topics discussed by the sub-committees. This Agenda outlines the areas of focus for the IMO, emphasizing that naval architecture and marine engineering education should be consistent with these focus areas. The topics are linked to relevant SDGs to assess the alignment of ITU and YTU's naval architecture and marine engineering curricula. It appears that the ITU and YTU curricula primarily contribute to the topics of IMO 2, IMO 4, IMO 5, IMO 6, and IMO 8. The "Human element, training and watchkeeping (IMO 5)" topic is mainly supported by courses related to SDG 4 and SDG 8 within the ITU and YTU curricula. 51% of the ITU curriculum's courses and 49% of the YTU curriculum's courses correspond to this topic. "Implementation of IMO Instruments (IMO 8)" is another IMO topic effectively covered by the ITU and YTU curricula. Courses related to SDG 4 and SDG 16 provide the main contribution to the IMO 8 topic. 45% of the ITU curriculum and 41% of the YTU curriculum consist of courses related to this topic. The ITU and YTU curricula adequately meet the requirements of the IMO 2 and IMO 6 topics. 45% of the courses in the YTU curriculum are related to the "Ship design and construction (IMO 2)" topic, and 39% of the courses in the ITU curriculum are as well. The "Carriage of cargoes and containers (IMO 6)" topic is covered by 33% of the courses in the ITU curriculum and 31% of the courses in the YTU curriculum. Courses under SDG 2 provide the main support to the IMO 2 topic, while courses under SDG 8 make the primary contribution to the IMO 6 topic. Another IMO topic to which both curricula make a significant contribution is "Ship systems and equipment (IMO 4)". The courses most relevant to this topic are categorized under SDG 12, and 41% of the YTU curriculum and 37% of the ITU curriculum consist of courses that cover this topic. When the ITU and YTU curricula are evaluated with respect to other IMO topics, SDG 9 courses provide the main contribution to the "Safety of navigation, communication, and search and rescue (IMO 1)" topic, SDG 12 courses effectively cover "Pollution prevention and response (IMO 3)", and SDG 7 courses are directly related to "Reduction of greenhouse gas emissions from ships (IMO 7)".

Table 8. The relation between IMO Topics and SDGs.

IMO Topics	SDG-related	
	Directly	Partly
IMO 1- Safety of navigation, communication and search and rescue	11, 14	9, 17
IMO 2- Ship design and construction	9, 12, 13	14, 17
IMO 3- Pollution prevention and response	6, 12, 13, 14	15, 17
IMO 4- Ship systems and equipment	9, 12	3
IMO 5- Human element, training and watchkeeping	3, 4	8, 17
IMO 6- Carriage of cargoes and containers	8, 14	13, 17
IMO 7- Reduction of greenhouse gas emissions from ships	7, 13, 14	6, 15
IMO 8- Implementation of IMO instruments	16, 17	4

It must be also mentioned that another crucial organization the International Towing Tank Conference (ITTC) which is recognized as an NGO with observer status to IMO. The ITTC serves as a global reference point in the performance analysis of naval architecture and marine structures. It addresses numerous topics covered within the naval engineering curriculum, either directly or indirectly. However, it does not directly shape education or provide curriculum recommendations. The recommended procedures and guidelines contribute to setting standards within the maritime industry. The Executive Committee oversees the daily operations of the ITTC and reports its findings, on technical matters relevant to the sector. The topics covered by the technical committees include topics about ship resistance and propulsion conducting test procedures and calculations, such as resistance tests, various propulsion tests, cavitation analyses, hydrodynamic noise and energy saving methods thereby supporting SDG 9, SDG12 and SDG13. Additionally, it contributes to SDG 14 (Life Below Water) through its procedures for noise measurements. The procedures about maneuvering, maneuvering in waves, ships operations at sea, stability, stability in waves covered by the technical committees of Maneuvering Committee, Seakeeping Committee and Stability in Waves committee covers SDG 11 and SDG 14. Among the topics addressed by ITTC are speed and power trials necessary for calculating the Energy Efficiency Design Index as mandated by the IMO. Its contributions to environmental sustainability, efficiency, and high-quality instrumentation are undeniable, establishing a direct connection to SDG 12 and SDG 9. ITTC's contribution to SDG 8 is reflected in its support for the shipbuilding industry, ship operators, and designers,

provided by its professional team. By including procedures for offshore wind turbines and wave energy structures, in Ocean Engineering committee, ITTC supports SDG 7, SDG 9, SDG 11 SDG 12 and SDG 13, significantly. Lastly, ITTC's Executive Committee maintains communication with organizations such as IMO, as highlighted in the article, thereby aligning with SDG 17.

3.4. Annual Based Analysis of Curricula Regarding SDGs

Considering year-based analysis, the alignment with SDGs varies as each course is introduced in different semesters/years. The Figure 3 demonstrates the a) ITU and b) YTU distribution of curricula's annual based contribution. The figure is designed considering four year and the X-axis shows the end of the year.

As an outcome of this analysis, ITU's first year indicates the highest emphasis on SDG 4 (Quality Education), with receiving a 57% of priority for the first year, considering the amount of SDG support of courses throughout the year. SDG 8 (Decent work and economic growth) and SDG 16 (Peace, Justice and strong intuitions) are in 2nd and 3rd place with 14% both. For YTU, SDG 4 is also in the first place by 50% and followed by SDG 8 and SDG 17(Partnerships for the goals) with 17% contribution.

For the second-year assessment, ITU's curriculum has the most courses oriented towards SDG 12 (Responsible consumption and production), the rate makes it the top priority with 44%. SDG 4 is in 2nd place for the year with 22%. Additionally, SDG 7, SDG 9, SDG 17 have the same share for supported by 11% of the courses. For YTU's 2nd year evaluation, SDG 12 is again the top priority. Despite SDG 4 and SDG 8 being in second place, there is a significant proximity with SDG 9 (Industry, innovation and infrastructure) in the curriculum, with relevance levels of 28%, 20%, and 16% for both, respectively.

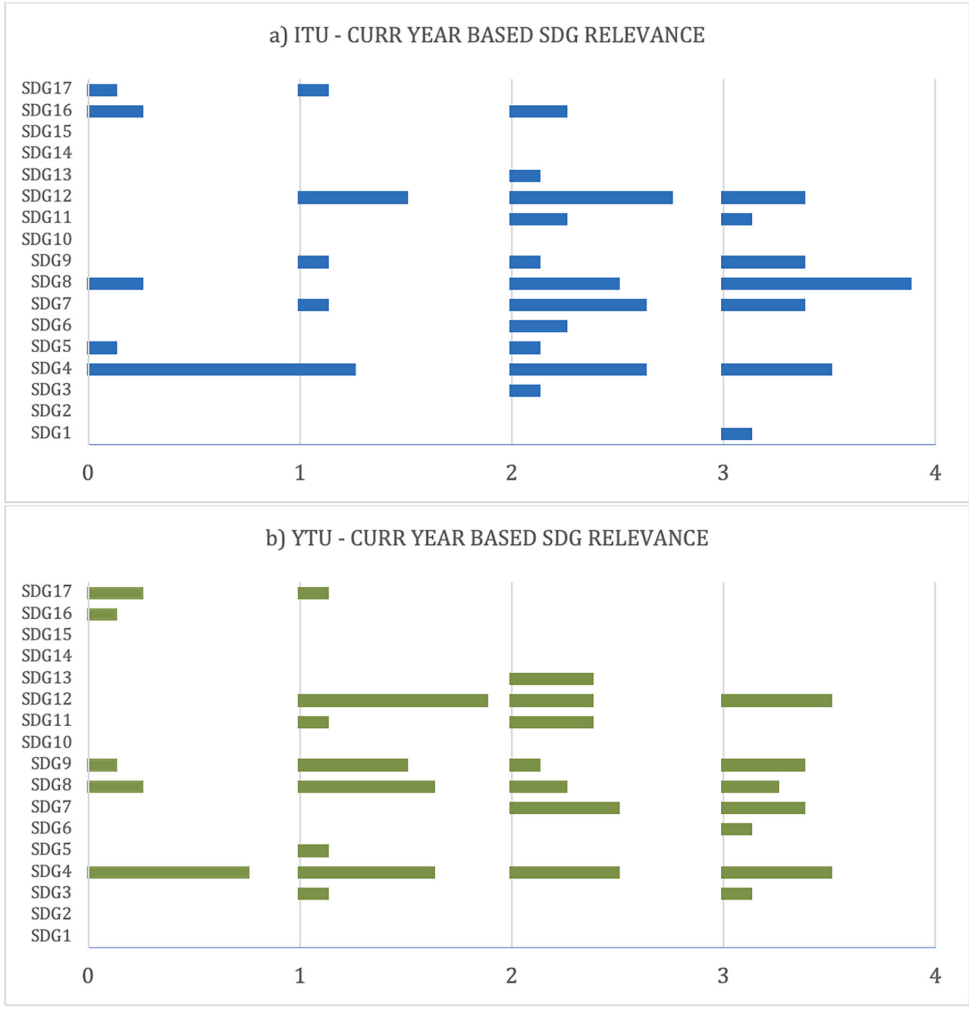

Figure 3. Year based analysis of ITU (a) and YTU (a) curriculum.

ITU: Istanbul Technical University, YTU: Yıldız Technical University

In the third year, with the increase in vocational courses, there is a broader distribution. In ITU's curriculum, SDG 12, SDG 7 (Affordable and clean energy), SDG 4, and SDG 8 are prioritized with relevance levels of 20%, 17%, 17%, and 13%, respectively. On the other hand, in YTU's third year, SDG 7 and SDG 4 are supported by 20% of the courses, while SDG 11 (Sustainable cities and communities), SDG 12, and SDG 13 (Climate action) are supported at 15% level.

In the fourth year, ITU's curriculum stands out for its association with SDG 8, with a relevance level 32% of the courses and followed by SDG 4 18%, SDG 7, SDG 9, and SDG 12 with 14% support level. For YTU's curriculum, SDG 4 and SDG 12 are prominent, with a relevance level of 22%. SDG is at the fifth order with 11% after the SDG7 and SDG9 17% both support by courses.

3.5. Overall Assessment of Curricula with SDGs

This section will analyze the collective contributions of the curricula as consecutive process of the year-based assessments. The comprehensive evaluation of the curriculum allows for a clear identification of its strengths and weaknesses by analyzing the extent to which the courses a student will take over the four-year education period contribute to the SDGs. Figure 4 presents a comparative analysis for both ITU and YTU, showing the percentage of courses within each curriculum that contribute to the relevant SDGs.

In evaluating both curricula within the scope of the SDGs, the most notable aspect is their contribution to SDG 4 (Quality Education). This is an expected outcome, as education has been emphasized as a priority in the context of sustainability goals, even in the MDGs. SDG 4 receives the highest level of support in the both curricula, with 40% of the courses in the ITU curriculum and 39% in the YTU curriculum contributing to this goal. These percentages indicate that 20 courses within the naval architecture and marine engineering programs contribute to this goal during a student's education. Additionally, another SDG that both curricula strongly support is SDG 12 (Responsible Consumption and Production), with 28% and 29% of the courses in ITU and YTU curricula, respectively contributing to this goal.

Figure 4. Program comparison of the two universities with respect to SDGs.

In the third position among the SDGs supported by the curricula, SDG 8 (Decent Work and Economic Growth) is again observed in both curricula. SDG 8 is supported by 28% at ITU and 24% at YTU. A divergence is observed in the fourth most supported SDGs. While the ITU curriculum supports SDG 7 (Affordable and Clean Energy) at a rate of 20%, the YTU curriculum supports SDG 9 (Industry, Innovation, and Infrastructure) at the same rate. In the fifth position, SDG 7 is supported by 16% at YTU, while SDG 9 is supported by 12% at ITU, reversing the positions seen in the previous fourth order. As the ranking decreases, there is a significant decline and differentiation in the level of support. For instance, SDG 16 (Peace, Justice, and Strong Institutions) is supported by 10% in the ITU curriculum, ranking sixth, whereas it is supported by 4% in the YTU curriculum, ranking tenth. Conversely, SDG 11 (Sustainable Cities and Communities) is supported by 10% in the YTU curriculum, ranking sixth, while it is supported by 8% in the ITU curriculum, ranking tenth. In the seventh position, both curricula support SDG 17 (Partnerships for the Goals), with ITU providing 6% support and YTU 8%. Additionally, in the seventh position, the ITU curriculum also supports SDG 5 (Gender Equality) and SDG 6 (Clean Water and Sanitation), while the YTU curriculum ranks SDG 13 (Climate Action) as seventh. As for the least supported SDGs, in the ITU curriculum, SDG 1 (No Poverty) and SDG 13 (Climate Action) are supported at 4%, ranking tenth. SDG 2 (Zero Hunger), SDG 3 (Good Health and Well-being), SDG 14 (Life Below Water), and SDG 15 (Life on Land) are the least supported, with a support rate of 2%. In the YTU curriculum, SDG 3 (Good Health and Well-being) is ranked ninth with 6% support, while SDG 6 (Clean Water and Sanitation) is ranked tenth. The least supported SDGs in the YTU curriculum, with 2% support, are SDG 1 (No Poverty), SDG 2 (Zero Hunger), SDG 5 (Gender Equality), SDG 14 (Life Below Water), and SDG 15 (Life on Land). Overall, it is notable that the least supported SDGs are common in both curricula.

Although some SDGs are directly related to the naval architecture industry, their integration into the curriculum

appears to be weak. These include SDG 3, SDG 13, and SDG 14. A reason for this outcome is that these SDGs are more often included as topics in elective courses. For instance, SDG 14 involves marine biology, which is not a compulsory course in the curricula of Naval Architecture and Marine Engineering. Additionally, its limited coverage within mandatory courses contributes to this result. Introducing a course addressing ship recycling and its environmental impacts or a course examining the environmental dimensions of port management could support this SDG. Similarly, SDG 13 is another underrepresented SDG. This gap might stem from the limited coverage of machinery-related courses. Including the topic of "energy management" in courses on ship production or shipyard management could enhance contributions to this area. SDG 3 also holds significant importance for the shipbuilding industry. However, its weak connection is likely due to its limited integration into mandatory courses. Furthermore, having a course exclusively dedicated to this topic, while increasing focus, may have adversely impacted its distribution across the curriculum. It is essential to remember that habits and skills are not developed instantaneously. As the proverb says, "Slow and steady wins the race".

The study was prepared by reviewing the course catalogues. It may vary to some extent depending on practical/physical opportunities of universities and the experience of the instructors. However, the course catalogues reliably referenced in this study, which serve as a central tool for the European Credit Transfer and Accumulation System (ECTS), aim to enhance transparency in studies and courses and make national education systems more internationally comparable. The ECTS also supports the evaluation, planning, and delivery of HE programs, representing learning based on clearly defined learning outcomes. The use of ECTS systems in the accredited educational institutions has enabled a bottom-up methodology for evaluating the overall educational curriculum within the framework of the SDGs. This evaluation, based on weekly plans in course catalogues, is limited to the curriculum itself. To assess the competencies acquired by engineers, GAs, detailed course evaluation surveys, including thoroughly analyzed student grades, are required. However, this would constitute the further study of this long-term and comprehensive research.

4. Conclusion

Universities are among the most significant actors in the development of new technologies and the transmission of existing knowledge and experience to future generations. Considering the urgency of the SDGs, and the challenges and needs of the era, it is essential for universities worldwide to integrate the concept of sustainable development into the curricula, particularly in the education of engineers who consider economic, environmental, and social responsibilities through their work, as well as in other disciplines.

The study focuses on the relevancy of SDG with naval architecture curriculum and aims to reveal strengths and weaknesses regarding SDGs. The strengths within the curricula are identified as SDG 4 (Quality Education), SDG 12 (Responsible Consumption and Production), SDG 8 (Decent Work and Economic Growth), SDG 7 (Affordable and Clean Energy), and SDG 9 (Industry, Innovation, and Infrastructure). On the other hand, SDG 1 (No Poverty), SDG 2 (Zero Hunger), SDG 3 (Good Health and Well-being), SDG 13 (Climate Action), SDG 14 (Life Below Water), and SDG 15 (Life on Land) have been identified as the weakly supported SDGs of the naval architecture and marine engineering curricula. The results may vary according to disciplines of the curricula, and their content. In order to leverage the relevancy with SDGs, the proposal of elective courses regarding SDGs may be incentivized for instructors. The curricula have compulsory courses, and the weekly course plan of the courses may be reconsidered with SDG perspective, and efforts to encourage students not only to increase their awareness but to internalize the concept of sustainability through education will facilitate the acceleration of this transition process. It should also be emphasized that as the need for sustainable development continues to grow in line with the demands of the era, the responsibility of universities will likewise continue to increase.

Footnotes

Authorship Contributions

Concept/Design: **Ç**. Dere, and S. Bulut, Data Collection or Processing: **Ç**. Dere, and S. Bulut, Analysis or Interpretation: **Ç**. Dere, and S. Bulut, Literature Review: **Ç**. Dere, and S. Bulut, Writing, Reviewing and Editing: **Ç**. Dere, and S. Bulut.

Conflict of Interest: No conflict of interest was declared by the authors.

Financial Disclosure: The authors declared that this study received no financial support.

5. References

[1] United Nations General Assembly (UN), "Development and international economic co-operation: environment report of the world commission on environment and development: our common future." Accessed: July 31, 2024. [Online]. Available: https://sswm.info/sites/default/files/reference_attachments/UN%20WCED%201987%20Brundtland%20Report.pdf

[2] United Nations (UN), "Transforming our world: the 2030 agenda for sustainable development." Accessed: July 31, 2024. [Online]. Available: https://sdgs.un.org/2030agenda

[3] P. Alina, "The paradigm of sustainable development in maritime education and training," Master of Science Dissertation, World Maritime University (WMU), Malmö, Sweden, 2013.

[4] M. S. Rowihil, and Y. B. A. Farag, *Sustainable development in maritime education and training; trends, challenges and the way forward*, Strathclyde, Scotland: Strathprints, 2021.

[5] F. M. Reimers, "The sustainable development goals and education, achievements and opportunities", *International Journal of Educational Development*, vol. 104, no. 102965, Jan 2024.

[6] L. F. Walter, *Implementing Sustainability in the Curriculum of Universities: Approaches, Methods and Projects.* Hamburg, Germany: Springer, 2018.

[7] International Engineering Alliance (IEA), "Graduate attributes and professional competencies, version 2021.1." Accessed: Aug 12, 2024. [Online]. Available: http://www.ieagreements.org

[8] UNESCO, "Education for sustainable development." Accessed: July 28, 2024. [Online]. Available: https://www.unesco.org/en/sustainable-development/education

[9] UNCTAD, "United Nations conference on trade and development review of maritime transport 2019." Accessed: July 30, 2024. [Online]. Available: https://unctad.org/topic/transport-and-trade-logistics/review-of-maritime-transport

[10] B. Zincir, "Analyzing marine engineering curriculum from the perspective of the sustainable development goals," *Marine Science and Technology Bulletin*, vol. 11, no. 2, pp. 158-168, Jun 2022.

[11] H. Mennatullah, J. Mahreen, and A. Amin, "Integrating sustainable development goals into the architecture curriculum: Experiences and perspectives", *City and Environment Interactions,* vol. 21, no. 100138, 2024.

[12] M. J. Upvall, and G. Luzincourt, "Global citizens, healthy communities: Integrating the sustainable development goals into the nursing curriculum," *Nursing Outlook,* vol. 67, no. 6, pp. 649-657, Nov-Dec 2019.

[13] X. Qikun, "Increasing commitment to the sustainable development goals across universities worldwide," *Sustainable Horizons,* vol. 2, no. 100021, Mar 2022.

[14] L. Barrera, "The 2030 agenda for sustainable development in engineering education: a criteria statement proposal for graduate attributes and professional competencies," in *2022 International Symposium on Accreditation of Engineering and Computing Education (ICACIT),* Cusco, Peru, November, 2022.

[15] B. Lazzarini, A. Pérez-Foguet, and A. Boni, "Key characteristics of academics promoting sustainable human development within engineering studies," *Journal of Cleaner Production,* vol. 188, pp. 237-252, Jul 2018.

[16] International Maritime Organization (IMO), "IMO preparations for the sustainable development goals." Accessed: July 29, 2024. [Online]. Available: https://www.unevaluation.org/document/download/3499

[17] MUDEK, "Association for Evaluation and Accreditation of Engineering (MÜDEK) Programs List of Accredited Programs." Accessed: July 25, 2024. [Online]. Available: https://www.mudek.org.tr/en/akredit/akredite2024.shtm

[18] ABET, "Accredited Programs." Accessed: July 25, 2024. [Online]. Available: https://amspub.abet.org/aps/name-search?searchType=institution&keyword=Istanbul%20Technical%20University&exactMatch=true&historical=true

[19] A. Carpenter, J. A. Skinner, and T. M. Johansson, *Sustainability in the maritime domain, conclusions: connecting sustainable development goals to the maritime domain.* Berlin, Germany: Springer, 2021.

[20] Y. Leclerc, D. Murray, and M.Ircha, *Sustainability in the maritime domain, canadian ports sustainability: a strategic response to disruptive paradigms such as COVID-19*. Berlin, Germany: Springer, 2021.

[21] K. R. Aldosari, *Sustainability in the maritime domain, the applicability of the international and regional efforts to prevent oil pollution: comparative analysis between the Arabian Gulf Region and the North Sea*. Berlin, Germany: Springer, 2021.

[22] A. Christodoulou, and J. E. Fernández, *Sustainability in the maritime domain, maritime governance and international maritime organization instruments focused on sustainability in the light of United Nations' sustainable development goals.* Berlin, Germany: Springer, 2021.

[23] A. Sharma, T. E. Kim, and S. Nazir, *Sustainability in the maritime domain, implications of automation and digitalization for maritime education and training*. Berlin, Germany: Springer, 2021.

[24] A. Pastra, and M. Swoboda, *Sustainability in the maritime domain, mind the gap: women in the boardroom, on board and in the port.* Berlin, Germany: Springer, 2021.

[25] A. Carpenter, T. M. Johansson, and J. A. Skinner, *Sustainability in the maritime domain, introducing sustainability in the maritime domain.* Berlin, Germany: Springer, 2021.

[26] E. V. Hooydonk, Port Labour in the EU: *Labour market qualifications & training health & safety, volume I - The EU perspective.* Brussels, Belgium: Study commissioned by the European Commission, 2014.

[27] M. L. Lancaster, P. Winsor, and A. Dumbrille, *Sustainability in the maritime domain, underwater noise from shipping: a special case for the Arctic.* Berlin, Germany: Springer, 2021.

[28] A. Pastra, P. Zachariadis, and A. Alifragkis, *Sustainability in the maritime domain, the role of slow steaming in shipping and methods of CO_2 reduction.* Berlin, Germany: Springer, 2021.

RESEARCH ARTICLE

DOI: 10.54926/jnamt.2025.2411

J Nav Architect Mar Technol 2024;226(2):65-79

An Investigation of Maritime Accidents in Turkish Territorial Waters

Kaan Ünlügençoğlu

Yıldız Technical University Faculty of Naval Architecture and Maritime, Department of Marine Engineering, İstanbul, Türkiye

To cite this article: K. Ünlügençoğlu. An investigation of maritime accidents in Turkish territorial waters. *J Nav Architect Mar Technol*. 2024;226(2):49-64.

Received: 26.11.2024 - **Revised:** 16.01.2025 - **Accepted:** 21.01.2025 - **Epub:** 29.01.2025 - **Publication Date:** 31.01.2025

Abstract

Maritime accidents pose significant challenges to both global and regional safety, often resulting in severe environmental, economic, and human consequences. Understanding the underlying patterns and factors contributing to these accidents is crucial for developing effective safety measures and regulatory frameworks. This study presents a comprehensive analysis of 498 marine accidents that occurred in Turkish territorial waters between 2016 and 2022, examining relationships between accident types, temporal trends, accident characteristics, and vessel-specific factors. The dataset, obtained from the Directorate General of Coastal Safety, underwent rigorous data cleaning to ensure accuracy and reliability. Statistical methods, including frequency analyses, chi-square association tests, and Kruskal-Wallis H tests, were employed to investigate patterns and differences across variables such as accident season, type, region, vessel tonnage and length, and casualty numbers. Key findings revealed that hull/equipment failure was the most common accident type, with general cargo vessels and the Turkish Straits System (TSS) region experiencing the highest frequencies. Grounding accidents were more prevalent in smaller vessels (<1000 GT), while sinking accidents occurred primarily in medium-sized vessels (1000-3000 GT). The Kruskal-Wallis tests identified significant differences in casualty rates based on vessel length, with larger vessels (>200 meters) associated with higher casualty rates compared to medium-sized vessels. Accidents were most frequent during the winter season, and the TSS region exhibited the highest accident density, underscoring its critical role in maritime safety due to dense traffic and challenging navigational conditions. These findings highlight the importance of vessel type-specific safety measures and region-focused regulations, offering valuable insights for the development of effective accident prevention strategies.

Keywords: Maritime accident, statistics, accident trends, chi-square

1. Introduction

Maritime transport is a sector that carries out more than 80% of world trade and is recognized as one of the key factors of the global [1,2]. Despite facing significant challenges due to the global crises in recent years, the sector has shown remarkable resilience. Moreover, maritime trade is expected to grow by more than 2% annually between 2024 and 2028 [3]. While this highlights the economic and strategic importance of maritime transport, it also raises debates concerning its environmental impacts and sustainability. Increasing maritime trade volume can have serious consequences, such as maritime accidents, human losses, environmental destruction and economic damage [4]. Maritime accidents, especially in central areas with heavy traffic such as the Turkish Straits, are not only local, but can also negatively affect international trade and security. In this context, analyzing the causes of marine accidents and their changes over time is of critical importance for

Address for Correspondence: Kaan Ünlügençoğlu, Department of Marine Engineering, Yıldız Technical University Naval Architecture and Maritime Faculty, İstanbul, Türkiye
E-mail: kunlu@yildiz.edu.tr
ORCID ID: orcid.org/0000-0002-3092-148X

J Nav Architect Mar Technol
2024;226(2):49-64

both improving safety standards and preventing future accidents [5]. Extensive research has explored various factors contributing to maritime accidents, including human error, vessel characteristics, environmental conditions, and operational variables, often using statistical and machine learning techniques to identify risk patterns. However, despite the increasing complexity of maritime operations and rising traffic density, studies providing a comprehensive analysis of accident patterns, particularly in high-risk regions like the Turkish territorial waters, remain limited. To establish a robust contextual basis for this study, the following section critically reviews the existing literature on maritime accident analysis, summarizing key methodologies and findings while identifying gaps that warrant further investigation into accident patterns and risk assessment.

1.1. Literature Review

There are numerous studies on marine accidents in the literature. Luo and Shin [6] conducted a comprehensive analysis of 572 articles on marine accidents, revealing a shift in research focus from maritime technology to human error and socio-economic factors. The authors emphasized the need for future research to adopt an interdisciplinary approach, incorporate multiple data sources, and apply advanced research methods to better understand the complex interactions influencing maritime safety. Fan et al. [7] proposed a novel methodology for developing maritime accident prevention strategies from a human factor's perspective, employing Bayesian Networks and the TOPSIS method within a multi-criteria decision-making framework. Their findings highlighted that the most effective strategies for reducing human error involved improving information flow, providing clear orders, and fostering a strong safety culture. Chen et al. [8] analyzed global maritime accident data from 1998 to 2018, covering 16 ship types and 13 sea regions. Using a TOPSIS model, they evaluated the significance of various accident factors, identifying foundering, stranding, and fires/explosions as the most critical contributors. Jiang et al. [9] developed a Bayesian network-based risk analysis model to assess maritime accidents along the Maritime Silk Road. Their analysis, based on accident reports, identified key risk factors such as accident type, location, ship type, speed, and vessel age. Scenario analysis revealed that hijacking posed the highest risk, while contact accidents were the least severe. Cao et al. [10] conducted a bibliometric analysis and systematic review of 491 maritime accident publications from 2000 to 2022. The study highlighted emerging research hotspots, including human factors in remote-controlled ships and accident prevention strategies for Arctic waters. It also emphasized the growing use of machine learning and big data mining techniques, offering a theoretical basis and future directions for maritime safety research. Pilatis et al. [11] performed a statistical analysis of 213 ship accidents involving collisions, groundings, and hull failures that occurred between 1990 and 2020 using IBM SPSS Statistics software. Their findings established significant correlations between accident characteristics such as ship type, ship age, damage location, and cause of the accident, with human error identified as the leading cause of marine accidents. Lan et al. [12] applied association rule mining to analyze the causes of total loss marine accidents using data from 1554 incidents recorded between 2010 and 2020. The study identified hull/machinery damage (52%) and water ingress (20.9%) as the most common causes of total losses. Additionally, vessel age exceeding 20 years and cargo condition were found to be primary indicators of accident severity and human casualties. Liu et al. [13] developed a Bayesian Network combined with advanced machine learning techniques to investigate the causes of maritime accidents in Chinese coastal waters. Their findings indicated that small general cargo ships were the riskiest vessel type, with adverse weather conditions frequently contributing to accidents. Minor accidents were more prevalent in regions with lower traffic density. Wang et al. [14] examined the injury severity outcomes of maritime accidents using a zero-inflated ordered probit regression model. They investigated factors such as accident type, ship characteristics, seafarer experience, and environmental conditions. Their analysis found that capsizing, poor sea conditions, and short rank periods significantly increased the likelihood of injury-prone accidents, while large gross tonnage and water depth were associated with more severe injuries. The study provides valuable insights for maritime safety authorities to develop strategies aimed at reducing injury severity in maritime accidents. Demirci and Gülmez [15] conducted a Human Factors Analysis and Classification System (HFACS) analysis of 30 Ro-Ro ship accidents, identifying human error as the cause in 93.27% of the cases. Unsafe actions, particularly routine violations, were the most frequently observed error types. The study emphasized the importance of compliance with established regulations and the need for proper maintenance and inspections to reduce human error.

Previous studies have provided a broad understanding of maritime accidents on a global scale, examining accident types, frequencies, and contributing factors through various analytical approaches. Building on this foundation, the present study focuses specifically on accidents occurring within the Turkish Straits System (TSS) and Turkish territorial waters. Relevant studies conducted in these regions are summarized below. Uğurlu et al. [16] analyzed 850 maritime accidents in the Turkish Straits between 2001 and 2010, identifying human error as the primary cause. Among these accidents, 89 resulted in economic losses, while 11 led to injuries or

fatalities. The accidents were categorized into collisions, groundings, sinkings, fires/explosions, and machinery failures, highlighting their significant economic and safety impacts. Essiz and Dagkiran [17] evaluated accident risks in the Istanbul and Çanakkale Straits by conducting a risk analysis of ship accidents and their consequences. Their findings revealed that 153 out of 240 reported accidents over the past 13 years occurred in the Ahırkapı anchorage area, with collisions, groundings, and clashes being the most common. The authors recommended expanding or creating new anchorage areas and reducing supply operation times for transit vessels to enhance maritime safety. Korçak and Balas [18] investigated collision risks between ships navigating the İstanbul Strait and domestic ferries crossing the same route. Using simulation modeling, they identified collision hotspots and calculated collision probabilities. Their results suggested that optimized transit schedules could reduce collision risk by 7.2%, highlighting schedule management as a cost-effective mitigation measure. Yılmaz and İlhan [19] analyzed 182 maritime accidents involving Turkish-flagged vessels or incidents within the Turkish Search and Rescue Region from 2002 to 2014. Their findings indicated that 56.6% of incidents were categorized as maritime accidents, with capsizing (31.3%) and collisions (12.6%) being the most common accident types. The study also reported that vessels under 3000 GRT and 90 meters in length, particularly recreational yachts, private boats, and passenger ships, were most frequently involved. Balık et al. [20] examined traffic density, waiting times, and maritime accidents in the Istanbul and Çanakkale Straits between 2006 and 2020. They observed a gradual decrease in the number of vessels transiting the straits, while the total tonnage and vessel size, particularly in the Çanakkale Strait, increased. Additionally, the number of accidents in the Istanbul Strait showed a notable reduction over time, with an average of 7 accidents per year between 2004 and 2019. Ece [21] analyzed 857 maritime accidents in the Strait of Istanbul between 1982 and 2018 using both qualitative and quantitative statistical methods, including frequency distribution, chi-square test, Cramer's V, and regression analysis. The results identified collisions and groundings as the most common accident types, with cargo ships being the most frequently involved vessels. The study also established strong correlations between accident rates and variables such as current velocity, foggy and snowy days, wind conditions, and ship tonnage. In another study, Ece [22] further investigated maritime accidents in the Strait of Istanbul between 1994 and 2019 using similar statistical methods. Collisions were identified as the most frequent accident type (45.6%), followed by groundings and contact incidents (17.5%). The study also highlighted that cargo ships accounted for 49.8% of the accidents, while 71.5% of the vessels involved were operating without a pilot. Human error was again identified as the primary cause across all accident types. Additionally, a statistically significant relationship was found between accident type and variables such as ship type, pilot usage, and accident year. Yildiz et al. [23] examined the impact of operational conditions on marine accidents in narrow waterways, focusing on the İstanbul Strait and the Dover Strait between 2004 and 2020. They used GIS-based Kernel Density Analysis to create maritime accident density maps and conducted chi-square independence tests to explore relationships between operational factors and accident characteristics. Expert opinions validated their findings, emphasizing the influence of ship size, type, age, transit time, traffic density, and channel-specific risks on accident likelihood. The study stressed the importance of dynamic passage planning, vessel-specific risk assessments, and operational measures such as mandatory pilotage and tugboat assistance. Görçün and Burak [24] assessed maritime traffic risks in the Bosphorus between 2001 and 2010 using both qualitative and quantitative risk assessment methods. Their findings identified collisions as the most common accident type (41%), followed by groundings (22%). Navigational errors, unknown factors, and vessel-related issues were highlighted as the primary causes. The study also observed that accident risk was highest during nighttime hours and winter months, especially January and February. Bulk carriers were identified as the highest-risk vessel type, involved in 63% of accidents, while vessels under 200 meters exhibited a notably higher accident rate (69%). Arıcan [25] investigated maritime accidents in Turkish territorial waters, focusing on violations of international maritime conventions using multiple linear regression and frequency analysis. The study revealed that vessels under 500 GRT were more frequently involved in accidents occurring in Turkish territorial waters. Kamal and Çakır [26] analyzed 418 ship accidents in the İstanbul Strait between 2016 and 2021, exploring probabilistic relationships between accident types and factors such as ship size, age, type, wind speed, visibility, and current velocity. Their findings indicated that small vessels under 300 GRT were particularly prone to drift accidents, while older ships demonstrated a higher risk of machinery failures, underscoring the importance of regular maintenance.

1.2. Research Objectives and Scope

The aim of this study was to conduct an in-depth analysis of marine accidents that occurred within Turkish territorial waters, encompassing maritime zones extending up to 12 nautical miles from the baseline, in accordance with international law, between 2016 and 2022. The analysis focused on four major regions: the TSS - including the İstanbul Strait, the Çanakkale Strait, and the Marmara Sea,

the Aegean Sea, the Mediterranean Sea, and the Black Sea. The dataset, which was sourced from the Directorate General of Coastal Safety, included detailed records of 498 marine accidents. To uncover patterns and relationships in the data, statistical methods such as frequency analysis, chi-square tests, and the Kruskal-Wallis H test (a non-parametric statistical procedure for comparing multiple independent groups) were applied. The analysis aimed to identify key accident characteristics, examine the influence of regional and vessel-specific factors, and assess casualty distributions across different categories.

This study was distinguished by its comprehensive focus on Turkish territorial waters and the use of robust statistical methods applied to a large dataset spanning multiple years. Unlike previous studies, which often focused on specific accident types or smaller datasets, this research provided a holistic examination of marine accidents, contributing valuable insights into regional and vessel-specific safety dynamics. The findings of this study held important implications for developing targeted safety measures and regulatory strategies to mitigate marine accidents in Turkish territorial waters.

The study was structured as follows: Section 2 detailed the dataset and methodological framework employed to analyze maritime accidents, including statistical approaches such as frequency analysis, chi-square tests, and Kruskal-Wallis H tests. Section 3 presented the results, offering an in-depth discussion of key findings related to accident patterns, vessel characteristics, and regional variations. Finally, Section 4 concluded the study by synthesizing the main insights and proposing recommendations aimed at enhancing maritime safety.

2. Materials and Methods

The data set used in this study is taken from the official records of the Directorate General of Coastal Safety and the reported accidents of bulk carriers, container ships, general cargo, passenger/RoRo, tugboat and tanker type vessels occurring in Turkish territorial waters between 2016-2022 are taken into consideration After the accident records with repetitive, incorrect or incomplete information (such as the absence of the ship name/ship's IMO registration) were removed from the raw data, it was seen that the regions where 498 accident records took place were Mediterranean, TSS, Aegean Sea and Black Sea. Different parameters were assessed in analysing these accidents: year (from 2016 to 2022) and season of the accident (spring, summer, autumn, winter), type of accident (allision/collision, fire, grounding, hull/equipment failure, man over board, sinking and others), type of vessel (bulk carrier, container ship, general cargo, passenger/RoRo, tugboat and tanker), the region in which the accident occurred (Mediterranean Sea, TSS, Aegean Sea and Black Sea), the tonnage of the vessel (<1000 GT, between 1000-3000 GT and >3000 GT), the length of the vessel (between 0-99 meters, between 100-200 meters, higher than 200 meters) and the number of casualties (dead/missing).

Various statistical methods were applied to gain insights into the marine accident dataset. First, frequency analysis, a common statistical tool for understanding the descriptive characteristics of data, was conducted using graphical representations. In addition, the chi-square test was employed to evaluate the significance of relationships between categorical parameters utilized in the study. The chi-square test, a non-parametric statistical method, assesses whether a significant relationship exists between two categorical variables [27]. Two hypotheses were tested: the null hypothesis (H_0), indicating no significant relationship, and the alternative hypothesis (H_1), indicating a significant relationship. Following a significant chi-square test result, the Bonferroni correction was applied as a post-hoc test to identify which groups exhibited significant differences. While the chi-square test examines whether an overall difference is present, post-hoc tests specifically determine between which categories these differences occur. To assess variations in casualty numbers across groups defined by vessel-specific factors (e.g., vessel type and gross tonnage) and accident region, Kruskal-Wallis H tests were conducted. This robust non-parametric method identifies significant differences in the median values of a continuous variable (e.g., casualty numbers) across more than two independent groups. Unlike One-Way ANOVA (analysis of variance), which compares means and assumes normality and homogeneity of variances, the Kruskal-Wallis H test focuses on medians and does not require these assumptions. This flexibility makes it particularly suitable for datasets with skewed distributions, heteroscedasticity, or ordinal data. While One-Way ANOVA is preferred for datasets meeting its assumptions, the Kruskal-Wallis H test is a more adaptable option for datasets that deviate from these conditions, such as the casualty data analyzed in this study. The Kruskal-Wallis H test examines two hypotheses: the null hypothesis (H_0), which posits no significant differences in casualty distributions across groups, and the alternative hypothesis (H_1), which indicates that at least one group differs significantly. A p-value below 0.05 was considered significant, prompting further post-hoc analyses. The mean rank values generated by the Kruskal-Wallis H test represent the relative rankings of casualty numbers across groups, with higher values indicating relatively greater casualty numbers. The Kruskal-Wallis H value, as the test statistic, measures the variability among groups, while its associated p-value determines the significance of observed differences. Even

when the results are not significant, the mean rank values provide insights into group rankings. For significant results, pairwise comparisons (post-hoc tests) were conducted to identify which groups were responsible for the differences. These analyses offered critical insights into the influence of vessel-specific and regional factors on casualty distributions.

All statistical analyses were performed using the R programming language, with key packages such as ggplot2 for visualization, chisq.posthoc.test for post-hoc analysis, stats for statistical computations, and dplyr and tibble for data manipulation. This methodological approach ensured a rigorous and reproducible analysis of the data.

3. Results and Discussion

3.1. Frequency and chi-square Analysis

As shown in Figure 1, accidents between 2016 and 2022 occurred most frequently during the winter season (n=151, 30.3%). Furthermore, 2022 was the year with the highest frequency of accidents within the period considered in the study (n=110, 22.1%). When analyzing the distribution of accidents occurring in the winter months by year, it was observed that 28.5% (n=43) of the accidents took place in 2022, 17.9% (n=27) in 2019, 15.9% (n=24) in 2020, 13.9% (n=21) in 2021, 11.9% (n=18) in 2017, 9.3% (n=14) in 2018, and 2.6% (n=4) in 2016. Additionally, results from the chi-square test confirmed that there was a significant relationship between the year and the season, X2 (18, n=498) =55.627, p-value <0.001. This result indicated that vessel accidents were more or less frequent in certain seasons during specific years. Given the significant relationship between year and season, a series of post hoc tests were conducted. In the autumn of 2016 and the summer of 2017, it is noteworthy that ship accidents occurred more frequently (p-values <0.001) compared to other years. In other words, the frequency of vessel accidents during these years and seasons was higher than expected. Figure 2 shows the distribution of vessel types involved in accidents according to seasons. It was observed that general cargo vessels were more prominent compared to other vessel types in terms of accident frequency (n=209, 42%). Following general cargo vessels, the frequency distribution of vessel types involved in accidents was as follows, from highest to lowest: bulk carriers (n=143, 28.7%), tankers (n=67, 13.5%), container ships (n=36, 7.2%), passenger/RoRo vessels (n=33, 6.6%), and tugboats (n=10, 2%). The chi-square test, which examined whether there was a relationship between vessel types and the season in which the accidents occurred, confirmed a non-significant relationship, χ^2 (15, n=498) =18.227, p-value =0.251. This suggests that the distribution of vessel accidents is not meaningfully influenced by seasonal variations, implying other factors may be at play in determining accident frequency across different vessel types.

Figure 3 shows the frequency distribution of accident types and the vessel types involved in the accidents. The most common cause of accidents for all vessel types was hull/equipment failure (n=171, 34.3%). The frequency distribution of other accident causes was as follows: allision/collision (n=162, 32.5%), grounding (n=50, 10%), others

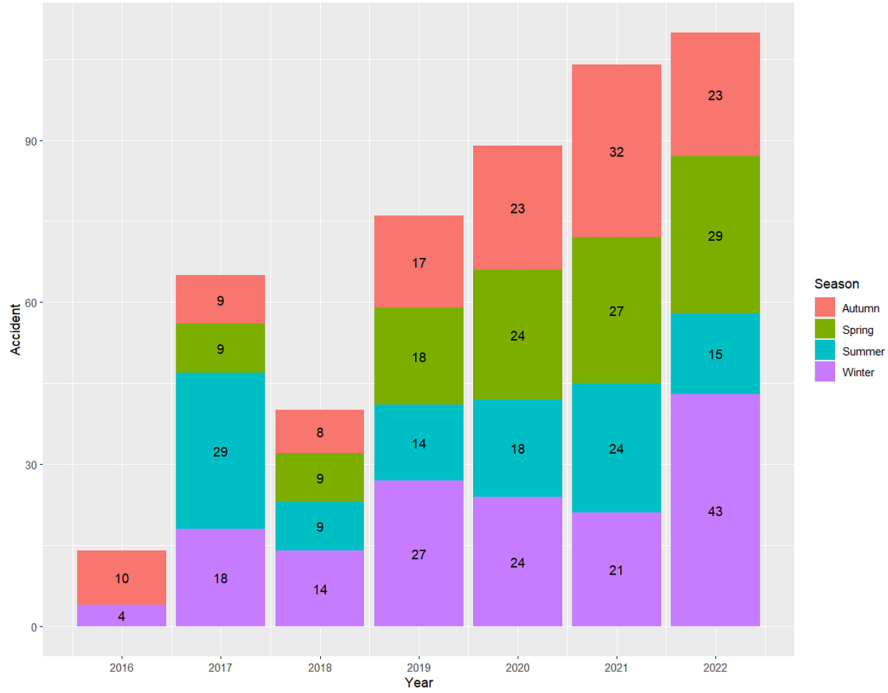

Figure 1. Distribution of accident season by years.

(n=41, 8.2%), fire (n=33, 6.6%), sinking (n=23, 4.6%), and man overboard (n=18, 3.6%). When hull/equipment accidents were examined in detail, it was found that the vessel type with the highest frequency of these accidents was the bulk carrier (n=61, 35.7%). Following bulk carriers, 32.2% (n=55) of hull/equipment accidents occurred on general cargo vessels, 15.8% (n=27) on tankers, 8.2% (n=14) on container ships, 5.3% (n=9) on passenger/RoRo vessels, and 2.9% (n=5) on tugboats. When the causes of accidents were examined separately for each vessel type, it was observed that the most common accident type for bulk carriers, container ships, tankers, and tugboats was hull/equipment failure (n=61, 42.7%; n=14, 38.9%; n=27, 40.3%; n=5, 50%, respectively). For general cargo vessels,

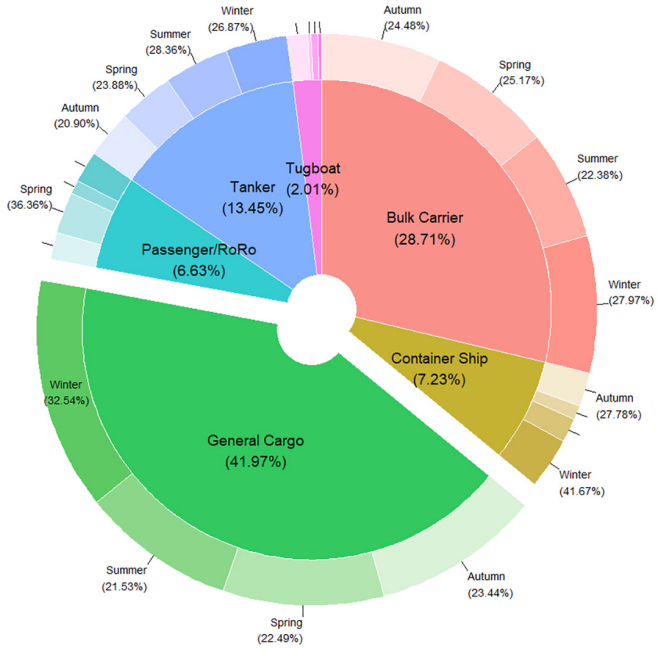

Figure 2. Distribution of the vessel types by season.

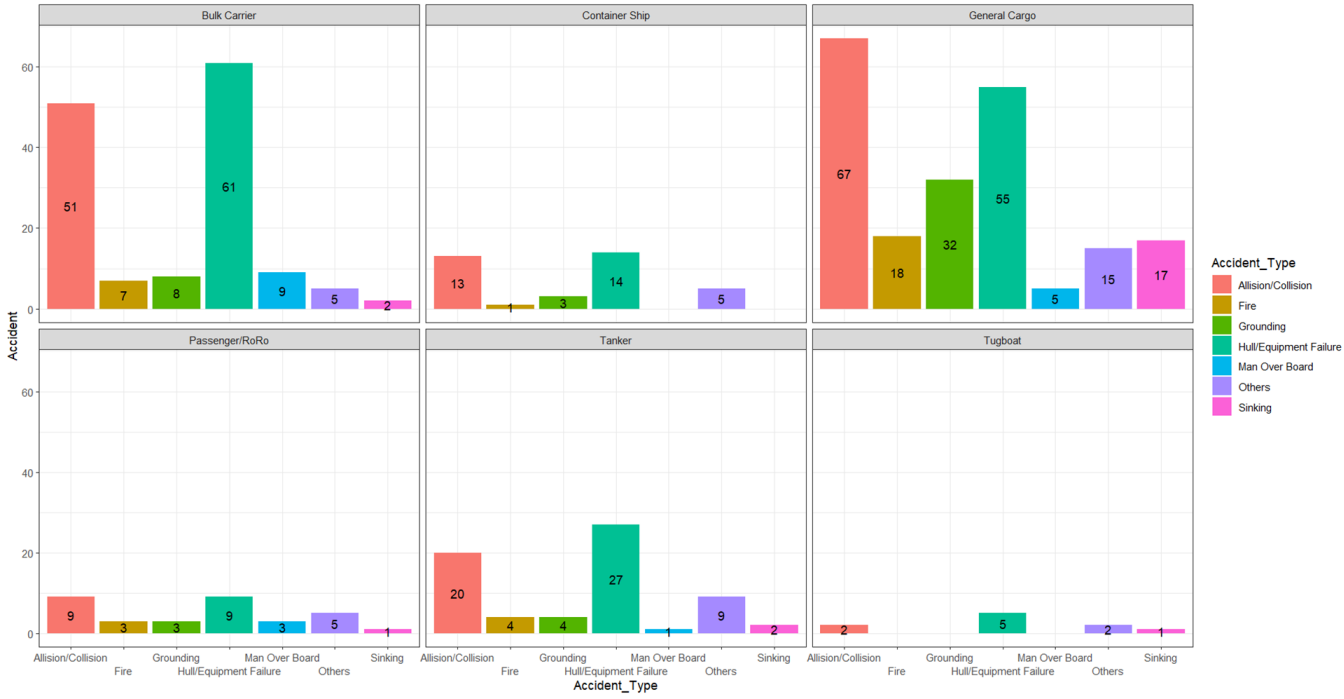

Figure 3. Distribution of the vessel types by accident type.

the most common accident type was allision/collision (n=67, 32.1%). In passenger/RoRo vessels, allision/collision and hull/equipment failure occurred with equal frequencies (n=9, 27.3%). The chi-square test results revealed a significant association between vessel type and accident type, χ^2 (30, n=498) =56.927, p-value =0.002. This finding suggests that certain accident types were more or less likely to occur in specific vessel types. However, except for general cargo vessels, post-hoc analyses for all other vessel types did not show significant differences, indicating that there were no statistically significant differences between vessel types for accident types (i.e., the differences between observed and expected frequencies were not significant). A statistically significant difference was observed for grounding-type accidents in general cargo vessels (p=0.03), indicating that grounding occurred more frequently in this vessel type compared to other types of accidents.

When examining the frequency distribution of accident types by season (Figure 4), it was observed that the winter season stands out as having the highest frequency of the most common accident type, namely hull/equipment failure, with 28.07% (n=48) of such accidents occurring in winter. Additionally, winter recorded the highest frequency of allision/collision accidents (n=49, 30.2%), grounding accidents (n=20, 40%), and other accident types (n=15, 36.6%). Conversely, the autumn season saw the highest occurrence of sinking accidents (n=10, 43.5%), while the summer season recorded the highest frequency of man-overboard accidents. Finally, fire-related accidents were most common in the spring season (n=9, 27.3%). A chi-square test was conducted to investigate whether there was a statistically significant relationship between accident types and the seasons in which they occurred. The p-value was greater than the 5% significance level, indicating that the null hypothesis (H_0), which stated that no relationship exists, could not be rejected, χ^2 (18, n=498)=20.303, p-value =0.316. In other words, the analysis showed that the season does not have a statistically significant effect on the occurrence of specific accident types. This finding was further supported by post-hoc analyses, which revealed that no individual accident type exhibited a significant association with any particular season. Therefore, the distribution of accidents by type appears consistent across different seasons, without notable seasonal influence on specific accident types.

Figure 5 illustrates the frequency distribution of vessel accident types by region. When analyzing the regions where accidents occurred, it was notable that the TSS had the highest frequency of accidents (n=362, 72.7%). In other words, 72.7% of the vessel accidents recorded between 2016 and 2022 took place in the TSS region. The Mediterranean (n=53, 10.6%), Aegean (n=49, 9.8%), and Black Sea (n=34, 6.8%) followed as the next most frequent regions for accidents. When examining hull/equipment failure, which was the most common accident type in the analyzed data set, it was observed that this type of accident occurred most frequently in the TSS (n=143, 83.6%). Hull/equipment failure was also the most common accident type in the Mediterranean region (n=13, 24.5%). In contrast, the Aegean and Black Sea regions

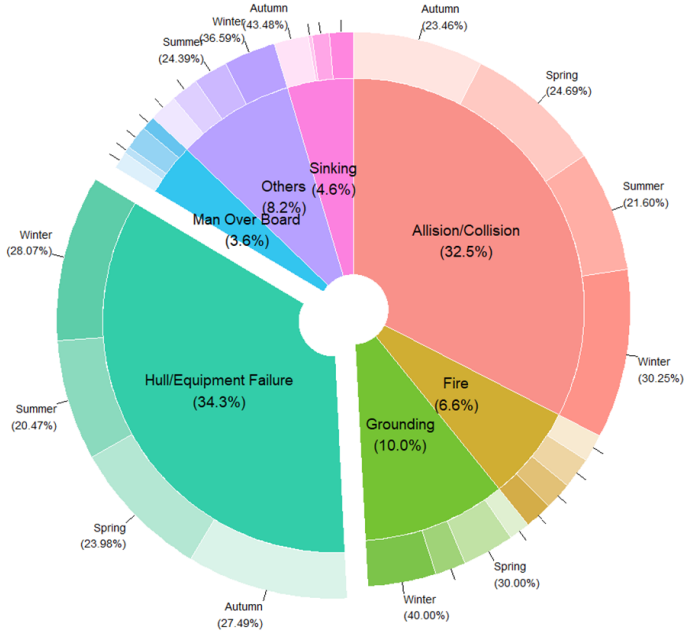

Figure 4. Distribution of the accident types by season.

showed different patterns. The Aegean region experienced the highest frequency of allision/collision accidents (n=16, 32.7%), while the most frequent accident types in the Black Sea region were allision/collision and grounding, both with equal frequency (n=7, 20.6%). Results from the chi-square test confirmed a significant relationship between accident type and region, χ^2 (18, n=498)= 64.443, p-value <0.001. This indicates that certain accident types were more or less frequent in specific regions. Post-hoc comparisons for allision/collision, grounding, man-overboard, and other accident types were not significant, showing no statistically significant differences between regions for these types of accidents (i.e., the difference between observed and expected frequencies was not statistically significant). However, there was a statistically significant difference for fire-type accidents in the TSS region compared to other regions (p-value =0.007), indicating that fire-type accidents occurred less frequently there. Additionally, sinking-type accidents were found to occur more frequently in the Black Sea Region (p-value =0.004). Hull/equipment failure accidents occurred more frequently in the TSS region (p-value =0.002), while sinking-type accidents occurred less frequently in this region compared to others (p-value =0.006).

Figure 6 illustrates the distribution of accidents of vessel types across different regions. It was observed that the TSS were the regions where the highest number of accidents occurred across all vessel types. For instance, 77.6% (n=111) of the accidents involving bulk carriers took place in this region, followed by the Mediterranean region with 11.6% (n=17). Also, the frequency of general cargo type vessels having accidents in this region was quite high compared to other regions (n=141, 67.5%). For passenger/RoRo and tugboat vessels, the TSS recorded the highest number of accidents, with the Mediterranean being the second most frequent region for these incidents. After the TSS, the Aegean Sea was the region with the second highest number of accidents for container ships and tankers (n=6, 16.7%; n=6, 9%, respectively). For general cargo vessels, on the other hand, the Black Sea was the second most frequent region (n=24, 11.5%). The chi-square test results indicated a significant relationship between vessel type and region, χ^2 (15, n=498) =27.632, p-value =0.02. This finding suggests that certain vessel types experienced accidents more or less frequently in specific regions. Post-hoc comparisons for bulk carriers, container ships, passenger/RoRo, tankers, and tugboats were not significant, leading to the conclusion that there was no statistically significant difference in accident rates between regions for these vessel types. However, a statistically significant difference (p-value =0.01) was found for general cargo type vessels in the Black Sea region, where the number of accidents observed was significantly higher than expected compared to other regions.

A new categorical variable was created based on gross tonnage, dividing vessels into three groups: those with a gross tonnage below 1000 GT, those between 1000 and 3000 GT, and those above 3000 GT. Subsequent analyses were performed using this classification. As shown in Figure 7, the dataset comprised 9.8% (n=49) vessels with a gross

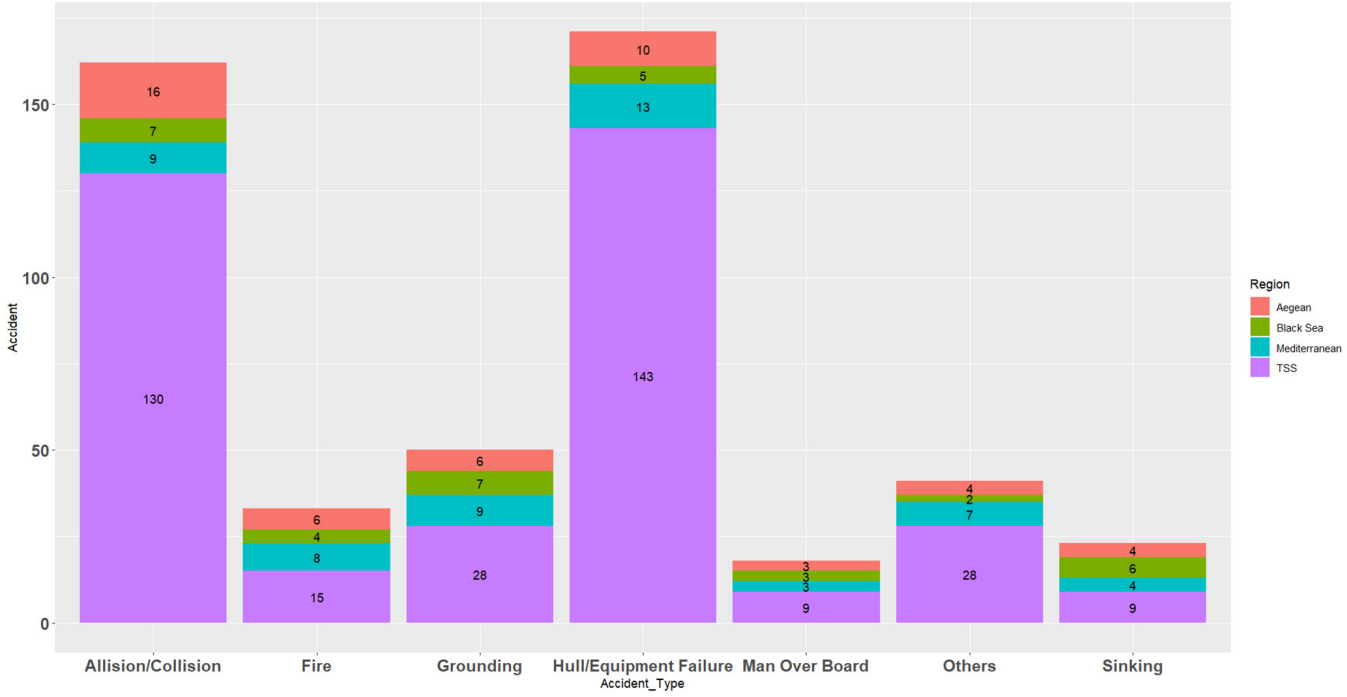

Figure 5. Distribution of the accident types by region.

tonnage below 1000 GT, 24.7% (n=123) vessels with a gross tonnage between 1000 and 3000 GT, and 65.5% (n=326) vessels with a gross tonnage above 3000 GT. Notably, the most common type of accident in two of the gross tonnage categories was hull/equipment failure, occurring in 35.8% (n=44) of vessels between 1000 and 3000 GT and 35.9% (n=117) of vessels above 3000 GT. In contrast, the most frequent accident type in the first category (vessels with a gross tonnage below 1000 GT) was grounding, with an occurrence rate of 30.6% (n=15). Additionally, sinking-type accidents were observed to occur with the lowest frequency in the highest gross tonnage category (2.1%, n=7). Similarly, man overboard was notably infrequent in the 1000-3000 GT and >3000 GT categories, with occurrence rates of 2.4%

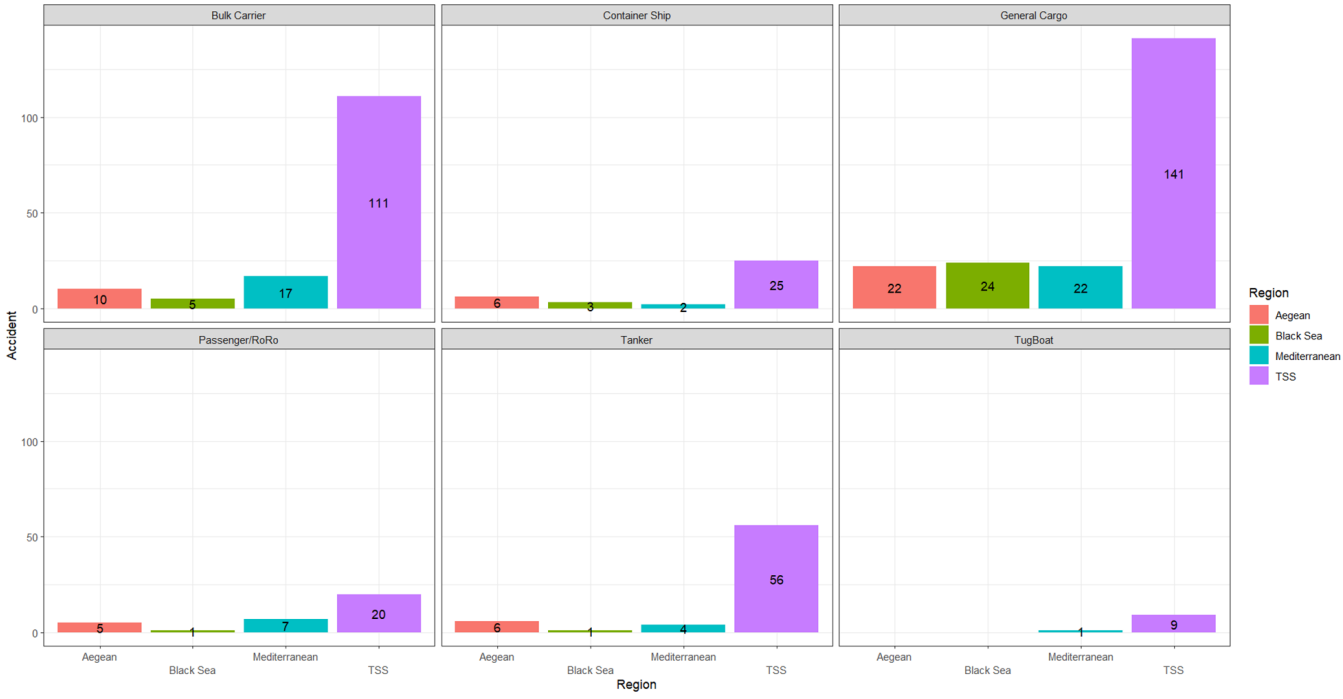

Figure 6. Distribution of the vessel types by region.

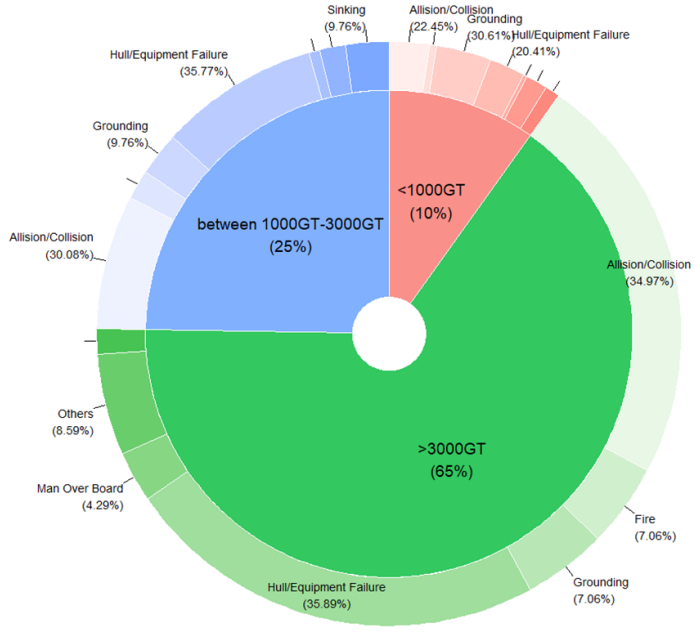

Figure 7. Distribution of the vessel gross tonnage by accident type.

(n=3) and 2% (n=1), respectively. The results of the chi-square test indicated a significant relationship between the vessel's gross tonnage category and the types of accident, χ^2 (12, n=498) =45.424, p=0.001. This suggests that, within the three gross tonnage categories, certain accident types occurred more or less frequently. The post hoc analysis using the Bonferroni correction was conducted to explore the significant differences in accident types across gross tonnage categories (<1000 GT, 1000-3000 GT, and >3000 GT). No statistically significant differences were found across the gross tonnage categories for allision/collision, fire, hull/equipment failure, man overboard, or other accident types, as all p-values exceeded the significance threshold after Bonferroni correction. The post hoc analysis revealed notable differences in the frequency of grounding and sinking accidents across gross tonnage categories. Grounding accidents were significantly more frequent in vessels with a gross tonnage of <1000 GT (p<0.01), whereas vessels in the >3000 GT category exhibited a significantly lower frequency of grounding accidents (p=0.047). No statistically significant differences were observed for the 1000-3000 GT category. Similarly, sinking accidents occurred significantly more frequently in vessels within the 1000-3000 GT category (p=0.037) but were significantly less frequent in vessels >3000 GT (p=0.006). No significant differences were found for vessels with a gross tonnage of <1000 GT. These findings suggest that grounding accidents are more prevalent in smaller vessels (<1000 GT), while sinking accidents are notably more frequent in medium-sized vessels (1000-3000 GT) but less common in larger vessels (>3000 GT).

3.2. Kruskal-Wallis H test

The first Kruskal-Wallis H test was conducted to examine whether the number of casualties (dead/loss) varied across different types of accidents, including sinking, allision/collision, man overboard, grounding, hull/equipment failure, fire, and others. The results indicated that there was no statistically significant difference in the number of fatalities between the accident types (Kruskal-Wallis H=5.059, p-value=0.536). This suggests that the distribution of casualties did not significantly differ depending on the type of accident, indicating that the type of accident may not have a direct impact on the number of casualties in the dataset. The mean ranks for each accident type, as shown in Table 1, provide a summary of the relative severity of casualties across different accident types. Although the test did not yield significant results, the mean ranks can offer insights into how the accident types were ordered in terms of casualties, with higher mean ranks indicating accident types associated with higher casualty numbers.

Another Kruskal-Wallis H test was conducted to investigate whether the number of casualties differed across the four regions: the TSS, the Aegean Sea, the Mediterranean Sea, and the Black Sea. The analysis revealed no statistically significant differences in the number of casualties between the regions (Kruskal-Wallis H =1.411, p-value =0.703). This suggests that the number of casualties did not vary significantly based on the region, indicating that the region of occurrence may not have a substantial effect on casualties outcomes. The mean ranks for each region, as shown in Table 2, provide a summary of the relative casualty outcomes in each region. Although the test did not yield significant results, the mean ranks can still offer insights into how casualties were distributed across the regions, with higher mean ranks indicating regions with higher casualty counts.

The last Kruskal-Wallis H test was performed to examine whether the number of casualties varied across the three vessel length categories: small (0-99 meters), medium (100-200 meters), and large (greater than 200 meters). The results (Table 3) indicated a statistically significant difference in

Table 1. Kruskal-Wallis test results (accident type-number of casualties).

Accident type	n	Mean Rank	Kruskal-Wallis H
Sinking	23	236.00	Test Stat=5.059 p-value=0.536
Allision/collision	162	251.37	
Man over board	18	264.03	
Grounding	50	250.76	
Hull/equipment failure	171	246.29	
Fire	33	243.45	
Others	41	260.00	

Table 2. Kruskal-Wallis test results (region-number of casualties).

Region	n	Mean Rank	Kruskal-Wallis H
Mediterranean	53	245.56	Test Stat=1.411 p-value=0.703
TSS	362	249.73	
Aegean	49	256.38	
Black Sea	34	243.24	

Table 3. Kruskal-Wallis test results (vessel length-number of casualties).

Vessel length	n	Mean Rank	Kruskal-Wallis H
Small	161	253.07	Test Stat=6.130 p-value=0.04
Medium	269	244.28	
Long	68	261.72	

the number of casualties between the length categories (Kruskal-Wallis H =6.130, p=0.04). This finding suggests that vessel length significantly influenced the number of casualties, with variations observed across the different length categories. The mean ranks for each category, presented in Table Y, offer a summary of the relative casualty outcomes for each vessel length group. These mean ranks indicated that casualty outcomes varied across vessel sizes. While small vessels had a slightly lower mean rank compared to large vessels, the difference between medium and small vessels appeared relatively modest. The higher mean rank for long vessels suggested that they might have experienced more casualties than medium-sized vessels, although the differences between medium and small vessels were less pronounced. Post-hoc tests revealed that the differences between small-medium and small-large vessel categories were not statistically significant (p-value =0.097 and p-value =0.374, respectively). However, the comparison between medium and long length vessels revealed a statistically significant difference (p-value =0.048), indicating that long length vessels were associated with a significantly higher number of casualties compared to medium-sized vessels. This result implies that, although both medium and long length vessels may experience casualties, large vessels tend to have a notably higher casualty rate.

This study analyzed 498 marine accidents involving various vessel types (bulk carriers, container ships, general cargo, passenger/RoRo, tugboats, and tankers) between 2016 and 2022. The accidents occurred in the Mediterranean, TSS, Aegean Sea, and Black Sea. Several parameters, including vessel type, accident type, region, gross tonnage, vessel length, and casualties (dead/missing), were examined. Statistical methods, such as frequency analysis, chi-square tests, and Kruskal-Wallis H tests, were employed to explore patterns and relationships. Significant differences in accident characteristics and casualty distributions were found across different parameters. Post-hoc analyses further identified specific differences between groups, offering valuable insights into the factors influencing accident severity and casualty outcomes.

4. Discussion

Analysis of the accident frequency between 2016 and 2022 indicated that incidents were most commonly observed during the winter months, with the highest frequency recorded in 2022. Chi-square tests and subsequent post-hoc analyses identified significant year-season variations, particularly highlighting increased accident frequencies in autumn 2016 and summer 2017. These findings underscore the influence of temporal patterns on maritime accident rates, aligning with the studies of Akten [28] and Liu et al. [29], who emphasized the role of temporal dynamics and operational conditions in shaping maritime incident trends. The variation in accident numbers between 2016 and 2022 may also reflect improvements in reporting and investigation practices in Türkiye in recent years. Enhanced focus on maritime safety and systematic documentation likely contributed to the higher number of recorded incidents in 2022 compared to the potential underreporting in 2016. This limitation should be considered when interpreting temporal trends in the dataset.

Regarding vessel types, general cargo vessels were involved in the highest number of accidents compared to other vessel types. However, the chi-square test revealed no significant relationship between vessel types and the seasons in which the accidents occurred, indicating that seasonal factors do not play a major role in the occurrence of these accidents. This result aligns with previous studies that highlight the greater influence of other factors, such as vessel-specific characteristics, operational challenges, and traffic density, in investigating accident patterns rather than seasonal changes [30].

An examination of accident types revealed that hull/equipment failure was the most common type of accident across all vessel types, with bulk carriers experiencing the highest frequency of such incidents. The chi-square test revealed a significant relationship between vessel type and accident type, indicating that certain types of accidents were more prevalent in specific vessel categories. However, post-hoc tests found no statistically significant differences for most vessel types, except for general cargo vessels, where grounding accidents occurred more frequently than expected. This finding is consistent with studies in the literature showing that certain types of ships are more prone to specific types of accidents [31,32].Seasonal variations in accident patterns were also explored, revealing that winter had the highest frequency of hull/equipment failure, as well as allision/collision, grounding, and other accident types. Conversely, autumn, summer, and spring had the highest occurrences of sinking, man-overboard, and fire-related accidents, respectively. However, the chi-square test indicated no statistically significant relationship between accident types and seasons, suggesting that the occurrence of specific accident types is not significantly influenced by seasonal variations. Post-hoc analyses confirmed a consistent distribution of accident types across different seasons. These results are consistent with prior research, indicating that while certain accident types may exhibit seasonal peaks in frequency, such patterns often lack statistical significance when analyzed comprehensively [33,34].Regional differences in accident frequency were also evident, with the TSS region exhibiting the highest

frequency of vessel accidents, particularly involving hull/equipment failure. Other regions, such as the Mediterranean, Aegean, and Black Sea, showed varying accident patterns, with allision/collision and grounding being more common in the latter two. Chi-square analysis confirmed a significant relationship between accident type and region, reflecting distinct regional accident trends. Notably, fire-type accidents were significantly less frequent in the TSS, highlighting that strict safety regulations, traffic control, and advanced fire safety measures aboard vessels contribute to the reduced occurrence of such incidents. The shorter transit times and more predictable weather patterns in this region may also play a role in mitigating the risk factors associated with fire incidents. Conversely, hull/equipment failure accidents were found to be particularly common in this region with post-hoc comparisons, consistent with the findings of several key studies [35,36]. These studies suggest that the high frequency of hull/equipment failures in the TSS can be attributed to the complex navigational conditions, dense traffic, and operational difficulties typical of the area. In addition, post hoc test results revealed that sinking-type accidents were more prevalent in the Black Sea, a finding consistent with previous important studies that attribute the higher frequency of such incidents to the Black Sea region's challenging environmental conditions, including weather patterns, difficult navigation routes, and rough seas [37,38].

The regional distribution of vessel accidents indicated that the TSS experienced the highest frequency of incidents across all vessel types. Specifically, for passenger/RoRo and tugboat vessels, the TSS recorded the highest accident counts, followed by the Mediterranean region. Conversely, the Aegean Sea ranked second for container ship and tanker accidents, while the Black Sea held the second position for general cargo vessel incidents. The chi-square test revealed a significant association between vessel type and accident region, suggesting certain vessel types were more susceptible to accidents in particular areas. However, post-hoc analyses identified no significant regional differences for most vessel types, except for general cargo vessels, which exhibited a significantly higher accident frequency in the Black Sea compared to other regions. Existing studies, such as [39,40] emphasize the elevated accident risk for general cargo vessels in the Black Sea, attributing this trend to operational and navigational challenges, complex maritime traffic, adverse weather conditions, poor visibility, and high traffic density.

The frequency analysis revealed that the dataset consisted of vessels classified into three gross tonnage categories: below 1000 GT, between 1000 and 3000 GT, and above 3000 GT. Hull/equipment failure was the most common accident type in the two larger categories (1000-3000 GT and >3000 GT). In contrast, grounding accidents were the most frequent among vessels with a gross tonnage below 1000 GT. Sinking accidents occurred at significantly higher rates in medium-sized vessels (1000-3000 GT), while both grounding and sinking accidents were notably less frequent in the highest gross tonnage category (>3000 GT). The chi-square test indicated a significant relationship between gross tonnage categories and accident types, confirming that accident frequencies vary depending on vessel tonnage. Post-hoc analysis revealed that grounding accidents were significantly more frequent in smaller tonnage vessels (<1000 GT) and significantly less frequent in larger tonnage vessels (>3000 GT). Similarly, sinking accidents were significantly more prevalent in medium-tonnage vessels (1000-3000 GT) compared to the other categories. These findings partially align with prior research suggesting that smaller tonnage vessels are more prone to grounding accidents due to their limited stability and vulnerability to harsh weather conditions, as noted by Chen et al. [41]. Furthermore, the elevated occurrence of sinking accidents in medium-tonnage vessels (1000–3000 GT) observed in this study underscores the operational challenges and safety issues highlighted by Akten [42], which are often associated with vessels in this tonnage range.

In addition to frequency analysis and chi-square procedures, this study conducted three Kruskal-Wallis H tests to examine the factors influencing the number of casualties in maritime accidents. The first analysis evaluated whether casualty numbers varied across different accident types, including sinking, allision/collision, man overboard, grounding, hull/equipment failure, fire, and others. Notably, the analysis showed no statistically significant differences in the number of casualties across various accident types, suggesting that accident type alone does not have a substantial effect on casualty outcomes. Instead, factors such as vessel size, weather conditions, and human error appear to play a more critical role in influencing the severity of casualties. These findings are consistent with prior research [41,43] which highlights the importance of vessel-specific and situational factors, such as emergency response capabilities and crew preparedness, in determining casualty outcomes. This study reinforces the need for targeted safety measures that address these broader influences rather than focusing solely on accident types. The second Kruskal-Wallis H test investigated whether casualty numbers differed across four regions: the TSS, the Aegean Sea, the Mediterranean Sea, and the Black Sea. The findings indicated no statistically significant differences between regions, implying that the geographical location of accidents does not play a major role in determining casualty outcomes. Despite the lack of statistical significance, the mean rank values offered a comparative understanding of casualty distributions

across regions. The Marine Accident Investigation Branch (MAIB) report on accidents in Scottish waters concluded that casualty severity was more closely related to vessel characteristics, human error, and operational factors than to the geographical region of the accident [44]. Also, recent studies reinforce the notion. For instance, a by Zhang et al. [45], it was emphasized that marine accidents do not differ according to geographical region and accident outcomes are generally determined independently of geographical location. The results of a last Kruskal-Wallis test revealed a significant relationship between vessel length and casualty rates, showing that larger vessels (those over 200 meters) had higher casualty rates compared to medium-sized vessels. Post-hoc analyses further confirmed that long vessels were associated with a significantly greater number of casualties than medium-length vessels, emphasizing the role of vessel size in casualty outcomes. Various studies have investigated the relationship between vessel size and the severity of casualties in maritime accidents. Montewka et al. [46] indicated that larger vessels have an increased risk of collision and that these risks are particularly pronounced in narrow waterways and heavy maritime traffic. Similarly, Chen et al. [41] noted that the high tonnage and large volume of large vessels tend to result in more serious consequences in collision and grounding situations. Furthermore, Gao et al. [47] suggested that ship tonnage increases the severity of collision accidents, thus larger ships cause more serious damage and loss of life. These studies collectively underscore the importance of vessel size in determining the severity of casualties in maritime accidents.

5. Conclusion

In conclusion, this study provides a comprehensive analysis of maritime accidents recorded between 2016 and 2022, based on data from the official records of the Directorate General of Coastal Safety, emphasizing the influence of temporal patterns, vessel types, accident types, and regional differences on accident frequencies and casualty outcomes across the Mediterranean, TSS, Aegean Sea, and Black Sea regions. The findings reveal a concentration of accidents in winter months, with a peak in 2022, possibly linked to improved reporting practices. General cargo vessels were the most involved in accidents, though seasonal influences were minimal, with vessel-specific factors playing a greater role. The TSS recorded the highest accident frequencies, while the Black Sea saw a higher prevalence of sinking accidents due to environmental challenges. Smaller vessels were more prone to grounding, while medium-tonnage vessels experienced more sinking incidents. Larger vessels showed higher casualty rates, emphasizing the need for improved design and emergency strategies.

By providing a comprehensive analysis of vessel accidents across different types, regions, and accident categories over a six-year period, this study offered significant insights into maritime accident patterns. By examining the role of vessel type, region, and temporal factors, the research contributed to understanding the complex dynamics of maritime accidents. Overall, this research enhanced the understanding of maritime safety by revealing significant relationships between accident characteristics, casualties, and environmental variables, and provides valuable insights for the development of more effective maritime safety policies and strategies to prevent future accidents.

Footnotes

Financial Disclosure: The author declared that this study received no financial support.

6. References

[1] UNCTAD, "Review of maritime transport 2017," in *United Nations Conference on Trade and Development*, Oct 2017. Accessed: Aug. 15, 2024. [Online]. Available: https://unctad.org/system/files/official-document/rmt2017_en.pdf

[2] D. Elrhoul, M. Romero Gómez, and M. Naveiro, "Review of green hydrogen technologies application in maritime transport," *International Journal of Green Energy*, vol. 20, pp. 1800-1825, 2023.

[3] UNCTAD, "Review of Maritime Transport 2023," in *United Nations Conference on Trade and Development,* Sep. 2023. Accessed: Aug. 15, 2024. [Online]. Available: https://unctad.org/system/files/official-document/rmt2023_en.pdf

[4] H. Wang, Z. Liu, X. Wang, T. Graham, and J. Wang, "An analysis of factors affecting the severity of marine accidents," *Reliability Engineering & System Safety*, vol. 210, 107513, 2021.

[5] T. Olgaç, and O. Bayazit, "An investigation of the maritime accident in the Aegean Sea Turkish search and rescue region," *Aquat Res*, vol. 6, pp. 83-96, 2023.

[6] M. Luo, and S.-H. Shin, "Half-century research developments in maritime accidents: Future directions," *Accident Analysis & Prevention*, vol. 123, pp. 448-460, 2019.

[7] S. Fan, J. Zhang, E. Blanco-Davis, Z. Yang, and X. Yan, "Maritime accident prevention strategy formulation from a human factor perspective using Bayesian Networks and TOPSIS," *Ocean Engineering*, vol. 210, pp. 107544, 2020.

[8] J. Chen, W. Bian, Z. Wan, Z. Yang, H. Zheng, and P. Wang, "Identifying factors influencing total-loss marine accidents in the world: Analysis and evaluation based on ship types and sea regions," *Ocean Engineering*, vol. 191, pp. 106495, 2019.

[9] M. Jiang, J. Lu, Z. Yang, and J. Li, "Risk analysis of maritime accidents along the main route of the Maritime Silk Road: a Bayesian network approach," *Maritime Policy & Management*, vol. 47, pp. 815-832, 2020.

[10] Y. Cao, X. Wang, Z. Yang, J. Wang, H. Wang, and Z. Liu, "Research in marine accidents: A bibliometric analysis, systematic review and future directions," *Ocean Engineering*, vol. 284, pp. 115048, 2023.

[11] A. N. Pilatis, D.-N. Pagonis, M. Serris, S. Peppa, and G. Kaltsas, "A Statistical Analysis of Ship Accidents (1990-2020) Focusing on

Collision, Grounding, Hull Failure, and Resulting Hull Damage," *Journal of Marine Science and Engineering*, vol. 12, Art. no. 1, pp. 122, 2024.

[12] H. Lan, X. Ma, L. Ma, and W. Qiao, "Pattern investigation of total loss maritime accidents based on association rule mining," *Reliability Engineering & System Safety*, vol. 229, pp. 108893, 2023.

[13] K. Liu, Q. Yu, Z. Yuan, Z. Yang, and Y. Shu, "A systematic analysis for maritime accidents causation in Chinese coastal waters using machine learning approaches," *Ocean & Coastal Management*, vol. 213, pp. 105859, 2021.

[14] H. Wang, Z. Liu, X. Wang, D. Huang, L. Cao, and J. Wang, "Analysis of the injury-severity outcomes of maritime accidents using a zero-inflated ordered probit model," *Ocean Engineering*, vol. 258, pp. 111796, 2022.

[15] E. C. Demirci, and S. Gülmez, "Ro-Ro gemi kazalarının vaka bazlı HFACS analizi," *Marine and Life Sciences,* vol. 3, no. 2, pp. 105-114, 2021.

[16] Ö. Uğurlu, S. Erol, and E. Başar, "The analysis of life safety and economic loss in marine accidents occurring in the Turkish Straits," *Maritime Policy & Management*, vol. 43, no. 3, pp. 356–370, 2016.

[17] B. Essiz, and B. Dagkiran, "Accidental risk analyses of the Istanbul and Canakkale Straits," *IOP Conf. Ser.: Earth Environ. Sci.*, vol. 95, no. 4, pp. 042042, 2017.

[18] M. Korçak, and C. E. Balas, "Reducing the probability for the collision of ships by changing the passage schedule in Istanbul Strait," *International Journal of Disaster Risk Reduction*, vol. 48, pp. 101593, 2020.

[19] F. Yılmaz, and M. N. İlhan, "Türk Bayraklı Gemilerin Karıştığı Deniz Kazaları ve Denizcilere Etkilerine İlişkin Bir Analiz," *GDT*, no. 211, pp. 80-95, 2018.

[20] İ. Balık, S. Z. Aydın, and F. Bitiktas, "Türk Boğazları Trafik Yoğunluğu, Bekleme Süreleri ve Deniz Kazaları," *Kent Akademisi*, vol. 15, no. 1, pp. 262-276, 2022.

[21] N. J. Ece, "Analysis of marine accidents in the strait of İstanbul using qualitative & quantative methods," *MEUJMAF*, vol. 1, no. 1, pp. 1-9, 2019.

[22] N. J. Ece, "Statistical analysis of marine accidents in the strait of İstanbul using chi-square test," *MEUJMAF*, vol. 3, no. 1, pp. 17-27, Jun. 2021.

[23] S. Yildiz, Ö. Uğurlu, S. Loughney, J. Wang, and F. Tonoğlu, "Spatial and statistical analysis of operational conditions influencing accident formation in narrow waterways: A Case Study of Istanbul Strait and Dover Strait," *Ocean Engineering*, vol. 265, pp. 2001, 2022.

[24] Ö. F. Görçün, and S. Z. Burak, "Formal Safety Assessment for Ship Traffic in the Istanbul Straits," *Procedia - Social and Behavioral Sciences*, vol. 207, pp. 252–261, Oct. 2015, doi: 10.1016/j.sbspro.2015.10.094.

[25] O. H. Arıcan, "Türk karasularında gerçekleşen gemi kazalarının denizcilik sözleşmeleri ihalleri üzerine araştırma," *Gemi ve Deniz Teknolojisi*, no. 225, pp. 73-89, 2024.

[26] B. Kamal, and E. Çakır, "Data-driven Bayes approach on marine accidents occurring in Istanbul strait," *Applied Ocean Research*, vol. 123, pp. 103180, 2022.

[27] T. M. Franke, T. Ho, and C. A. Christie, "The Chi-Square Test: Often Used and More Often Misinterpreted," *American Journal of Evaluation*, vol. 33, no. 3, pp. 448-458, 2012.

[28] N. Akten, "Shipping accidents: a serious threat for marine environment," *Journal of Black Sea / Mediterranean Environment*, vol. 12, no. 3, Art. no. 3, 2006.

[29] X. Liu, Q. Yu, Y. Hu, W. Lu, A. Zhanga, and X. Bo, "Cause Analysis of Ship Accidents Based on Chi-Square Test," presented at the Proceedings of the 2nd International Conference on Big Data Economy and Digital Management, BDEDM 2023, January 6-8, 2023, Changsha, China, Jun. 2023. Accessed: Nov. 13, 2024. [Online]. Available: https://eudl.eu/doi/10.4108/eai.6-1-2023.2330244

[30] W. K. Talley, D. Jin, and H. Kite-Powell, "Determinants of the severity of cruise vessel accidents," *Transportation Research Part D: Transport and Environment*, vol. 13, no. 2, pp. 86-94, 2008.

[31] A. L. Tunçel, E. Yüksekyıldız, E. Akyuz, and O. Arslan, "Probability-based extensive quantitative risk analysis: collision and grounding case studies for bulk carrier and general cargo ships," *Australian Journal of Maritime & Ocean Affairs*, vol. 15, no. 1, pp. 89-105, 2023.

[32] P. Kujala, M. Hänninen, T. Arola, and J. Ylitalo, "Analysis of the marine traffic safety in the Gulf of Finland," *Reliability Engineering & System Safety*, vol. 94, no. 8, pp. 1349-1357, 2009.

[33] C. Macrae, "Human factors at sea: common patterns of error in groundings and collisions," *Maritime Policy & Management*, vol. 36, no. 1, pp. 21-38, 2009.

[34] C. Hetherington, R. Flin, and K. Mearns, "Safety in shipping: The human element," *Journal of Safety Research*, vol. 37, no. 4, pp. 401-411, 2006.

[35] E. Doğan, and S. Burak, "Ship-Originated Pollution in the Istanbul Strait (Bosphorus) and Marmara Sea," *Journal of Coastal Research*, vol. 23, no. 2 (232), pp. 388-394, 2007.

[36] Ö. S. Ulusçu, B. Özbaş, T. Altıok, and İ. Or, "Risk Analysis of the Vessel Traffic in the Strait of Istanbul," *Risk Analysis*, vol. 29, no. 10, pp. 1454-1472, 2009.

[37] Ö. Uğurlu, S. Yıldız, S. Loughney, J. Wang, S. Kuntchulia, and I. Sharabidze, "Analyzing collision, grounding, and sinking accidents occurring in the Black Sea utilizing HFACS and Bayesian networks," *Risk Analysis*, vol. 40, no. 12, pp. 2610–2638, 2020.

[38] D. Huang, T. Liang, S. Hu, S. Loughney, and J. Wang, "Characteristics analysis of intercontinental sea accidents using weighted association rule mining: Evidence from the Mediterranean Sea and Black Sea," *Ocean Engineering*, vol. 287, p. 115839, 2023.

[39] N. Akten, "Maritime traffic accident statistics and risk factors in the Black Sea," *Marine Safety and Risk Analysis*, vol. 7, no. 1, pp. 21–34, 2006.

[40] P. Georgiev, and Y. Garbatov, "Multipurpose Vessel Fleet For Short Black Sea Shipping Through Multimodal Transport Corridors," *Brodogradnja : An International Journal of Naval Architecture and Ocean Engineering for Research and Development*, vol. 72, no. 4, pp. 79-101, 2021.

[41] J. Chen, W. Bian, Z. Wan, S. Wang, H. Zheng, and C. Cheng, "Factor assessment of marine casualties caused by total loss," *International Journal of Disaster Risk Reduction*, vol. 47, pp. 101560, 2020.

[42] N. Akten, "Analysis of ship accidents and factors affecting marine safety in the Black Sea," *Maritime Research Journal*, vol. 40, no. 4, pp. 251–262, 2006.

[43] N. J. Ece, "Analysis of ship accidents in the strait of Istanbul," *Dokuz Eylül Üniversitesi Denizcilik Fakültesi Dergisi*, vol. 4, no. 2, Art. no. 2, 2012.

[44] Marine Accident Investigation Branch, "Investigation into maritime accidents in the Scottish waters." MAIB Annual Report, 2007. [Online]. Available: https://assets.publishing.service.gov.uk/media/5e81d604d3bf7f133f849387/2007-SD3-MAIBSafetyDigest.pdf

[45] Y. Zhang, X. Sun, J. Chen, and C. Cheng, "Spatial patterns and characteristics of global maritime accidents," *Reliability Engineering & System Safety*, vol. 206, pp. 107310, 2021.

[46] J. Montewka, T. Hinz, P. Kujala, and J. Matusiak, "Probability modelling of vessel collisions," *Reliability Engineering & System Safety*, vol. 95, no. 5, pp. 573-589, 2010.

[47] X. Gao, L. Yu, Q. Yu, and W. Dai, ""Analyzing influential factors of ship collision accidents severity using ordered probit model," in *2023 7th International Conference on Transportation Information and Safety (ICTIS)*, vol. 8, pp. 1-8, 2023.

RESEARCH ARTICLE

DOI: 10.54926/jnamt.2025.249

J Nav Architect Mar Technol 2024;226(2):80-90

A Practical Approach to the Design of Long Sandwich Plates

Erkin Altunsaray, Gökdeniz Neşer

Dokuz Eylül University, Institute of Marine Sciences and Technology, Department of Naval Architecture, İzmir, Türkiye

To cite this article: E. Altunsaray, and G. Neşer. A practical approach to the design of long sandwich plates. *J Nav Architect Mar Technol*. 2024;226(2):80-90.

Received: 30.10.2024 - **Revised:** 23.12.2024 - **Accepted:** 29.01.2025 - **Publication Date:** 31.01.2025

Abstract

Sandwich materials in plate form, crafted from advanced composite face sheets and lightweight core materials, are extensively utilized in marine structures, particularly in pleasure boats. This is due to their high specific strength, ease of formability, high rigidity, and cost-effectiveness. Given their complex internal structures, there is a pressing need for practical methods to accurately analyze the behavior of sandwich plates during the preliminary design phase, where time constraints can heavily impact the designer's decisions. Although rule-based approaches are often seen as a quick and suitable solution for reaching initial design assumptions, they can result in heavier structures compared to those achieved through optimization using more time-intensive numerical methods, ultimately leading to suboptimal designs.This study presents a practical method for obtaining a lightweight sandwich structure without the necessity of numerical analyses, utilizing a parametric approach specifically developed for this purpose. The approach is tailored to address the design of a sandwich plate representing the bottom of a boat. It features carbon fiber-reinforced epoxy face sheets and a PVC foam core, which is simply supported at the edges while being subjected to compressive loads that can induce buckling along the long edges. Ansys was also used to select the lightest one among 12 different sandwich plate combinations. The optimization was carried out on the basis of critical buckling loads obtained by the Long Sandwich Plate Method.

Keywords: Critical buckling load, Long Sandwich Plate Method (LSPM), structural optimization, ship structural analysis

1. Introduction

Sandwich plate materials made from polymer-based composites are extensively used in the marine industry, serving various purposes, from the hull structures of ships to their components. These plates are utilized by ships and in structures that generate marine renewable energy, such as wind turbines and wave energy converters, as well as in modern technologies like unmanned marine vehicles [1-6]. These materials have proven to be an excellent choice due to their superior specific strength, meaning they are lightweight while maintaining high strength. Additionally, they offer advantages in logistics and production with low emissions and have a long lifespan primarily because of their resistance to environmental factors. This aligns well with current environmental concerns that drive industries toward sustainability in design and production. Other benefits of sandwich structures in marine applications include good buckling resistance and crashworthiness, reduced construction weight, and the ability to support large spans without additional stiffening. This results in increased usable volume, greater design flexibility, fewer parts, and reduced assembly time.The marine industry can widely use sandwich materials made from polymer-based composites. This includes innovative applications that ensure time-saving designs and allow designers to work freely. Because

Address for Correspondence: Erkin Altunsaray, Dokuz Eylül University Institute of Marine Sciences and Technology, Department of Naval Architecture, İzmir, Türkiye

E-mail: erkin.altunsaray@deu.edu.tr

ORCID ID: orcid.org/0000-0003-3099-6059

these materials can easily produce complex forms that cannot be achieved with metal or alloy equivalents, this flexibility in design allows for innovative shapes and structures that can enhance performance and aesthetic appeal. Glass or carbon fiber-reinforced epoxy or vinyl ester composites are commonly used as face sheets. At the same time, closed or open-cell foam, balsa of various densities, and aluminum honeycombs serve as cores. These materials are notable components of sandwich structures made from polymer-based composites, which are widely utilized in the boatbuilding industry.

The loads that the structural elements of ships, especially those sailing in rough seas, must carry are quite variable in terms of their magnitude, the direction of action (compression, tension, shear, compound, bending, torsion, buckling, etc.), and behavior (cyclic, randomly variable over time, singular, shock, etc.). The selection and dimensioning of the materials of the structural elements are made by taking into account the various loads that a ship in the design phase may encounter throughout its life. In marine conditions, buckling comes to the forefront as the inevitable load that elements in plate form will be exposed to.

Research on buckling, recognized as the most critical load that sandwich plates encounter, focuses on optimizing both the geometry and lamination of these plates under the relevant loads [7-9] and selecting the appropriate materials. When addressing complex challenges, such as designing the bottom sandwich plates of high-speed marine vehicles, buckling loads are typically analyzed using various plate theories, considering them as uniformly distributed axial and biaxial in-plane loads [10,11].

It is worth noting that the first scientific publication on sandwich plates was a study by Marquerre in 1944 on the behavior of these structures under buckling loads, which was cited in [12]. Most research investigating the buckling behavior of sandwich composite plates focuses on enhancing the mechanical properties of the facesheet and core components by using auxiliary materials, such as modifications with multi-walled carbon nanotubes [13-15]. Additionally, at an analytical level, studies that aim to determine buckling responses utilize approaches like Reddy's higher-order shear deformation theory [16] as well as numerical methods, including the Finite Element Method (FEM) and the Generalized Differential Quadrature Method [17].

In this study, the optimization of the components (face sheets and core) of rectangular sandwich plates with long length compared to their width and subjected to buckling load, representing the bottom structure of a small marine craft, was carried out with the Long Sandwich Plate Method (LSPM) [18,19]. The obtained analytical results were also verified with the help of the ANSYS software [20] based on the FEM. The study aims to propose practical tools for designers who design composite sandwich plates, whose numerical or analytical modeling requires expertise and time, such as the graph that gives the critical buckling loads depending on the plate dimensions presented at the end.

2. Materials and Methods

2.1. Governing Equations of Sandwich Plates Under Critical Buckling Load

Kirchhoff Plate Theory is applied to analyze thin plates undergoing small deformations. Under this theory, it is assumed that after deformation, the normal to the plane remains perpendicular to the reference plane and does not curve. The governing equations for plates and thin plates are presented below.

In the case of sandwich plates, the normal line remains straight but is not perpendicular to the reference plates (neutral axis) (Figure 1). The displacements at the x and y axis are given in Equation 1.

$$u = u^0 - z\chi_{xz} \quad v = v^0 - z\chi_{yz} \tag{1}$$

where, χ_{xz} and χ_{yz} are the rotations of the normals at the x-z and y-z planes, respectively.

From Figure 1, the first derivative of the deflection w^0 of reference plane with respect to x is

$$\frac{\partial w^0}{\partial x} = \chi_{xz} + \gamma_{xz} \tag{2}$$

and similarly the first derivative of the w^0 of reference plane with respect to y is,

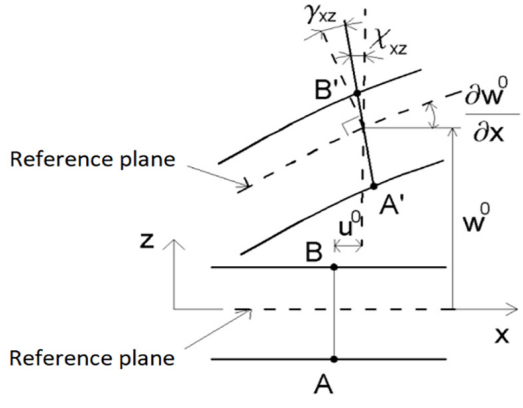

Figure 1. Deformation of a sandwich plates [18]

$$\frac{\partial w^0}{\partial y} = \chi_{yz} + \gamma_{yz} \tag{3}$$

As for the strains at the reference planes are,

$$\epsilon_x^0 = \frac{\partial u^0}{\partial x} \ , \ \epsilon_y^0 = \frac{\partial v^0}{\partial y} \ , \ \gamma_{xy}^0 = \frac{\partial u^0}{\partial y} + \frac{\partial v^0}{\partial x} \tag{4}$$

From Equations 2 and 3, transverse shear strains are

$$\gamma_{xz} = \frac{\partial w^0}{\partial x} - \chi_{xz} \ , \ \gamma_{yz} = \frac{\partial w^0}{\partial y} - \chi_{yz} \tag{5}$$

While shear deformation is zero, those expressions of curvatures of reference planes can be reached

$$\kappa_x = -\frac{\partial \chi_{xz}}{\partial x}, \quad \kappa_y = -\frac{\partial \chi_{yz}}{\partial y}, \quad \kappa_{xy} = -\frac{\partial \chi_{xz}}{\partial y} - \frac{\partial \chi_{yz}}{\partial x} \tag{6}$$

From these Equations 4-6, strain-displacement relations of the sandwich plates can be seen.

The section of the sandwich plate is illustrated in Figure 2, where t^t and t^b represent the thicknesses of the outer and inner (upper and lower) face sheets, respectively. In this study, t^t and t^b are equal, as they share the same thickness and symmetrical lamination sequence. Similarly, the reference plane is located at the midplane of the sandwich plate, which means that d^t and d^b are also equal. For these variables, the relationship d=c+t is shown in Figure 2.

To establish the force-strain relationship, the forces and moments are described in Equations 7 and 8, respectively.

$$\begin{aligned} N_x &= \int_{-h_b}^{h_t} \sigma_x dz \ , \ N_y = \int_{-h_b}^{h_t} \sigma_y dz, \\ N_{xy} &= \int_{-h_b}^{h_t} \tau_{xy} dz \ , M_x = \int_{-h_b}^{h_t} z\sigma_x dz, \\ M_y &= \int_{-h_b}^{h_t} z\sigma_y dz, \ M_{xy} = \int_{-h_b}^{h_t} z\tau_{xy} dz \end{aligned} \tag{7}$$

$$V_x = \int_{-h_b}^{h_t} \tau_{xz} dz \ , \quad V_y = \int_{-h_b}^{h_t} \tau_{yz} dz \tag{8}$$

N_i, M_i, and V_i are in plane forces, moments and transverse shear forces respectively. h_t and h_b are the distances from the reference plane to the surface of the plate.

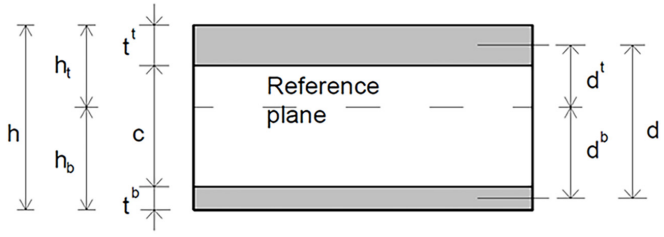

Figure 2. Sandwich plate geometry [18]

As for in-plane stresses,

$$\begin{Bmatrix} \sigma_x \\ \sigma_y \\ \tau_{xy} \end{Bmatrix} = \begin{bmatrix} \overline{Q}_{11} & \overline{Q}_{12} & \overline{Q}_{16} \\ \overline{Q}_{12} & \overline{Q}_{22} & \overline{Q}_{26} \\ \overline{Q}_{16} & \overline{Q}_{26} & \overline{Q}_{66} \end{bmatrix} \begin{Bmatrix} \epsilon_x \\ \epsilon_y \\ \gamma_{xy} \end{Bmatrix} \tag{9}$$

As for the strains at z distance from the reference plane:

$$\begin{aligned} \epsilon_x &= \frac{\partial u}{\partial x} = \frac{\partial u^0}{\partial x} - z\frac{\partial \chi_{xz}}{\partial x} \\ \epsilon_y^0 &= \frac{\partial v}{\partial y} = \frac{\partial v^0}{\partial y} - z\frac{\partial \chi_{yz}}{\partial y} \\ \gamma_{xy}^0 &= \frac{\partial u}{\partial y} + \frac{\partial v}{\partial x} = \frac{\partial u^0}{\partial y} + \frac{\partial v^0}{\partial x} - z\left(\frac{\partial \chi_{xz}}{\partial y} + \frac{\partial \chi_{yz}}{\partial x}\right) \end{aligned} \tag{10}$$

From the Equations 4th, 7th, 9th and 10th and the definitions of rigidity matrices [A], [B] and [D], following expressions can be obtained:

$$\begin{Bmatrix} N_x \\ N_y \\ N_{xy} \end{Bmatrix} = [A]\begin{Bmatrix} \epsilon_x^0 \\ \epsilon_x^0 \\ \gamma_{xy}^0 \end{Bmatrix} + [B]\begin{Bmatrix} -\frac{\partial \chi_{xz}}{\partial x} \\ -\frac{\partial \chi_{yz}}{\partial y} \\ -\frac{\partial \chi_{xz}}{\partial y} - \frac{\partial \chi_{yz}}{\partial x} \end{Bmatrix} \tag{11}$$

$$\begin{Bmatrix} M_x \\ M_y \\ M_{xy} \end{Bmatrix} = [B]\begin{Bmatrix} \epsilon_x^0 \\ \epsilon_x^0 \\ \gamma_{xy}^0 \end{Bmatrix} + [D]\begin{Bmatrix} -\frac{\partial \chi_{xz}}{\partial x} \\ -\frac{\partial \chi_{yz}}{\partial y} \\ -\frac{\partial \chi_{xz}}{\partial y} - \frac{\partial \chi_{yz}}{\partial x} \end{Bmatrix} \tag{12}$$

From the Equation 6, the Equations 11 and 12 can be written as;

$$\begin{Bmatrix} N_x \\ N_y \\ N_{xy} \end{Bmatrix} = [A]\begin{Bmatrix} \epsilon_x^0 \\ \epsilon_x^0 \\ \gamma_{xy}^0 \end{Bmatrix} + [B]\begin{Bmatrix} \kappa_x \\ \kappa_y \\ \kappa_{xy} \end{Bmatrix} \tag{13}$$

$$\begin{Bmatrix} M_x \\ M_y \\ M_{xy} \end{Bmatrix} = [B]\begin{Bmatrix} \epsilon_x^0 \\ \epsilon_x^0 \\ \gamma_{xy}^0 \end{Bmatrix} + [D]\begin{Bmatrix} \kappa_x \\ \kappa_y \\ \kappa_{xy} \end{Bmatrix} \tag{14}$$

The relation between transverse shear forces and transverse shear stress can be given as,

$$\begin{Bmatrix} V_x \\ V_y \end{Bmatrix} = \begin{bmatrix} \breve{S}_{11} & \breve{S}_{12} \\ \breve{S}_{12} & \breve{S}_{22} \end{bmatrix} \begin{Bmatrix} \gamma_{xz} \\ \gamma_{yz} \end{Bmatrix} \tag{15}$$

where $[\breve{S}]$ is the shear stiffness matrix (rigidity matrix) of the sandwich plate.

At the boundary conditions for simple support, deflection, w^0, boundary moment, M_x, torsion moment M_{xy}, and in-plane forces N_x and N_{xy} are zero.

$$w^0 = 0,\ M_x = M_{xy} = 0,\ N_x = N_{xy} = 0 \tag{16}$$

so, governing equations of thin plates can be given below

Force-strain relations:

$$\begin{Bmatrix} N_x \\ N_y \\ N_{xy} \\ M_x \\ M_y \\ M_{xy} \end{Bmatrix} = \begin{bmatrix} A_{11} & A_{12} & A_{16} & B_{11} & B_{12} & B_{16} \\ A_{12} & A_{22} & A_{26} & B_{12} & B_{22} & B_{26} \\ A_{16} & A_{26} & A_{66} & B_{16} & B_{26} & B_{66} \\ B_{11} & B_{12} & B_{16} & D_{11} & D_{12} & D_{16} \\ B_{12} & B_{22} & B_{26} & D_{12} & D_{22} & D_{26} \\ B_{16} & B_{26} & B_{66} & D_{16} & D_{26} & D_{66} \end{bmatrix} \begin{Bmatrix} \epsilon_{lx}^0 \\ \epsilon_y^0 \\ \gamma_{xy}^0 \\ \kappa_x \\ \kappa_y \\ \kappa_{xy} \end{Bmatrix} \tag{17}$$

A_{ij}, B_{ij}, and D_{ij} in Equation 17th are the extensional, Aijbending-extension coupling, and bending stiffnesses matrices, respectively. These matrices are shown in the form of reduced stiffness matrices below,

$$\begin{aligned} A_{ij} &= \sum_{k=1}^{K} \left(\overline{Q}_{ij}\right)_k (z_k - z_{k-1}) \\ B_{ij} &= \frac{1}{2}\sum_{k=1}^{K} \left(\overline{Q}_{ij}\right)_k \left(z_k^2 - z_{k-1}^2\right) \\ D_{ij} &= \frac{1}{3}\sum_{k=1}^{K} \left(\overline{Q}_{ij}\right)_k \left(z_k^3 - z_{k-1}^3\right) \end{aligned} \tag{18}$$

The elements of the reduced stiffness matrix of $\left[\overline{Q}\right]$ are given below:

$$\begin{aligned} \overline{Q}_{11} &= c^4 Q_{11} + s^4 Q_{22} + 2c^2 s^2 \left(Q_{12} + 2Q_{66}\right) \\ \overline{Q}_{22} &= s^4 Q_{11} + c^4 Q_{22} + 2c^2 s^2 \left(Q_{12} + 2Q_{66}\right) \\ \overline{Q}_{12} &= c^2 s^2 \left(Q_{11} + Q_{22} - 4Q_{66}\right) + \left(c^4 + s^4\right) Q_{12} \\ \overline{Q}_{66} &= c^2 s^2 \left(Q_{11} + Q_{22} - 2Q_{12}\right) + \left(c^2 - s^2\right)^2 Q_{66} \\ \overline{Q}_{16} &= cs\left(c^2 Q_{11} - s^2 Q_{22} - \left(c^2 - s^2\right)\left(Q_{12} + 2Q_{66}\right)\right) \\ \overline{Q}_{26} &= cs\left(s^2 Q_{11} - c^2 Q_{22} + \left(c^2 - s^2\right)\left(Q_{12} + 2Q_{66}\right)\right) \end{aligned} \tag{19}$$

Here $c = \cos\theta$ and $s = \sin\theta$.

To determine the stiffness matrix of the sandwich plate, the following procedure will be used:

It is assumed that the thickness of the core is constant and in-plane stiffnesses of the core are neglected. By these assumptions, the stiffness matrices [A], [B], and [D] can be obtained by using the stiffnesses of face sheets and parallel axes theorem.

Since the upper and lower faceshetts are the same and have a symmetrical lamination sequence to their midplane, the bending-extension coupling stiffness matrix, [B], is zero while the bending-extension coupling matrix, [A], is the summation of the upper and lower extensional matrices.

$$[A] = 2\,[A]^t \tag{20}$$

and [D] is the bending stiffness matrix,

$$[D] = \frac{1}{2}d^2\,[A]^t + 2\,[D]^t \tag{21}$$

To determine the shear rigidity matrix, $[\breve{S}]$, the transverse shear stresses, τxz are distributed uniformly due to the assumption of neglecting in-plane stiffness of cores. Generally, the shear stress distribution of outer face sheets is like that shown in Figure 3a. This approach assumes a linear shear stress distribution (Figure 3b). Accordingly, the transverse shear force, V_x is

$$V_x = \int_{-h_b}^{h_b} \tau_{xz}\,\mathrm{d}z = \tau_{xz}^c + \tau_{xz}^c \frac{t^t}{2} + \tau_{xz}^c \frac{t^b}{2} = \tau_{xz}^c d \tag{22}$$

and

$$d = c + \frac{t^t}{2} + \frac{t^b}{2} \tag{23}$$

where the relations c, t, and b are core, outer (upper), and inner (lower) face sheets, respectively, while d is given in Figure 3.

Similarly, V_y is given below,

$$V_y = \tau_{yz}^c d \tag{24}$$

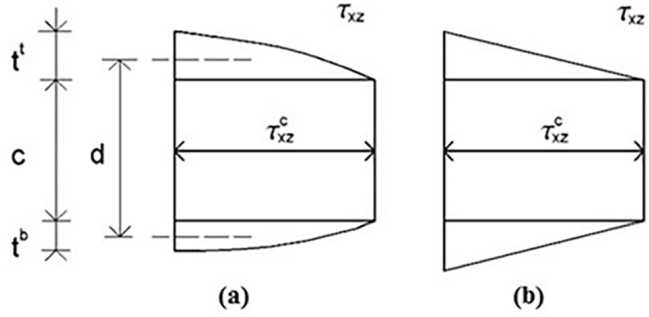

Figure 3. **(a)** Actual distribution, **(b)** approximate distribution of shear stress at the sandwich plate [18]

The relation between stress and strain in the core material is also given below.

$$\begin{Bmatrix} \tau_{xz}^{c} \\ \tau_{yz}^{c} \end{Bmatrix} = \begin{bmatrix} \overline{C}_{55}^{c} & \overline{C}_{45}^{c} \\ \overline{C}_{45}^{c} & \overline{C}_{44}^{c} \end{bmatrix} \begin{Bmatrix} \gamma_{xz}^{c} \\ \gamma_{yz}^{c} \end{Bmatrix} \tag{25}$$

Where $\overline{C}_{ij}^{c}$ is the element of the stiffness matrix of the core. In Equation 25, the shear deformations of the outer face sheets are neglected. By this approach, the transverse section of γ_{xz}^{c} is shown in Figure 4a. The mean shear deformation, γ_{xz} is also shown in the Figure 4b. As for Figure 4c. shows the relation between shear deformation and core deformation.

From Figure 4,

$$\gamma_{xz}^{c} = \frac{d}{c}\gamma_{xz}, \gamma_{yz}^{c} = \frac{d}{c}\gamma_{yz} \tag{26}$$

From the Equations 22-26, the relation between transverse shear forces and mean shear deformations yields:

$$\begin{Bmatrix} V_x \\ V_y \end{Bmatrix} = \frac{d^2}{c}\begin{bmatrix} \overline{C}_{55}^{c} & \overline{C}_{45}^{c} \\ \overline{C}_{45}^{c} & \overline{C}_{44}^{c} \end{bmatrix} \begin{Bmatrix} \gamma_{xz} \\ \gamma_{yz} \end{Bmatrix} \tag{27}$$

By substituting the Equation 15 into Equation 27:

$$\begin{bmatrix} \widetilde{S}_{11} & \widetilde{S}_{12} \\ \widetilde{S}_{12} & \widetilde{S}_{22} \end{bmatrix} = \frac{d^2}{c}\begin{bmatrix} \overline{C}_{55}^{c} & \overline{C}_{45}^{c} \\ \overline{C}_{45}^{c} & \overline{C}_{44}^{c} \end{bmatrix} \tag{28}$$

2.2. Buckling of Long Sandwich Plates

Long rectangular plates have length, b is quite larger compared to its width a ($b \gg a$). The boundary condition is simply supported at the edges of the plate. A uniform compressive force N_{x0} is applied along the long edges of the plate. The deflected surface of the plate can be assumed to be cylindrical at a significant distance from the short edges and is parallel to the axis.

The LPSM can be applied for orthotropic plates when the following inequality is satisfied [18]:

$$\frac{b}{a} > 3\sqrt[4]{\frac{D_{11}}{D_{22}}} \tag{29}$$

Where D_{11} and D_{22} are bending stiffness matrix elements. The equilibrium equations are given below

$$\frac{dV_x}{dx} - N_{x0}\frac{d^2w^0}{dx^2} = 0 \tag{30}$$

$$\frac{dM_x}{dx} - V_x = 0 \tag{31}$$

The sandwich plate is symmetrical to the midplane. The bending moment and the transverse shear force are given below

$$M_x = -D_{11}\frac{\partial \chi_{xz}}{\partial x}, V_x = \widetilde{S}_{11}\gamma_{xz} \tag{32}$$

From the Equations 30, 31, 32, and 2, the expressions of symmetrically laminated plates

$$-D_{11}\frac{d^3\chi}{dx^3} - N_{x0}\frac{d^2w^0}{dx^2} = 0 \tag{33}$$

$$D_{11}\frac{d^2\chi}{dx^2} + \widetilde{S}_{11}\left(\frac{dw^0}{dx} - \chi\right) = 0 \tag{34}$$

As for isotropic sandwich plates

$$-\widehat{EI}\frac{d^3\chi}{dx^3} - \widehat{N}_{x0}\frac{d^2w^0}{dx^2} = 0 \tag{35}$$

$$\widehat{EI}\frac{d^2\chi}{dx^2} + \hat{S}\left(\frac{dw}{dx} - \chi\right) = 0 \tag{36}$$

where $\widehat{EI}$ and $\hat{S}$ are the bending and shear stiffnesses, respectively, and $\widehat{N}_{x0}$ is the compressive load acting on the length of the plate.

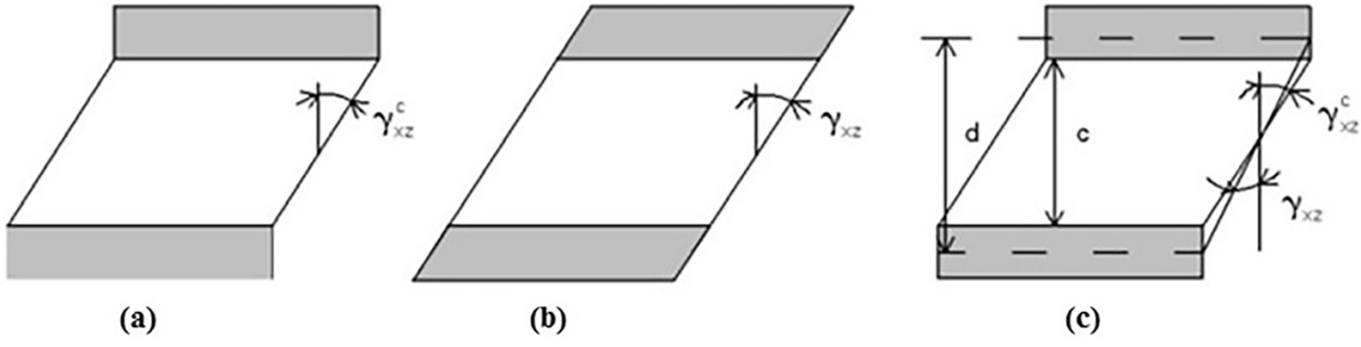

Figure 4. (a-c) Shear deformations of a sandwich plate [18]

By substituting D_{11}, $\tilde{S}_{11}$, and $\hat{N}_{x0}$ of the Equations 35 and 36 into $\widehat{EI}$, $\hat{S}$, and $\hat{N}_{x0}$, the buckling equation of by sandwich plates was obtained.

The critical buckling load of an isotropic sandwich beam for the simply supported boundary condition is given below:

$$\widehat{N_{cr}} = \left(\frac{a^2}{\pi^2 E I} + \frac{1}{\hat{S}}\right)^{-1} \tag{37}$$

The critical buckling load of a symmetrical laminated long sandwich plate for the simply supported boundary condition is given below

$$N_{x,cr} = \left(\frac{a^2}{\pi^2 D_{11}} + \frac{1}{\tilde{S}_{11}}\right)^{-1} \tag{38}$$

The shear stiffness matrix is given below

$$\begin{bmatrix} \tilde{S}_{11} & \tilde{S}_{12} \\ \tilde{S}_{12} & \tilde{S}_{22} \end{bmatrix} = \frac{d^2}{c}\begin{bmatrix} \overline{C}^c_{55} & \overline{C}^c_{45} \\ \overline{C}^c_{45} & \overline{C}^c_{44} \end{bmatrix} \tag{39}$$

where

$$\overline{C}^c_{55} = \overline{C}^c_{44} = \frac{E}{2(1+\nu)}, \overline{C}^c_{45} = 0 \tag{40}$$

for isotropic core material.

2.3. Sandwich Plate Forms, their Laminates, and Properties

The sandwich plates under investigation are illustrated in Figure 5, which includes the coordinate system used for analysis, as well as the dimensions of the short edge (a) and long edge (b) of the plates, their thickness, and the direction of the applied buckling load. The face sheets of these plates are made from symmetrically laminated, quasi-isotropic carbon fiber-reinforced epoxy composites, while the core material consists of PVC foam with varying densities. Notably, the long edge of the rectangular plate, referred to as 'b' in this study, is significantly longer than the short edge, designated as "a".

The properties of the components of 12 diferent sandwich panels are given in Table 1.

Some other specific properties (such as lamination sequences, core, and face sheet thicknesses) of twelve different sandwich plates considered in this study are given in Table 2. While laminating the face sheets of the plates, the carbon fibers were placed in three different directions, 0º, 45º, and 90º.

2.4. Numerical Approach

A commercial software application based on the FEM was used to calculate the critical buckling loads. The results obtained from this software were compared with those derived from the LSPM. In the numerical model, a rectangular four-point shell element was selected (refer to Figure 6). A square mesh with a size of 1/20 of the short edge of the sandwich

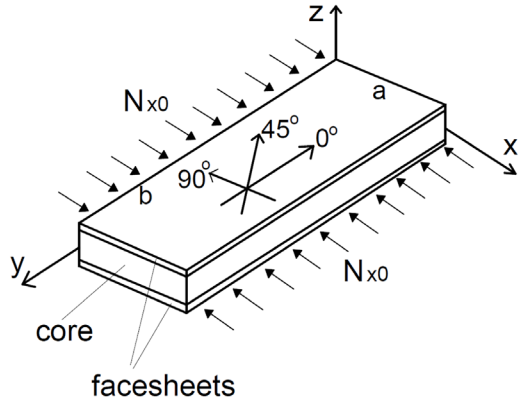

Figure 5. Form of sandwich plate studied and its buckling loads exposed

Table 1. Material properties

Facesheets (carbon/epoxy, T300-934) [18]								
Longitudinal Young's Modulus (E_{11}) (GPa)	148							
Transverse Young's Modulus (E_{22}) (GPa)	9.65							
Longitudinal Shear Modulus (G_{12}) (GPa)	4.55							
Longitudinal Poisson ratio (ν_{12})	0.3							
Lamina thickness (t) (m)	0.1×10^{-3}							
Density (ρ0) (kg/m^3)	1.5×10^3							
Core (PVC foam) [21]								
	H45	H60	H80	H100	H130	H160	H200	H250
Young's Modulus (E) (MPa)	55	75	95	130	175	205	250	320
Density (ρ0) (kg/m^3)	48	60	80	100	130	160	200	250
Poisson ratio (ν)	0.4							

Table 2. Sandwich plate studied LSPM

Plate no	Facesheets			Core			Plate			Bending stiffness values		LSPM
	The arrangement of layers on either side of the axis of symmetry	Thickness (mm)	Weight (gr)	Density (kg/m^3)	Thickness (mm)	Weight (gr)	Density (kg/m^3)	a (m)	b (m)	Weight (gr)	Density (kg/m^3)	D_{11} (N.m)	D_{22} (N.m)	$\frac{b}{a} > 3^{\sqrt[4]{\frac{D_{11}}{D_{22}}}}$
1	[90/-45/45/0]	1.6	298	1500	10	124	100	0.2	0.62	422	293	2916.9	2923.6	3.1 >2.9983
2	[902/-452/452/02]	3.2	595	1500	10	124	100	0.2	0.62	719	439	6742.9	6796.4	3.1 >2.9941
3	[903/-453/453/03]	4.8	893	1500	10	124	100	0.2	0.62	1017	554	11588	11768	3.1 >2.9884
4	[90/-45/45/0]	1.6	298	1500	5	62	100	0.2	0.62	360	439	842.8	849.5	3.1 >2.9941
5	[90/-45/45/0]	1.6	298	1500	15	186	100	0.2	0.62	484	235	6240.3	6247	3.1 >2.9992
6	[-452/452/902/02]	2.3	595	1500	10	124	100	0.2	0.62	719	439	6754.4	6763.3	3.1 >2.9990
7	[452/02/-452/902]	2.3	595	1500	10	124	100	0.2	0.62	719	439	6776.6	6749.8	3.1 >3.0030
8	[02/-452/452/902]	2.3	595	1500	10	124	100	0.2	0.62	719	439	6796.4	6742.9	3.1 >3.0059
9	[90/-45/45/0]	1.6	298	1500	34	421	100	0.2	0.62	719	163	3026.4	3027.1	3.1 >2.9998
10	[-45/45/90/0]	1.6	298	1500	34	421	100	0.2	0.62	719	163	3-026.6	3026.7	3.1 >3.0000
11	[45/0/-45/90]	1.6	298	1500	34	421	100	0.2	0.62	719	163	3026.8	3026.5	3.1 >3.0001
12	[0/-45/45/90]	1.6	298	1500	34	421	100	0.2	0.62	719	163	3027.1	3026.4	3.1 >3.0002

plate was employed. This element operates according to First Order Shear Deformation Theory, specifically the Mindlin-Reissner Shell Theory.

3. Results and discussions

In this study, the critical buckling loads were determined using LSPM and FEM-based numerical modeling. The related results are presented comparatively in Figure 7. $\tilde{S}_{11}$ was obtained using Equation 39 since the E is Young modulus of core, and v is Poisson ratios of core the only variable parameter in the calculation was D_{11}, which was derived from Equation 21. In this equation, d is a function of plate thickness, (A) is the extensional stiffness matrix of face sheets, and (D) is the bending stiffness matrix of face sheets. In long sandwich plates, the critical buckling value increases with the increase of the plate thickness and the elements of the A and D matrix.

Figure 7 shows that as the core thickness increases, the critical buckling load increases, as expected. Sandwich plates with thick core material have lower density but higher strength. In fact, a three-fold increase in core thickness increases the specific strength (load/density) based on the critical buckling load by 10 times.

The results clearly showed that at Plate 4, whose core thickness is the lowest, has the lowest critical buckling load. Since the plate has a thinner core (5 mm), it behaved as a single skin rather than a sandwich plate. This phenomenon also shows that the core thickness should be larger than a certain value. Without considering Plate no. 4, the results were very well fitted to a cubic polynomial given in Figure 8.

The results also showed that the critical buckling loads were independent of the rate of the aspect ratio (b/a) of the plates when it is larger than b/a=3.0. Almost the same results were found for b/a=3.1 and 4.0 (Figure 9).

The graph of the critical buckling loads that sandwich plates can withstand depending on their densities by changing the core materials is presented in Figure 10. In this graph, plate number 4, which was seen to be a single skin plate rather than a sandwich plate, was not taken into account. According to this figure, critical density range should be considered when designing sandwich plates. An approach that designers will use when choosing the right core materials is suggested in this graph. Namely, when designing a sandwich material, it is seen that it should prefer cores with a density of less than 300 kg.m^{-3} and more than 400 kg.m^{-3}.

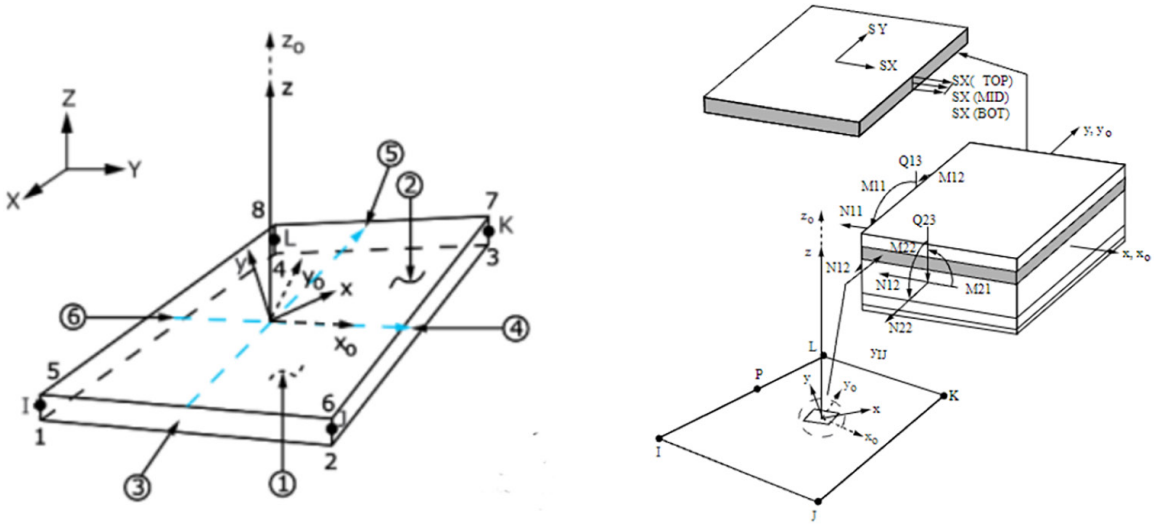

Figure 6. SHELL 181 element (ANSYS)

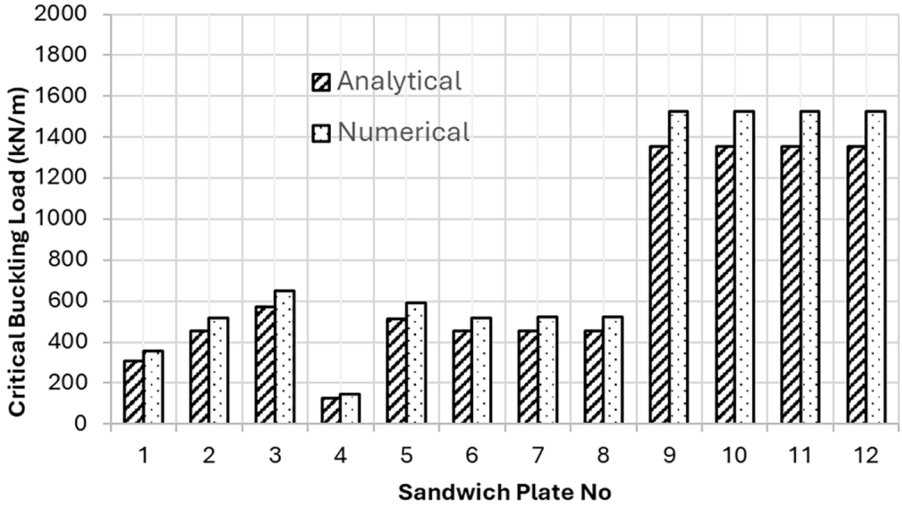

Figure 7. Critical buckling load of sandwich plates

In a comparison of eight sandwich plates with different face sheets and core materials, it was also found that there were no significant effects of lamination sequences on the critical buckling loads. It is also seen that sandwiches designed with thinner face sheets and thicker cores can carry higher critical buckling loads.

4. Conclusion

This study proposes a practical method to assist sandwich material designers based on the critical buckling load. This load is obtained both numerically (using the Ansys software based on the FEM) and analytically (using LSPM), which validate each other.

Critical buckling loads were systematically obtained for 88 plate combinations consisting of different core and face sheets. These plates were assumed simply supported at their four edges and subjected to axial compression loads along their long edges.

It has also been observed that the face sheets and edge dimensions of the sandwich plate are not effective in forming the critical buckling load. However, the thickness of the core material is more decisive as the lowest-density sandwich plate component. In practice, designers should choose this core thickness to give the plate a sandwich character and reduce the density.

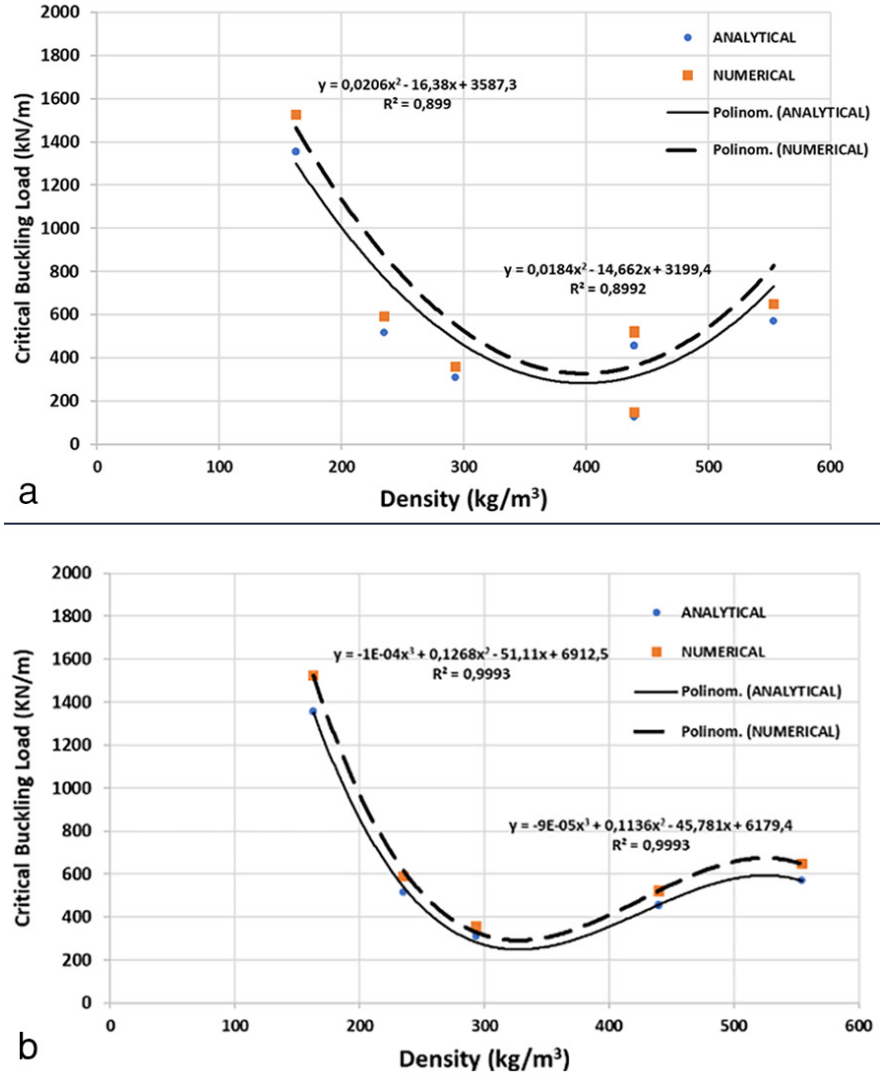

Figure 8. Critical buckling load versus density with **(a)** and without **(b)** Plate no. 4

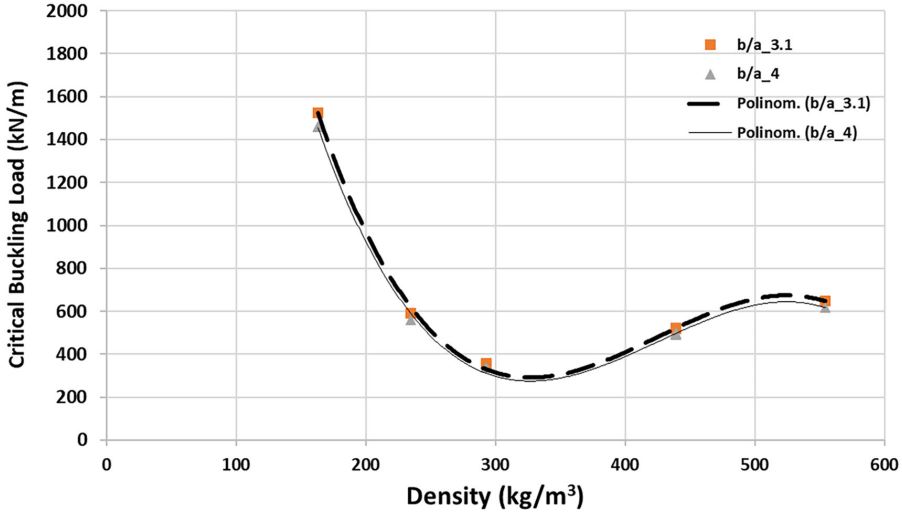

Figure 9. Results for different plate form ratios

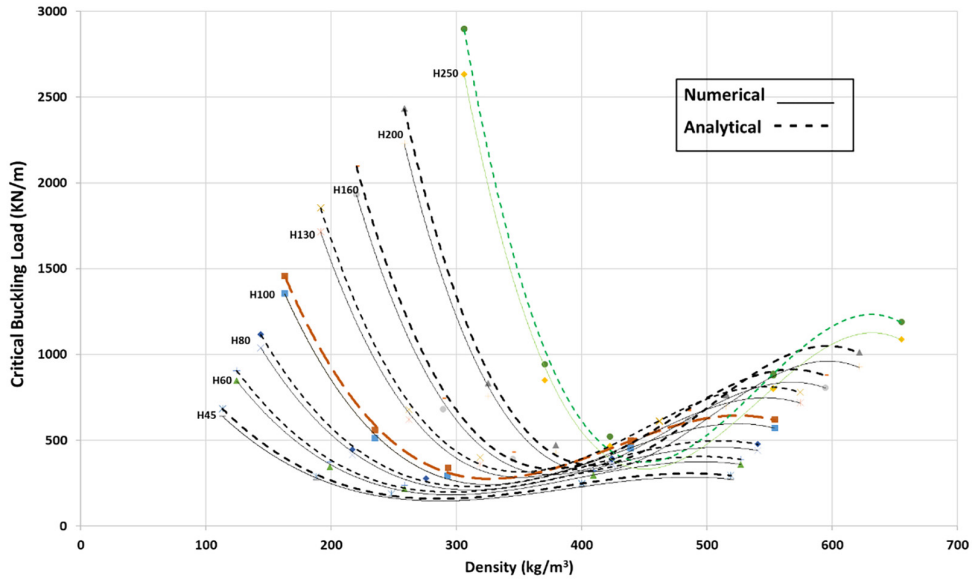

Figure 10. Change in critical buckling loads depending on core densities

It is clearly seen that the software developed in this study based on the LSPM is an effective tool for obtaining critical buckling loads in a shorter time than the commercial software based on FEM. By using this tool, the economy in time, labor, and budget can be provided while studying long sandwich plate optimization.

Footnotes

Authorship Contributions

Concept/Design: E. Altunsaray, and G. Neşer, Data Collection or Processing: E. Altunsaray, Analysis or Interpretation: E. Altunsaray, and G. Neşer, Literature Review: E. Altunsaray, Writing, Reviewing and Editing: G. Neşer.

Conflict of Interest: No conflict of interest was declared by the authors.

Financial Disclosure: The authors declared that this study received no financial support.

5. References

[1] S. Rudan, and L. Drobilo, "NFEM analysis of a composite made hull of autonomous underwater submersible", *Brodogradnja,* vol. 65, no. 3, pp. 101-115, 2014.

[2] F. Dominguez, and L. Carral, "A review of formulations to design an adhesive single-lap joint for use in marine applications", *Brodogradnja*, vol. 71, no. 3, pp. 89-118, 2020.

[3] J. G. Kang, M. C. Kim, I. R. Shin, and W. S. Jin, "Feasibility study on effect of structural flexibility of asymmetric pre swirl stator on propulsion performance for Kriso Container Ship(KCS)", *Brodogradnja*, vol. 72, no. 4, pp. 103-119, 2021.

[4] M. Calvario, Z. Li, and C. G. Soares, "Buckling strength of a composite material wave energy converter structure under slamming loads", *Ocean Engineering*, vol. 241, pp. 110044, 2021.

[5] M. Li, R. Yan, W. Shen, K. Qin, J. Li, and K. Liu, "Fatigue characteristics of sandwich composite joints in ships", *Ocean Engineering*, vol. 254, pp. 111254, 2022.

[6] E. P. Bilalis, M.S. Keramidis, N.G. Tsouvalis, "Structural design optimization of composite materials drive shafts", *Marine Structures*, vol. 84, pp. 103194, 2022.

[7] COReS, Best Practice Guide for Sandwich Structures in Marine Applications, 279.2013.

[8] V. Birman and G.A. Kardomateas, "Review of current trends in research and applications of sandwich structures", *Composites Part B: Engineering,* vol. 142, pp. 221-240, 2017.

[9] A. M. Zenkour, and M. Sobhy, "Thermal buckling of various types of FGM sandwich plates", *Composite Structures*, vol. 93, no. 1, pp. 93-102, 2010.

[10] M. A. Al-Shammari, and M. Al-Waily, "Analytical investigation of buckling behavior of honeycombs sandwich combined plate structure", *International Journal of Mechanical and Production Engineering Research and Development*, vol. 8, no. 4, pp. 803-818, 2018.

[11] M. A. Torabizadeh, "Buckling of the composite laminates under mechanical loads with different layups using different plate theories". *Advanced Composites Letters*, vol. 24, no. 1, pp. 12-20, 2015.

[12] R. Vescovini, M. D'Ottavio, L. Dozio, and O. Polit, "Buckling and wrinkling of anisotropic sandwich plates". *International Journal of Engineering Science*, vol. 130, pp. 136-156, 2018.

[13] S. Wang, et al. "Buckling analysis of hybrid fiber-reinforced composite sandwich panels with varying numbers of polyurethane cores", *Polymer Composites*, vol. 45, no. 16, pp. 15062-15085, 2024.

[14] H. Qian, et al. "Buckling analysis of sandwich plates reinforced with various loading of multi-walled carbon nanotubes", *Engineering Structures,* vol. 294, pp. 116765, 2023.

[15] L. He, A. Maalla, X. Zhou, and H. Tang, "Buckling and post-buckling of anisogrid lattice-core sandwich plates with nanocomposite skins", *Thin-walled Structures,* vol. 199, pp. 111828, 2024.

[16] V. M. Anh, N. D. Dat, and N. D. Duc, "Buckling and post-buckling of sandwich plate with functionally graded graphene origami reinforced core layer in hygrothermal environment", *VNU Journal of Science: Mathematics – Physics,* vol. 39. no. 4, pp. 14-25, 2023.

[17] G. D. Cara, M. d'Ottavio, and O. Polit, "Variable kinematics finite plate elements for the buckling analysis of sandwich composite panels", *Composite Structures,* vol. 330, pp. 117856, 2024.

[18] L. P. Kollar, and G. S. Springer, *Mechanics of composite structures,* Cambridge University Press, NY, USA, 2003.

[19] e. Altunsaray, "Parametric study of buckling of long sandwich rectangular plates". In *Proceedings of the 3rd International Congress on Engineering, Architecture and Design*, Kocaeli, Türkiye, May 04-05, 2018.

[20] ANSYS Academic, 2024R2.

[21] DiabGroup, "Divinycell H - Excellent mechanical properties to low weight", Accessed: Sep. 2024. [Online]. Available: https://www.diabgroup.com/products-services/divinycell-pvc/divinycell-h